Electronic Supplementary Material (ESI) for Chemical Science.
This journal is © The Royal Society of Chemistry 2023

Supporting Information

Near-infrared AIEgens with high singlet-oxygen yields for mitochondria-specific imaging and antitumor photodynamic therapy

Shasha Zhang,[a] Wenfang Yang,[a] Xiao Lu,[b] Xinyi Zhang,[a] Zhichao Pan,[a] Da-Hui Qu,[a] Dong Mei,*[b] Ju Mei* [a] and He Tian[a]

[a]Key Laboratory for Advanced Materials, Joint International Research Laboratory of Precision Chemistry and Molecular Engineering, Feringa Nobel Prize Scientist Joint Research Center, Frontiers Science Center for Materiobiology and Dynamic Chemistry, Institute of Fine Chemicals, School of Chemistry & Molecular Engineering, East China University of Science & Technology, Shanghai 200237, P.R. China. E-mail: daisymeiju@ecust.edu.cn

[b]Clinical Research Center, Beijing Children's Hospital, Capital Medical University, National Center for Children's Health, 56 South Lishi Road, Xicheng District, Beijing 100045, P. R. China. E-mail: meidong@bch.com.cn

Table of Contents

Materials and methods S-1

Table S1 Performance comparison of the present photosensitizers with the lately reported AIE photosensitizers for PDT S-5

Synthesis of $TPEPF_6$, $TPAPF_6$ and $DEAPF_6$ S-7

Scheme S1 The synthetic routes to $TPEPF_6$, $TPAPF_6$ and $DEAPF_6$ S-7

Fig. S1–**Fig. S25** ^1H NMR, ^{13}C NMR, and HRMS of the intermediates, $TPEPF_6$, $TPAPF_6$, and $DEAPF_6$ S-9–S-21

Table S2 Hole-electron analysis parameters of these three photosensitizers at five excited states S-22

Fig. S26 Singlet (*S*)- and triplet (*T*)-state energy levels of $TPEPF_6$, $TPAPF_6$ and $DEAPF_6$ S-22

Table S3 Calculated energy levels of the singlet (*S*) and triplet (*T*) excited states by density functional theory (DFT) S-23

Fig. S27 Cyclic voltammograms (CVs) of $TPEPF_6$, $TPAPF_6$ and $DEAPF_6$ in the DMF solution. S-23

Fig. S28 The UV-Vis and FL spectra of $TPEPF_6$ in different solvents with various polarities S-24

Fig. S29 The UV-Vis and FL spectra of $TPAPF_6$ in different solvents with various polarities S-24

Fig. S30 The UV-Vis and FL spectra of $DEAPF_6$ in different solvents with various polarities S-25

Fig. S31 FL spectra and I/I_0~f_w plots of $TPEPF_6$, $TPAPF_6$, and $DEAPF_6$ in the DMSO/water mixtures with different water fractions (f_ws) S-26

Fig. S32 Size distribution of $TPEPF_6$ in DMSO/water mixtures with different water fractions (f_ws), measured by dynamic light scattering (DLS) S-27

Fig. S33 Size distribution of $TPAPF_6$ in DMSO/water mixtures with different water fractions (f_ws), measured by dynamic light scattering (DLS). S-28

Fig. S34 Size distribution of $DEAPF_6$ in DMSO/water mixtures with different water fractions (f_ws), measured by dynamic light scattering (DLS) S-29

Fig. S35 The fluorescence spectra and I/I_0–1~concentration plots of $TPEPF_6$ in the DMSO/water mixtures (1/99, v/v) with different concentrations of $TPEPF_6$ S-30

Fig. S36 Size distribution of $TPEPF_6$ in the DMSO/water mixtures (1/99, v/v) with different concentrations of $TPEPF_6$, measured by DLS S-30

Fig. S37 The fluorescence spectra and I/I_0–1~concentration plots of $TPAPF_6$ in the DMSO/water mixtures (1/99, v/v) with different concentrations of $TPAPF_6$ S-31
Fig. S38 Size distribution of $TPAPF_6$ in the DMSO/water mixtures (1/99, v/v) with different concentrations of $TPAPF_6$, measured by DLS S-31
Fig. S39 The fluorescence spectra and I/I_0–1~concentration plots of $DEAPF_6$ in the DMSO/water mixtures (1/99, v/v) with different concentrations of $DEAPF_6$ S-31
Fig. S40 Size distribution of $DEAPF_6$ in the DMSO/water mixtures (1/99, v/v) with different concentrations of $DEAPF_6$, measured by DLS S-32
Fig. S41 FL spectra of $TPEPF_6$, $TPAPF_6$, and $DEAPF_6$ in the DMSO/toluene mixtures with different toluene fractions (f_Ts) S-32
Fig. S42 The UV-Vis spectra of $TPEPF_6$, $TPAPF_6$ and $DEAPF_6$ in the DMSO/toluene mixtures with different toluene fractions (f_Ts) S-33
Fig. S43 Size distribution of $TPEPF_6$, $TPAPF_6$ and $DEAPF_6$ in the DMSO/toluene mixtures with different toluene fractions(f_Ts), measured by dynamic light scattering (DLS)..... S-33
Fig. S44 TEM images of $TPEPF_6$ in the DMSO/toluene mixtures with different toluene fractions (f_Ts) S-34
Fig. S45 TEM images of $TPAPF_6$ in the DMSO/toluene mixtures with different toluene fractions (f_Ts)..... S-34
Fig. S46 TEM images of $DEAPF_6$ in the DMSO/toluene mixtures with different toluene fractions (f_Ts) S-34
Fig. S47 Zeta potentials of $TPEPF_6$, $TPAPF_6$ and $DEAPF_6$ characterized by DLS in the aqueous solution S-35
Fig. S48 Photostability of $TPEPF_6$, $TPAPF_6$ and $DEAPF_6$ under light irradiation for different time S-35
Table S4 Crystal data and structure refinement for $TPAPF_6$ S-36
Fig. S49 The single-crystal structure of $TPAPF_6$ S-37
Fig. S50 UV-Vis spectra of ABDA in the presence of a) $TPEPF_6$, b) $DEAPF_6$, or c) Rose Bengal, after being irradiated for different time by the white light S-37
Fig. S51 The absorption spectra of a) $TPEPF_6$, b) $TPAPF_6$, c) $DEAPF_6$, and d) Rose Bengal in the range of 400–800 nm. e) Time-dependent $^1O_2$ generation kinetics deduced from the decomposition rates of ABDA in the presence of different PSs under white-light irradiation in the mixture of DMSO/water (v/v = 1/100). The table shows the optical parameters of these PSs calculated according to ln (A_0/A) S-38
Fig. S52 UV-Vis spectra of ABDA in the presence of $TPAPF_6$ in the DMSO/water mixtures with different water fractions under white-light irradiation……..S-39
Fig. S53 Detection of intracellular $^1O_2$ by SOSG staining in 4T1 cells incubated with $TPEPF_6$ S-40
Fig. S54 Detection of intracellular $^1O_2$ by SOSG staining in SK-OV-3 cells incubated with $TPEPF_6$ S-41
Fig. S55 Detection of intracellular $^1O_2$ by SOSG staining in 4T1 cells incubated with $TPAPF_6$ S-42
Fig. S56 Detection of intracellular $^1O_2$ by SOSG staining in SK-OV-3 cells incubated with $TPAPF_6$ S-43
Fig. S57 Detection of intracellular $^1O_2$ by SOSG staining in 4T1 cells incubated with $DEAPF_6$ S-44
Fig. S58 Detection of intracellular $^1O_2$ by SOSG staining in SK-OV-3 cells incubated with $DEAPF_6$ S-45
Fig. S59 Co-staining experiments of $TPEPF_6$, $TPAPF_6$ and $DEAPF_6$ with MitoTracker® Deep Red FM, respectively S-46
Fig. S60 Relative viabilities of cancer cells (A549 and SK-OV-3 cells) and normal cells (293T cells) treated with $TPEPF_6$, $TPAPF_6$, or $DEAPF_6$, at various concentrations under darkness or white-light irradiation (100 mW/cm^2, 30 min) and further being incubated for 4, 12 or 24 h S-47
Table S5 Dark- and photo-cytotoxicity (IC_{50} [μM]) of $TPEPF_6$, $TPAPF_6$ and $DEAPF_6$ towards different cell lines S-48
Fig. S61 *In vivo* fluorescence imaging of $TPAPF_6$ S-48
Fig. S62 Photographs of 4T1 tumour-bearing mice in different groups on day 0, 5 and 12 during the treatment process S-49
Fig. S63 Weights of the tumors resected from the four groups of mice at day 12 after treatment S-49
Table S6 The ratio of tumor weight to body weight at day 12 post treatment S-50
Fig. S64 a) Tumour growth curves of mice after different treatments. b) The percentage of "body weight loss" at different time after treatment S-51
Fig. S65 H&E staining images, and the blood biochemistry indices of mice obtained at day 11 after treatment S-51
Reference S-52

Materials and methods

Materials

All chemical reagents, biological samples and materials were obtained from commercial suppliers, and all chemical reagents were used as purchased without purification. The silica gels (100–200 mesh, AR) were used for the purification of synthesized compounds. Spectrally pure dimethyl sulfoxide (DMSO) and 9,10-anthracenediylbis(methylene)dimalonic acid (ABDA, 90%) were purchased from J&K. Fetal bovine serum (FBS), penicillin and streptomycin were obtained from Gibco. Roswell Park Memorial Institute 1640 (RPMI 1640), Dulbecco's Modified Eagle Medium (DMEM) and phosphate buffered saline (PBS, 10 mM, pH = 7.4) were purchased from Gibco or Bioagrio. Cell Counting Kit-8 (CCK-8) were obtained from Solarbio. MitoTracker® Deep Red FM were purchased from BioDee. Singlet-oxygen sensor green (SOSG) were obtained from Sigma-Aldrich (MO, USA).

General instruments

^{1}H NMR spectra were recorded on a Brüker AV-400 spectrometer, using deuterated reagents ($CDCl_3$ or DMSO-d_6) as the solvents, and tetramethylsilane (TMS) as the internal standard. The high-resolution mass spectra (HRMS) were obtained on an HP 5958 mass spectrometer with the electronic spray ionization mode. Absorption and fluorescence spectra were obtained on a Varian Cary 500 UV-Vis spectrophotometer and Edinburgh FLS1000 photoluminescence spectrometer, respectively. Transmission electron microscopy (JEM-1400) studies were performed at the Instrumental Analysis Center of East China University of Science and Technology to investigate the morphology and size of nanoaggregates. Dynamic light scattering (DLS) and zeta potential measurement were conducted using Zetasizer Nano particle analyser series (Malvern Nano ZSE, UK) at room temperature. White light source for ROS generation experiment came from commercial LED lamps (SF-582, SF-T100). The cell imaging was implemented with a confocal laser scanning microscope (CLSM, Nikon) at the Instrumental Analysis Center of East China University of Science and Technology. The live mice were imaged with a Living Image system and the relative fluorescence intensity was analyzed by Living Image 4.3.1 software (Caliper).

Theoretical calculations

Theoretical calculation was carried out using the Gaussian 09 software. Optimization for the geometries of $TPEPF_6$, $TPAPF_6$ and $DEAPF_6$ at the ground state were operated at B3LYP/6-31G* level. Then calculation for HOMOs and LUMOs were performed at the same level. Excited triplet state was calculated at PBE0/6-31G* level by time-dependent density functional theory (TD-DFT). The electron-hole distribution analysis was based on TD-DFT unrelaxed excited-state densities as provided by the Multiwfn software.[S1]

The results suggested that the HOMO of $TPEPF_6$ is mainly distributed on the TPE unit and the adjacent cyano group, while its LUMO is basically dominated by the orbitals from the (*Z*)-4-(2-cyano-2-phenylvinyl)pyridin-1-ium moiety. It suggests the significant ICT from the acrylonitrile-substituted TPE moiety to the (*Z*)-4-(2-cyano-2-phenylvinyl)-pyridin-1-ium part. Likewise, marked ICT from the acrylonitrile-decorated TPA unit to the (*Z*)-4-(2-cyano-2-phenylvinyl)-pyridin-1-ium moiety is clearly revealed by the HOMO and LUMO of $TPAPF_6$. The case is similar but different in $DEAPF_6$. The electron clouds of HOMO are mainly situated on the DEA and the neighbouring 2-phenylacrylonitrile groups, while the LUMO is primarily occupied by the orbits from the (*Z*)-4-(2-cyano-2-phenylvinyl)pyridin-1-ium unit, implying the ICT from the 2-phenylacrylonitrile-furnished DEA to the (*Z*)-4-(2-cyanovinyl)pyridin-1-ium.

Spectral measurements

The stock solution of $TPEPF_6$, $TPAPF_6$ and $DEAPF_6$ were prepared in DMSO (10^{-3} M) and used for specific

experiments after appropriate preparation. All spectra of the solutions were obtained in 1 cm quartz cuvettes.

Investigation of size, zeta potential and morphology

Transmission electron microscopy (TEM) observation and dynamic light scattering (DLS) analysis were carried out to study the morphology of the aggregates of these three compounds formed in the DMSO/toluene mixtures with different toluene fractions (f_T = 50, 80, and 90 vol% for DLS measurement, and f_T = 80 and 90 vol% for TEM test). DLS measurement of AIE-PSs in DMSO/toluene mixtures with different toluene fractions was carried out using a Zetasizer Nano particle analyser series (Malvern Nano ZSE, UK) at 25 °C. Zeta-potentials of AIE-PSs in DMSO/H_2O (v/v = 1/99) were measured using the same instrument. Zetasizer software was used to process and analyze the data. TEM images were recorded by a JEM-1400 transmission electron microscope. Measurements were performed by dropping 10 μL samples onto carbon-coated copper grids. After removing the excess solution by blotting paper, the samples were dried under ambient conditions.

Crystallography analysis of $TPAPF_6$

Perfect single crystals of $TPAPF_6$ were successfully obtained by slowly evaporating the mixture of THF/hexane. The X-ray crystallography analysis helps to elucidate the molecular conformation and molecular arrangement of these analogue AIEgens. The crystal was resolved on Bruker APEX-II CCD with a radiation of CuK/α at a wavelength of 1.54178 (Å). The data was further analyzed with SHELXL-2018/3.

Detection of $^1O_2$ in solution

The $^1O_2$ production was determined by using 9,10-anthracenediylbis(methylene)dimalonic acid (ABDA) as an indicator. The stock solutions of ABDA and photosensitizers in DMSO were added into ultrapure water to afford the DMSO/water solutions (v/v, 1/100). Then the mixed solutions were exposed to white light (400–800 nm, 25 mW/cm^2) irradiation from 0 to 120 s. The absorbances of ABDA at 378 nm were recorded at different irradiation time to obtain the decay rates of the photosensitizing processes. The effectiveness of photosensitizer-generated $^1O_2$ was evaluated by A/A_0, where A_0 is the initial absorbance at 378 nm, while A represents the final absorbance at 378 after white-light irradiation.

Singlet-oxygen quantum yield calculation

The singlet-oxygen quantum yields of $TPEPF_6$, $TPAPF_6$ and $DEAPF_6$ (Φ_{PS}) were determined using Rose Bengal (RB) as the standard reference. To conduct the experiments, ABDA was added into AIE-PSs or RB solution to give a working concentration of 50 μM (DMSO/H_2O = 1/100, v/v). To eliminate the inner-filter effect, the absorption maxima were controlled at *ca.* 0.2. The singlet-oxygen quantum yields are calculated using the following equation:

$$\Phi_{PS} = \Phi_{RB} \frac{\kappa_{PS} \times A_{RB}}{\kappa_{RB} \times A_{PS}}$$

where κ_{PS} and κ_{RB} represent the decomposition rate constants of the photosensitizing process determined by the plot of ln(A_0/A) *versus* light irradiation time, A_0 is the initial absorbance of ABDA while A is the ABDA absorbance after irradiation for different time; A_{RB} and A_{PS} refer to the light absorbed by RB and AIE-PSs, respectively, calculated by the integration of their absorption spectra from 400 to 800 nm; Φ_{RB} is the singlet-oxygen quantum yield of RB, which is 0.75 in water.[S2]

Cell culture and cell imaging

Five cancer cell lines, namely mouse breast cancer cells (4T1), human embryonic kidney 293T cells (293T), human lung adenocarcinoma cells (A549), and ovarian cancer cells (SK-OV-3) were obtained commercially. 4T1, SK-OV-3, and A549 cells were cultured in modified 1640 medium containing 10% fetal bovine serum (FBS) and 1% penicillin-streptomycin (complete 1640). 293T cells were cultured in DMEM medium containing 10% FBS and 1%

penicillin-streptomycin (complete DMEM). All cells were incubated at 37 °C in a humidified atmosphere of 5% CO_2. Cells were seeded in cell culture dishes for 2 days and passed at 95% cell confluency. Before the experiment, the medium was removed and the attached cells were washed 3 times with PBS buffer to remove the remaining growth medium.

4T1 and SK-OV-3 cells in exponential phase were cultured individually on 35 mm-glass-bottom dishes for 24 hours before confocal microscopic imaging of the cells with the AIE-PSs, reaching approximately 80% confluency. On the day of treatment, the cell staining was conducted by replacing the cell culture medium with AIE-PS-containing culture medium. Then the cells were washed with 1 mL of PBS for three times at room temperature and 1 mL of complete medium was added and observed via confocal laser scanning microscope (CLSM).

Detection of singlet-oxygen in living cells

The intracellular ROS generation under white-light irradiation was detected by using SOSG as an indicator and studied by CLSM. 4T1 cells and SK-OV-3 cells were seeded and cultured in confocal plates (35 mm-glass-bottom culture dishes) for 12 h. Then the culture media were replaced with 1 mL of fresh medium containing AIE-PSs (10 μM) and the cells were incubated for another 1 h at 37 °C, the cells were irradiated by white light (100 mW/cm^2) for different periods of time. Afterwards, the cells were incubated with 1 mL of fresh medium containing 5 mM SOSG (10 μL) for 30 min at 37 °C. Finally, the cells were rinsed with PBS for three times and the fluorescence signals of the cells were captured by CLSM imaging. For the collection of fluorescence signal given by $TPEPF_6$, the excitation was 405 nm and the emission was collected at 570–620 nm. For the collection of fluorescence signal given by $TPAPF_6$ or $DEAPF_6$, the excitation was 488 nm and the emission was collected at 660–730 nm. For the collection of fluorescence signal given by SOSG, the excitation was 488 nm and the emission was collected at 500–530 nm. No background fluorescence of cells was detected under the set conditions.

Co-staining assay by CLSM

The SK-OV-3 and 4T1 cells were selected for the co-staining assay experiments. When the cells achieved around a confluence of 80%, the cells in 35 mm-glass-bottom dishes were cultured with AIE-PSs for 1 h and washed for three times with PBS solution (1 mL). Then, the cells were incubated with MitoTracker® Deep Red FM (commercially purchased fluorescent dye for the mitochondria-specific staining) for 1 h under standard operation conditions. Afterwards, the cells were washed three times with PBS solution (1 mL), and fluorescence images were taken by a CLSM (Laser wavelength: 647 nm for MitoTracker® Deep Red FM; 405 nm for $TPEPF_6$; 488 nm for $TPAPF_6$ and $DEAPF_6$; the emission filter: MitoTracker® Deep Red FM: 650–670 nm; $TPEPF_6$: 570–620 nm; $TPAPF_6$ and $DEAPF_6$: 660−730 nm). The false color of MitoTracker® Deep Red FM was given as green and the false color of AIE-PSs was given as red.

Cell viability test

The cell viability of 293T, A549, SK-OV-3, and 4T1 cells was determined after incubation with AIE-PSs under white-light irradiation (100 mW/cm^2, 30 min) using a Cell-Counting-Kit-8 (CCK-8). Briefly, on a 96-well plate, the cells were inoculated at a density of 1×10^4 cells/well in 100 μL of complete medium and cultured at 37 ºC with 5% CO_2. After the cells being incubated for 12 h, the old medium was replaced with 200 μL fresh medium containing different concentrations of AIE-PSs (0, 1, 2, 5, 10, 20, 50 and 100 μM) and the cells were further incubated at 37 °C. After 1 h, the plates were irradiated with white light (400–800 nm, 100 mW/cm^2) for 30 min. All cells with or without light irradiation were cultivated for another 4, 12 or 24 h to support the cell proliferation. After culturing for different time, 100 μL of serum-free medium containing 10% CCK-8 was added to each well, and the 96-well plate was subsequently incubated at 37 °C for 2 h. Finally, their optical density (OD) values were read at 450 nm, the cell viability rates were calculated by $(OD_{sample}–OD_{blank})/(OD_{control}–OD_{blank})$ ×100%. The results were presented as a mean ± standard

deviation obtained from six samples.

Animals and tumor model

The female BALB/*c* mice were obtained from Vital River and fed under standard housing conditions. 4T1 cells (5×10^5) in 50 μL PBS were subcutaneously inoculated into the hip of each mouse. The tumor growth was monitored every day, and the volume of tumor was measured with a vernier caliper and quantified using (tumor length)×(tumor width)^2/2. When the tumors grew to a certain size, the 4T1 tumor-bearing mice were used for fluorescence imaging and further therapy studies. All the mice used were handled strictly in accordance with governmental and international guidelines on animal experimentation. Mice were free to obtain sterile food and water. The animal experiments have been approved by the Laboratory Animal Ethics Committee of East China University of Science and Technology (No. ECUST-2021-03001).

***In vivo* study on tumor visualization**

The Living Image 4.3.1 software (Caliper) was utilized to image the mice. Mice bearing 4T1 tumors were randomly divided into three groups (PBS, $TPAPF_6$ and $TPAPF_6$+light) and intratumorally injected with 50 μL of $TPAPF_6$ (4 mg/kg, w_{probe}/w_{mouse}) or PBS (n = 3 per group); For the $TPAPF_6$+light group, mice were treated by light illumination for 10 min. *In vivo* fluorescence imaging of 4T1 tumor in mice at different time points after intratumor injection of PBS or $TPAPF_6$ was conducted afterwards. The excitation wavelength applied was 465 nm, and the fluorescence signals were collected at 700 nm and 760 nm, respectively. At 24 h post injection, the mice were sacrificed while the tumor and major organs were isolated and imaged, then the fluorescence images were taken by the same equipment using the same conditions as those for the mice bodies.

***In vivo* therapy study**

In this experiment, BALB/*c* mice bearing 4T1 subcutaneous tumors were divided into four groups (n = 5 per group) in random. Thereafter, the mice were treated by intratumor injection of (1) PBS (100 μL) without white-light irradiation, or (2) PBS (100 μL) and subjected to white-light irradiation, or (3) $TPAPF_6$ (100 μL of probe solution, w_{probe}/w_{mouse} = 8 mg/kg) without white-light irradiation, or (4) $TPAPF_6$ (100 μL of probe solution, w_{probe}/w_{mouse} = 8 mg/kg) and then irradiated with white light. Four hours later, mice of groups (2) and (4) were irradiated with white light (200 mW/cm^2) for 20 min. The treatments were conducted every two days and spanned a therapy duration of 12 days for all groups. The tumoricidal capacity was also continually estimated by tumor volume and mice body weight after various treatment every day. The volume of tumor was measured with a vernier caliper and quantified using (tumor length) × (tumor width)^2/2. On day 11 after treatment, blood was taken from the eye socket of each mouse for serum biochemical analysis. Furthermore, the mice in all these four groups were sacrificed and their tumor tissues were then excised to measure the tumor volume after treatment for 12 days. The main organs including heart, liver, spleen, lung, and kidney were resect for H&E staining.

Statistical analysis

Statistical analyses were carried out by Stata software and the differences between various groups were performed by Student's *t*-test. All the data were expressed as mean ± standard deviation (SD). A value of $P < 0.05$ was considered significant and was indicated with asterisks, such as $*P < 0.05$, $**P < 0.01$, and $***P < 0.001$. Statistical analysis was performed by Graph pad Prism 8.0. Each experiment included at least three replicates.

Table S1 Performance comparison of the present photosensitizers (PSs) with the lately reported AIE PSs for PDT

Photosensitizer	λ_{ex} (nm)	λ_{em} (nm)	ROS yield	ΔE_{ST} (eV)	In vivo experiments	Organelle specificity	References
$TPAPF_6$	476	783	3.170	0.460	Yes	Mitochondria	This work
$TPEPF_6$	419	662	5.110	0.460	No	Mitochondria	This work
$DEAPF_6$	495	768	0.880	0.560	No	Mitochondria	This work
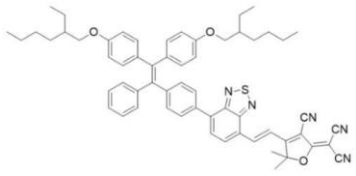 TBTC8	550	820	0.478		Yes	No	*Adv. Funct. Mater.* **2019**, *29*, 1901791
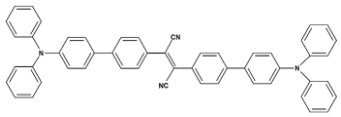 TPATCN	490	665	0.276		No	No	*Nano-Micro Lett.* **2021**, *13*, 58
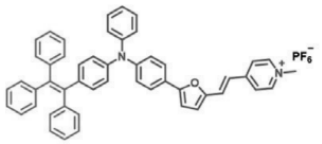 TPE-TFPy	490	672	0.630	1.043	Yes	Lysosome	*Angew. Chem. Int. Ed.* **2020**, *59*, 9610−9616
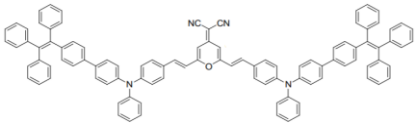 T-TTD dots	502	660	0.510		Yes	No	*ACS Nano* **2017**, *11*, 3922–3932
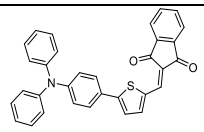 TTI	517	624	0.852		No	Lipid droplets	*Chem. Eng. J.* **2021**, 410,128186
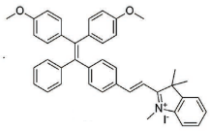 MTi	480	710	0.890	0.633	Yes	Mitochondria	*Small* **2019**, *15*, 1902352
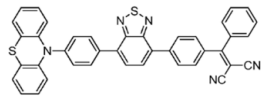 FBD NPs	400	735	0.520	0.001	Yes	No	*Chem. Mater.* **2021**, *33*, 5974–5980
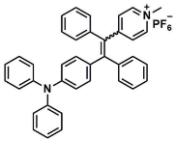 TPA-DPPy	420	625	0.245		No	Mitochondria	*Nanoscale* **2021**, *13*, 1195–1205
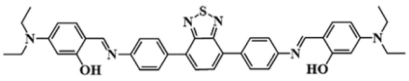 DSABBT NPs	450	625	0.350	0.951	No	No	*ACS Appl. Mater. Interfaces* **2021**, *13*, 7987–7996

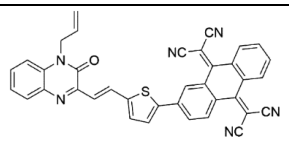 QCN NPs	530	800	0.690	0.071	Yes	No	*ACS Appl. Mater. Interfaces* **2020**, *12*, 42551–42557
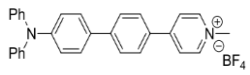 TPPM	442	601	3.170		No	Mitochondria	*ACS Appl. Mater. Interfaces* **2019**, *11,* 20715–20724
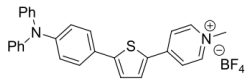 TTPM	448	607	3.710		No	Mitochondria	*ACS Appl. Mater. Interfaces* **2019**, *11,* 20715–20724
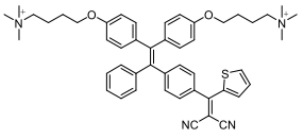 TPETH-Mito	350	635	0.692		No	Mitochondria	*ACS Appl. Mater. Interfaces* **2018**, *10*, 11546–11553
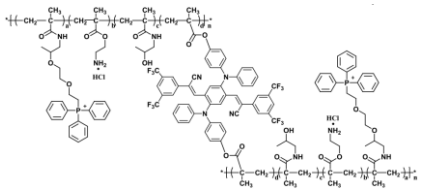 PAIE-TPP NPs	480	640	0.779	0.277	No	Mitochondria	*J. Mater. Chem. B* **2017**, *5*, 6277–6281
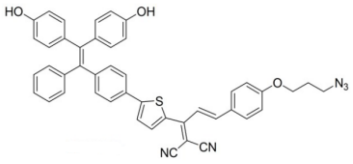 TPETF-N_3	420	650	0.330		No	No	*J. Mater. Chem. B* **2016**, *4*, 169–176
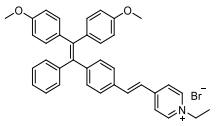 AIE-PS	400	625	0.785		No	No	*Mater. Chem. Front.* **2020**, *4*, 3074–3085
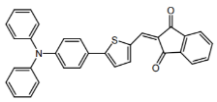 TTIE	542	650	0.129	0.680	No	Lipid droplets	*Chem. Commun.* **2021**, *57*, 1046–1049
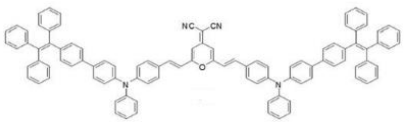 cRGD-siVEGF-TTD NPs	494	682	0.682		No	No	*Chem. Commun.* **2016**, *52*, 2752–2755
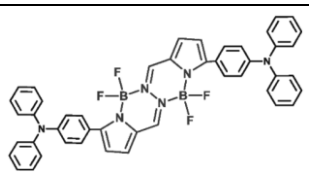 BOPHY-2TPA NPs	550	662	0.850	0.512	No	No	*ACS Appl. Nano Mater.* **2021**, *4*, 6012–6019

Synthesis of $TPEPF_6$, $TPAPF_6$ and $DEAPF_6$

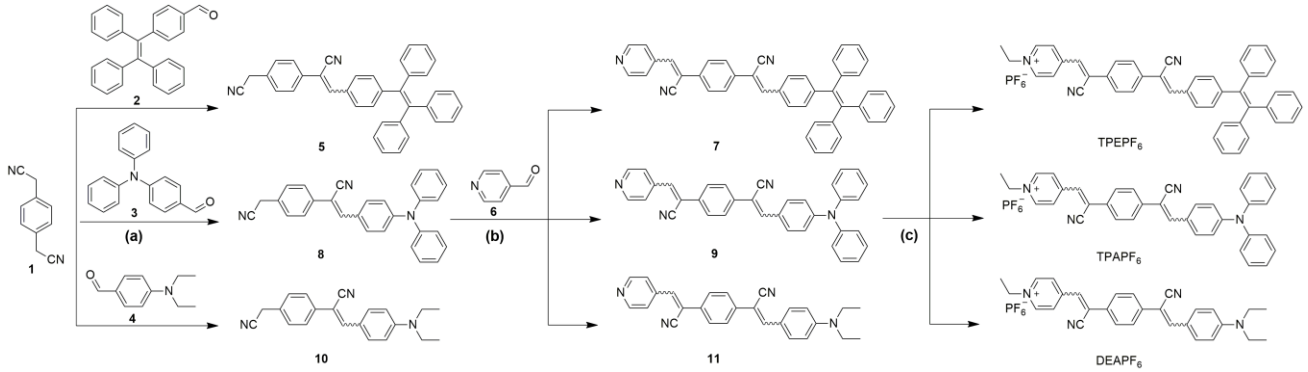

Scheme S1. The synthetic routes to $TPEPF_6$, $TPAPF_6$ and $DEAPF_6$. Conditions: (a) NaOH, EtOH/THF, R.T.; (b) Piperidine, EtOH, 90 °C; and (c) i) CH_3CH_2I, acetonitrile, 95 °C; ii) KPF_6, acetone, 65 °C.

4-(1,2,2-Triphenylvinyl)benzaldehyde (2): Compound **2** was prepared according to the methods reported in the literature.[S3] ^{1}H NMR (400 MHz, $CDCl_3$) δ 9.90 (s, 1H), 7.61 (d, J = 8.2 Hz, 2H), 7.19 (d, J = 8.2 Hz, 2H), 7.12 (dd, J = 6.2, 3.8 Hz, 9H), 7.02 (dt, J = 9.5, 5.0 Hz, 6H).

(*Z*)-2-(4-(Cyanomethyl)phenyl)-3-(4-(1,2,2-triphenylvinyl)phenyl)acrylonitrile (5): 2,2′-(1,4-Phenylene) diacetonitrile (**1**, 468.2 mg, 3.0 mmol) was added to a three-necked round-bottom flask, and 7.5 mL of THF and 2.5 mL of EtOH were added. 4-(1,2,2-Triphenylvinyl)benzaldehyde (**2**, 360.2 mg, 1.0 mmol) and sodium hydroxide (20.0 mg, 0.5 mmol) was dissolved in the mixture of THF (15 mL) and EtOH (5 mL), respectively, then added into the constant pressure dropping funnel. The flask was evacuated under vacuum and flushed with dry N_2 for three times. The reaction was started by slowly opening the constant pressure dropping funnel. The mixture was stirred for 6 h at R.T. and then was poured into water and extracted with dichloromethane for three times. The collected organic layers were concentrated by rotatory evaporation, and the residue was purified by the silica gel column chromatography with petroleum ether/ethyl acetate (20/1, v/v) as an eluent, and the pure product of compound **5** was obtained as a yellow-green solid (255.2 mg, 51.2%). ^{1}H NMR (400 MHz, $CDCl_3$), δ (TMS, ppm): 7.66 (dd, J = 8.3, 5.2 Hz, 4H), 7.44–7.36 (m, 3H), 7.20–7.09 (m, 11H), 7.08–6.99 (m, 6H), 3.79 (s, 2H). ^{13}C NMR (100 MHz, $CDCl_3$) δ (TMS, ppm): 146.85, 143.27, 143.14, 142.49, 139.95, 134.71, 131.99, 131.36, 131.29, 130.73, 128.87, 128.65, 127.89, 127.71, 126.94, 126.76, 126.62, 117.92, 117.37, 109.62, 23.37. HRMS for $C_{37}H_{26}N_2$ $[M]^-$, calculated: 497.2018; found: 497.2023.

(*Z*)-2-(4-((*Z*)-1-Cyano-2-(4-(1,2,2-triphenylvinyl)phenyl)vinyl)phenyl)-3-(pyridin-4-yl)acrylonitrile (7): Compound **5** (498.2 mg, 1.0 mmol) and compound **6** (114.6 μL, 1.2 mmol) were dissolved in 20 mL of EtOH, and piperidine (8.5 μL, 0.1 mmol) was then added dropwise into the reaction system. The mixture was heated to 90 °C and stirred for 12 h, after cooling to room temperature, the solvent was removed by rotatory evaporation. Dichloromethane (30 mL) was added and the organic phase was washed with water (50 mL×3). Then the organic phase was collected and dried by Na_2SO_4, and the solvent was removed under reduced pressure. The obtained residue was separated by silica-gel column chromatography (petroleum ether/ethyl acetate = 1/1) to obtain the desired product as orange-yellow solid (480.3 mg, 81.8%). ^{1}H NMR (400 MHz, $CDCl_3$) δ (TMS, ppm): 8.78 (d, J = 5.0 Hz, 2H), 7.81–7.72 (m, 6H), 7.70 (d, J = 8.4 Hz, 2H), 7.52 (d, J = 12.0 Hz, 2H), 7.19–7.09 (m, 11H), 7.09–7.00 (m, 6H). ^{13}C NMR (100 MHz, $CDCl_3$) δ (TMS, ppm): 150.51, 146.37, 142.79, 140.79, 138.70, 137.00, 133.76, 133.12, 131.09, 129.88, 129.70, 129.67, 129.60, 126.98, 126.87, 126.31, 125.87, 120.53, 118.44, 115.81, 108.85, 105.89. HRMS for $C_{43}H_{29}N_3$ $[M]^+$, calculated: 588.2440; found: 588.2414.

4-((*Z*)-2-Cyano-2-(4-((*Z*)-1-cyano-2-(4-(1,2,2 triphenylvinyl)phenyl)vinyl)phenyl)vinyl)-1-ethylpyridin-1-

ium ($TPEPF_6$): A mixture of compound **7** (588.2 mg, 1.0 mmol) and iodoethane (115.2 μL, 1.2 mol) was dissolved in 15 mL of acetonitrile under an atmosphere of nitrogen. The mixture was heated to 95 ºC and then refluxed for 6 h. After cooling to room temperature, the solvent was removed by rotatory evaporation. Then mixed residue was dissolved in 15 mL of acetone and added 3 mL of saturated aqueous solution of KPF_6. After being fully dissolved, the mixture was heated to 65 ºC and then refluxed for 3 h. After being cooled to room temperature, the solvent was removed under reduced pressure. The raw product was extracted three times using dichloromethane and water. The organic layers were combined and dried by anhydrous $MgSO_4$. After filtration, the solvent was removed under reduced pressure, and the resultant product was washed with ethyl acetate to give $TPEPF_6$ as a red solid (631.8 mg, 83.0% yield). ^{1}H NMR (400 MHz, DMSO-d_6) δ (TMS, ppm): 9.22 (d, J = 6.8 Hz, 2H), 8.48 (d, J = 6.7 Hz, 2H), 8.44 (s, 1H), 8.12 (s, 1H), 7.99 (q, J = 8.7 Hz, 4H), 7.78 (d, J = 8.4 Hz, 2H), 7.17 (dt, J_1 = 8.8 Hz, J_2 = 4.2 Hz, 11H), 7.07–6.95 (m, 6H), 4.66 (q, J = 7.3 Hz, 2H), 1.59 (t, J = 7.3 Hz, 3H). ^{13}C NMR (150 MHz, DMSO-d_6) δ (TMS, ppm): 193.41, 151.09, 150.47, 149.58, 141.29, 140.76, 136.61, 131.92, 126.77, 125.44, 122.72, 122.67, 122.64, 122.13, 119.19, 114.02, 100.15, 43.83, 12.41. HRMS for $C_{45}H_{34}N_3^+$ [M-PF_6], calculated: 616.2753; found: 616.2757.

(*Z*)-2-(4-(Cyanomethyl)phenyl)-3-(4-(diphenylamino)phenyl)acrylonitrile (8): Similar to the synthesis of compound **5**, except that the starting materials were compound **1** (468.2 mg, 3.0 mmol) and compound **3** (273.1 mg, 1.0 mmol). The crude product was purified by silica-gel column chromatography using petroleum ether/ethyl acetate (v/v, 15/1) as eluent to obtain the desired product as yellow solid (246.7 mg, 60.0%). ^{1}H NMR (400 MHz, DMSO-d_6) δ (TMS, ppm): 7.93 (s, 1H), 7.86 (d, J = 8.9 Hz, 1H), 7.75 (d, J = 8.4 Hz, 1H), 7.58–7.23 (m, 8H), 7.16 (p, J = 7.3 Hz, 4H), 7.06 (dd, J = 8.2, 4.1 Hz, 2H), 6.96 (d, J = 8.8 Hz, 1H), 6.67 (d, J = 8.8 Hz, 1H), 4.09 (t, J = 8.4 Hz, 2H). ^{13}C NMR (100 MHz, $CDCl_3$) δ (TMS, ppm): 150.22, 146.51, 142.28, 135.06, 130.84, 130.14, 129.60, 128.48, 126.37, 126.04, 125.89, 125.75, 124.46, 120.62, 118.60, 117.51, 106.52, 23.37. HRMS for $C_{29}H_{21}N_3$ $[M]^+$, calculated: 412.1814; found: 412.1805.

(*Z*)-2-(4-((*Z*)-1-Cyano-2-(4-(diphenylamino)phenyl)vinyl)phenyl)-3-(pyridin-4-yl)acrylonitrile (9): Similar to the synthesis of compound **7**, except that the starting materials were compound **8** (411.2 mg, 1.0 mmol) and compound **6** (114.6 μL, 1.2 mmol). The crude product was purified by silica-gel column chromatography using petroleum ether/ethyl acetate (v/v, 2/1) as eluent to obtain compound **9** as orange-red solid. Yield: 426.2 mg, 85.2%. ^{1}H NMR (400 MHz, DMSO-d_6) δ (TMS, ppm): 8.78 (dd, J = 4.5, 1.6 Hz, 2H), 8.20 (s, 1H), 8.06 (s, 1H), 7.97–7.87 (m, 6H), 7.83 (dd, J = 4.8, 1.4 Hz, 2H), 7.46–7.36 (m, 4H), 7.25–7.13 (m, 6H), 6.97 (d, J = 8.9 Hz, 2H). ^{13}C NMR (100 MHz, $CDCl_3$) δ (TMS, ppm): 150.51, 146.37, 142.75, 140.79, 138.72, 137.00, 135.62, 133.76, 133.12, 131.09, 129.88, 129.64, 126.98, 126.87, 126.31, 126.00, 124.67, 122.82, 120.53, 120.38, 116.67, 115.81, 108.85, 105.89. HRMS for $C_{35}H_{24}N_4$ $[M]^+$, calculated: 501.2079; found: 501.2073.

4-((*Z*)-2-Cyano-2-(4-((*Z*)-1-cyano-2-(4-(diphenylamino)phenyl)vinyl)phenyl)vinyl)-1-ethylpyridin-1-ium ($TPAPF_6$): Similar to the synthesis of $TPEPF_6$, except that the starting materials were compound **9** (250.2 mg, 0.5 mmol) and iodoethane (58.0 μL, 0.6 mmol). The crude product was washed with ethyl acetate to give $TPAPF_6$ as a black solid. Yield: 240.8 mg, 91.0%. ^{1}H NMR (400 MHz, DMSO-d_6) δ (TMS, ppm): 9.20 (d, J = 6.8 Hz, 2H), 8.48 (d, J = 6.7 Hz, 2H), 8.41 (s, 1H), 8.10 (s, 1H), 7.95 (dt, J = 16.7, 8.9 Hz, 6H), 7.42 (t, J = 7.8 Hz, 4H), 7.20 (dd, J = 16.3, 7.9 Hz, 6H), 6.97 (d, J = 8.9 Hz, 2H), 4.65 (q, J = 7.3 Hz, 2H), 1.59 (t, J = 7.3 Hz, 3H). ^{13}C NMR (150 MHz, DMSO-d_6) δ (TMS, ppm): 149.97, 145.80, 145.26, 135.20, 131.22, 129.93, 128.39, 127.49, 127.11, 126.19, 125.82, 124.96, 119.48, 83.89, 24.61. HRMS for $C_{37}H_{29}N_4^+$ [M–PF_6], calculated: 529.2392; found: 529.2392.

(*Z*)-2-(4-(Cyanomethyl)phenyl)-3-(4-(diethylamino)phenyl)acrylonitrile (10): Similar to the synthesis of compound **5**, except that the starting materials were compound **1** (468.2 mg, 3.0 mmol) and compound **4** (117.1 mg, 1.0 mmol). The crude product was purified by silica-gel column chromatography using petroleum ether/ethyl acetate (v/v, 15/1) as eluent to obtain the desired product as orange-yellow solid (129.8 mg, 41.2%). ^{1}H NMR (400 MHz, $CDCl_3$) δ (TMS, ppm): 7.85 (d, J = 8.6 Hz, 2H), 7.63 (d, J = 8.2 Hz, 2H), 7.40 (q, J = 16.1, 8.0 Hz, 4H), 7.26 (s, 1H),

3.78 (s, 2H), 3.43 (q, J = 7.0 Hz, 4H), 1.22 (t, J = 7.1 Hz, 6H). Please noted that due to the poor solubility of compound **10,** as suggested by the ^{1}H NMR measurement, we did not obtain the pure compound **10**. We have to use this not pure enough compound **10** as one of the raw material for the synthesis of compound **11** which is the intermediate of the targeted compound DEAPF$_6$.

(*Z*)-2-(4-((Z)-1-Cyano-2-(4-(diethylamino)phenyl)vinyl)phenyl)-3-(pyridin-4-yl)acrylonitrile (11): Similar to the synthesis of compound **7**, except that the starting materials were compound **10** (157.1 mg, 0.5 mmol) and compound **6** (57.3 μL, 0.6 mmol). The crude product was purified by silica-gel column chromatography using petroleum ether/ethyl acetate (v/v, 2/1) as eluent to obtain compound **11** as red solid. Yield: 162.1 mg, 80.2%. ^{1}H NMR (400 MHz, DMSO-d_6) δ (TMS, ppm): 8.77 (d, J = 5.7 Hz, 2H), 8.17 (s, 1H), 7.93–7.81 (m, 9H), 6.81 (d, J = 9.0 Hz, 2H), 3.45 (q, J = 7.0 Hz, 4H), 1.19–1.07 (m, 6H). HRMS for $C_{27}H_{24}N_4$ [M]$^+$, calculated:405.2079; found: 405.2077.

4-((Z)-2-Cyano-2-(4-((Z)-1-cyano-2-(4-(diethylamino)phenyl)vinyl)phenyl)vinyl)-1-ethylpyridin-1-ium (DEAPF$_6$): Similar to the synthesis of TPEPF$_6$, except that the starting materials were compound **11** (202.1 mg, 0.5 mmol) and iodoethane (58.0 μL, 0.6 mmol). The crude product was washed with ethyl acetate to give DEAPF$_6$ as a black solid (193.2 mg, 89.2%). ^{1}H NMR (400 MHz, DMSO-d_6) δ (TMS, ppm): 9.20 (d, J = 6.8 Hz, 2H), 8.47 (d, J = 6.8 Hz, 2H), 8.38 (s, 1H), 8.10–7.80 (m, 7H), 6.82 (d, J = 9.1 Hz, 2H), 4.65 (q, J = 7.3 Hz, 2H), 3.46 (q, J = 6.9 Hz, 4H), 1.58 (t, J = 7.3 Hz, 3H), 1.24–1.05 (m, 6H). ^{13}C NMR (150 MHz, DMSO-d_6) δ (TMS, ppm): 149.75, 148.83, 144.89, 137.83, 132.11, 131.05, 127.37, 126.66, 125.55, 119.83, 119.13, 118.81, 116.08, 111.08, 99.80, 56.23, 43.86, 16.06, 12.47. HRMS for $C_{29}H_{29}N_4^+$ [M–PF$_6$], calculated:433.2392; found: 433.2384.

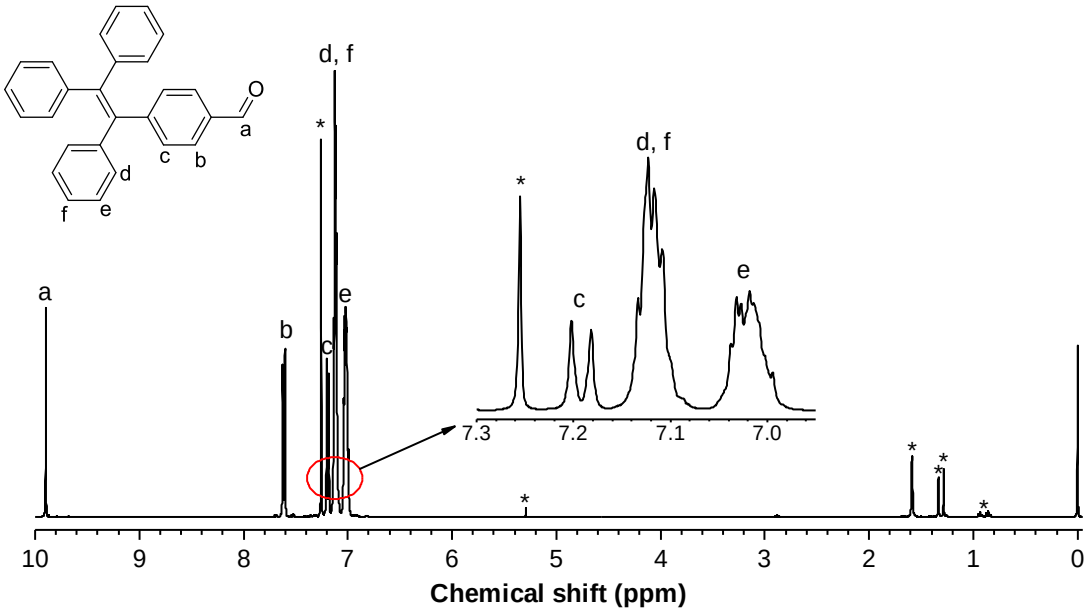

Fig. S1 The ^{1}H NMR spectrum of compound **2** in $CDCl_3$, where the solvent peaks are marked with asterisks.

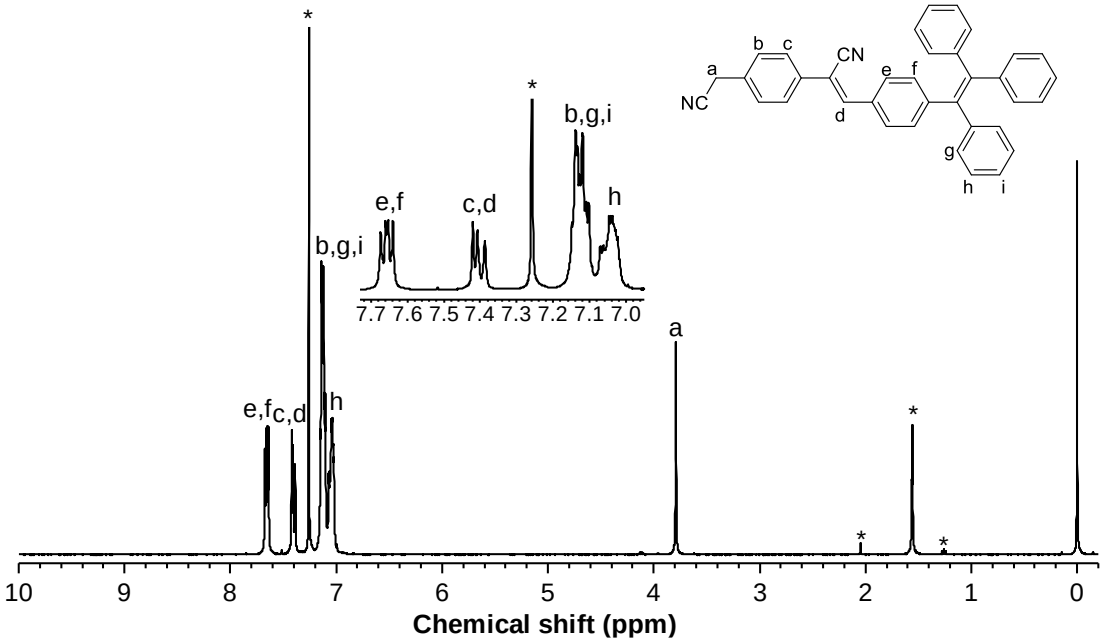

Fig. S2 The ^{1}H NMR spectrum of compound **5** in $CDCl_3$, where the solvent peaks are marked with asterisks.

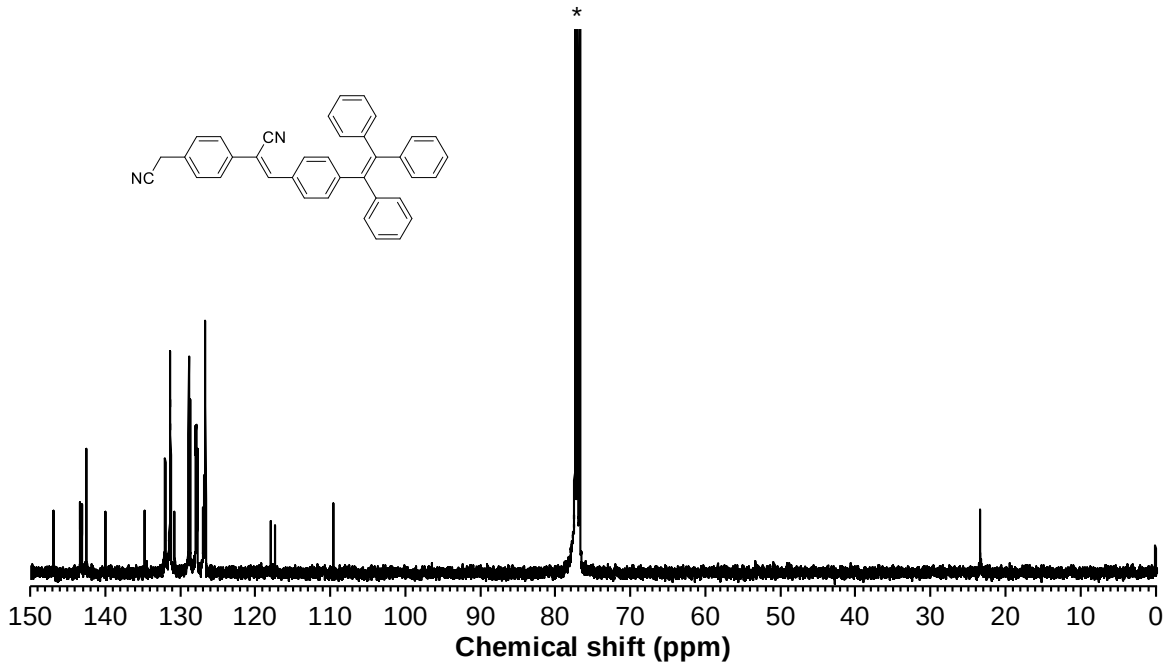

Fig. S3 The ^{13}C NMR spectrum of compound **5** in $CDCl_3$, where the solvent peaks are marked with asterisks.

Monoisotopic Mass, Even Electron Ions
3 formula(e) evaluated with 1 results within limits (up to 50 best isotopic matches for each mass)
Elements Used:
C: 0-37 H: 0-45 N: 0-2
J-MEI
MJ-ZSS-010 46 (0.517) Cm (46:53)

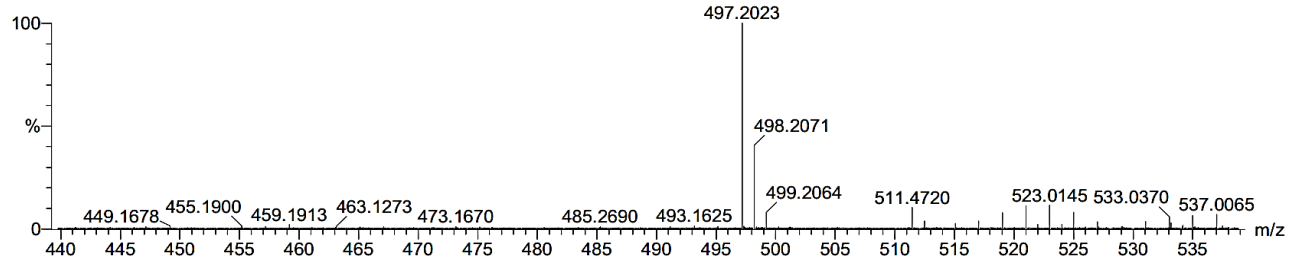

Minimum:				-1.5			
Maximum:		5.0	10.0	50.0			
Mass	Calc. Mass	mDa	PPM	DBE	i-FIT	i-FIT (Norm)	Formula
497.2023	497.2018	0.5	1.0	26.5	288.5	0.0	C37 H25 N2

Fig. S4 The HRMS of compound **5**.

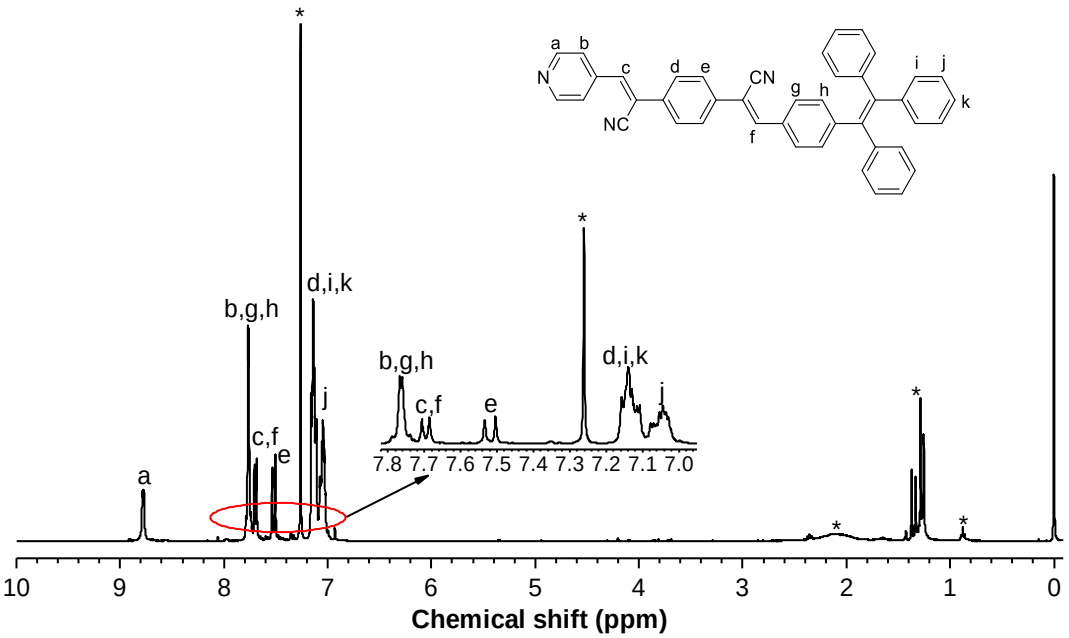

Fig. S5 The ^{1}H NMR spectrum of compound **7** in $CDCl_3$, where the solvent peaks are marked with asterisks.

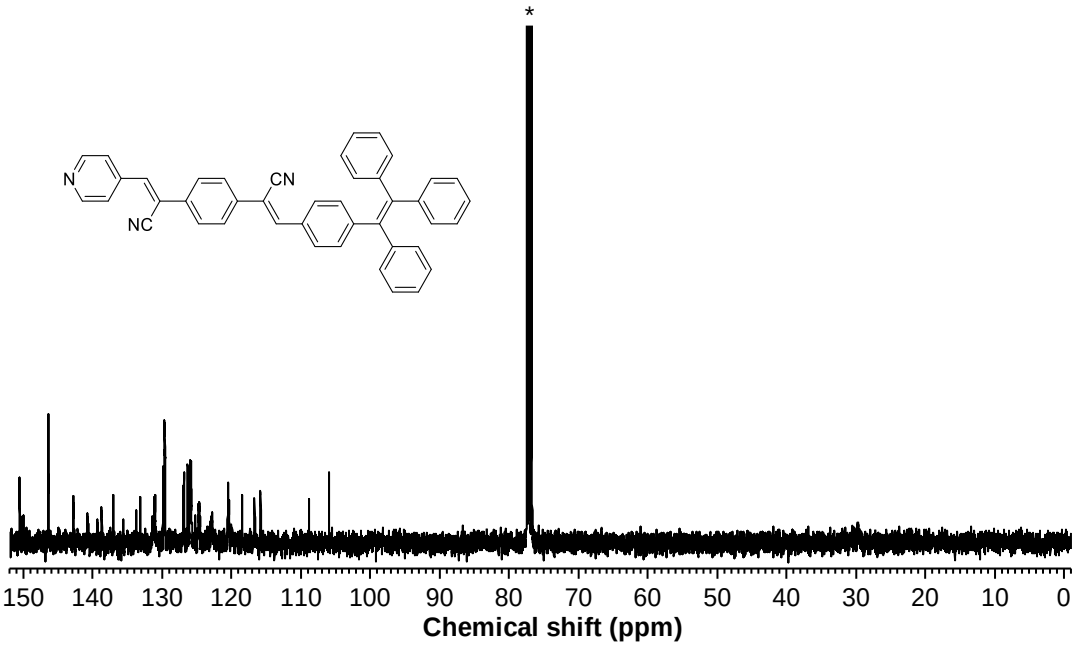

Fig. S6 The ^{13}C NMR spectrum of compound **7** in $CDCl_3$, where the solvent peaks are marked with asterisks.

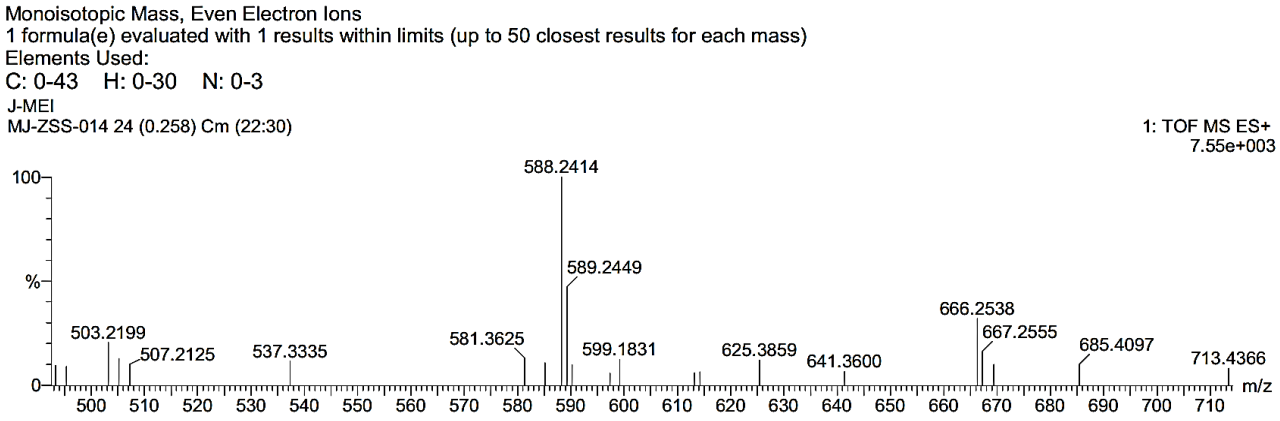

Minimum:				-1.5			
Maximum:		5.0	10.0	50.0			
Mass	Calc. Mass	mDa	PPM	DBE	i-FIT	i-FIT (Norm)	Formula
588.2414	588.2440	-2.6	-4.4	30.5	15.1	0.0	C43 H30 N3

Fig. S7 The HRMS of compound **7**.

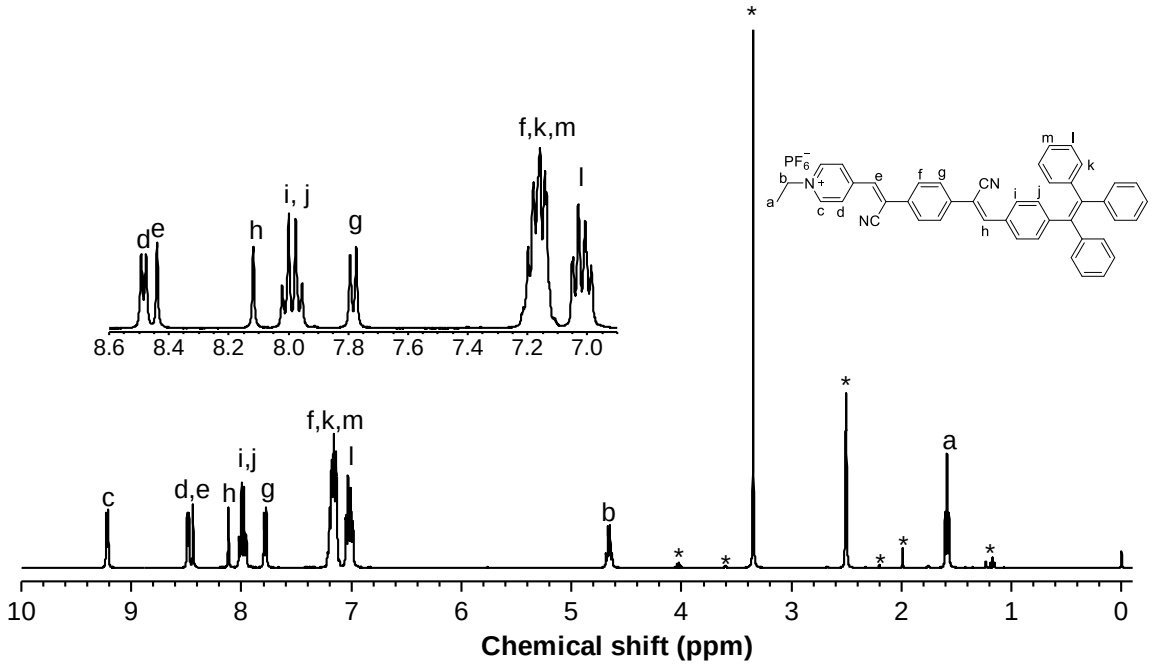

Fig. S8 The ^{1}H NMR spectrum of $TPEPF_6$ in DMSO-d_6, where the solvent peaks are marked with asterisks.

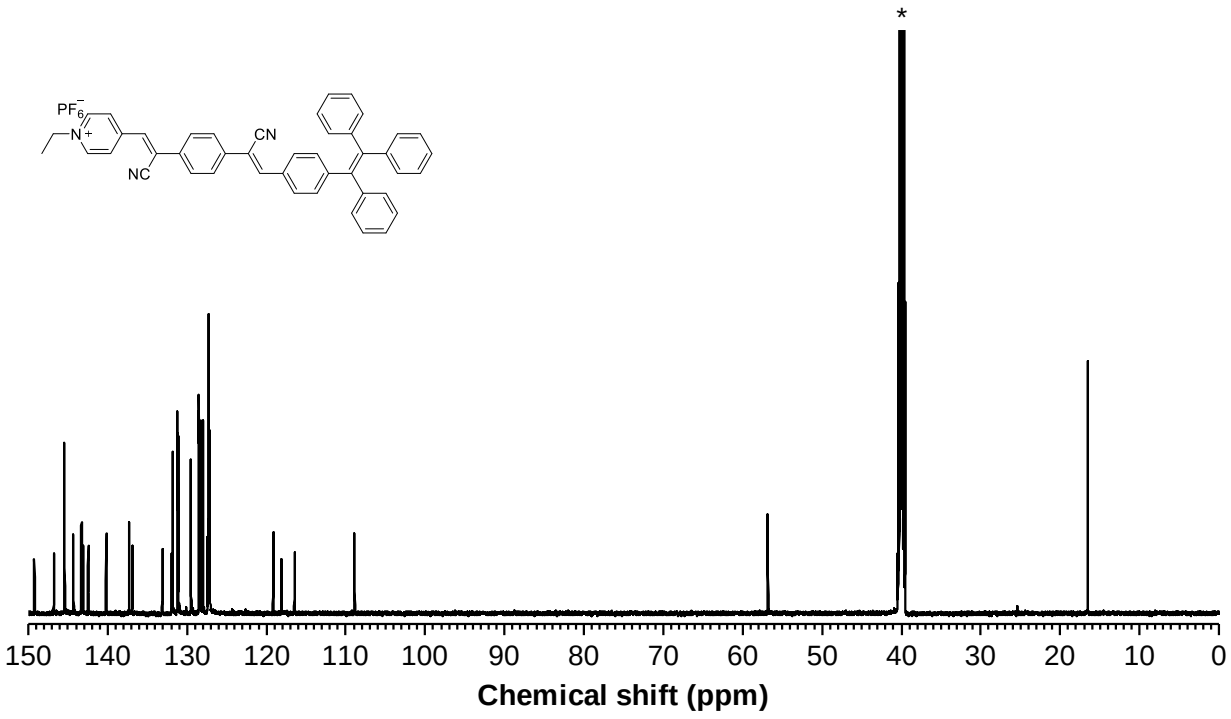

Fig. S9 The ^{13}C NMR spectrum of $TPEPF_6$ in DMSO-d_6, where the solvent peaks are marked with asterisks.

Monoisotopic Mass, Even Electron Ions
16 formula(e) evaluated with 1 results within limits (up to 50 closest results for each mass)
Elements Used:
C: 0-45 H: 0-99 N: 0-3
J-MEI
MJ-ZSS-019 71 (0.820) Cm (68:71)

1: TOF MS ES+
9.95e+002

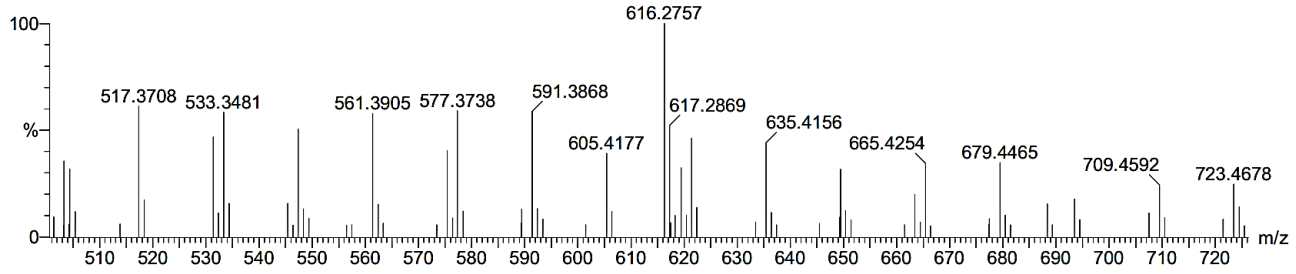

Minimum:				-1.5			
Maximum:		5.0	10.0	50.0			
Mass	Calc. Mass	mDa	PPM	DBE	i-FIT	i-FIT (Norm)	Formula
616.2757	616.2753	0.4	0.6	30.5	22.0	0.0	C45 H34 N3

Fig. S10 The HRMS of $TPEPF_6$.

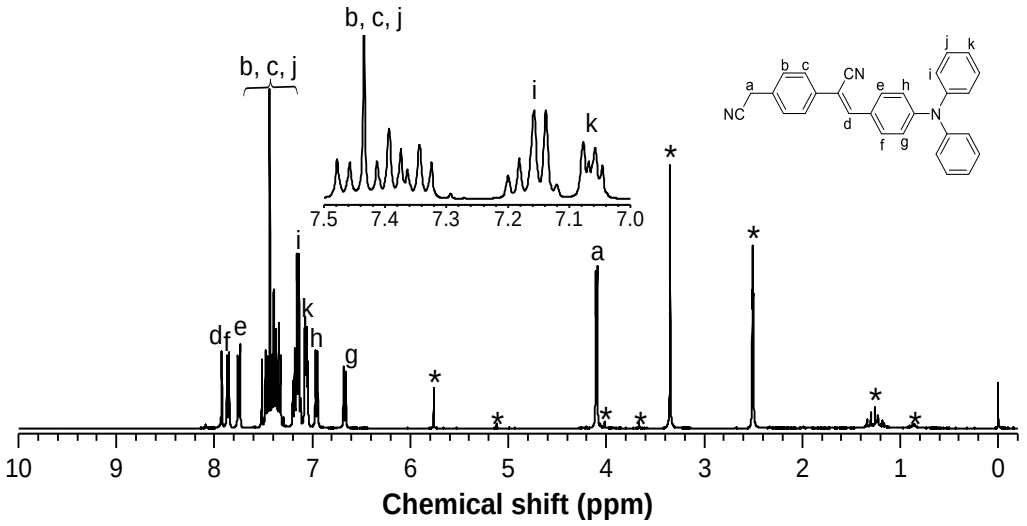

Fig. S11 The ^{1}H NMR spectrum of compound **8** in DMSO-d_6, where the solvent peaks are marked with asterisks.

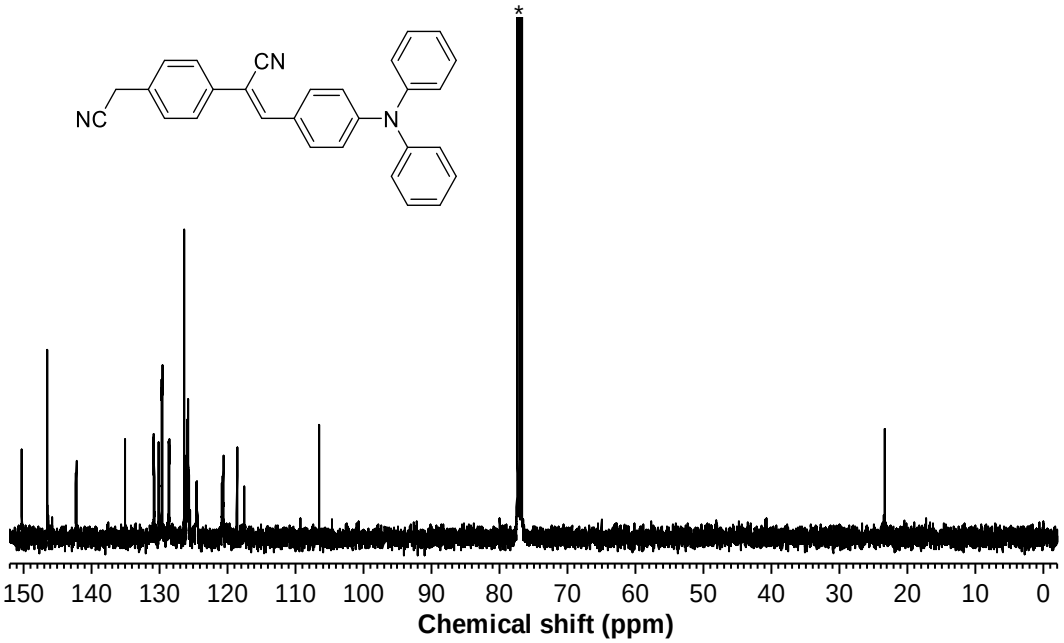

Fig. S12 The ^{13}C NMR spectrum of compound **8** in $CDCl_3$, where the solvent peaks are marked with asterisks.

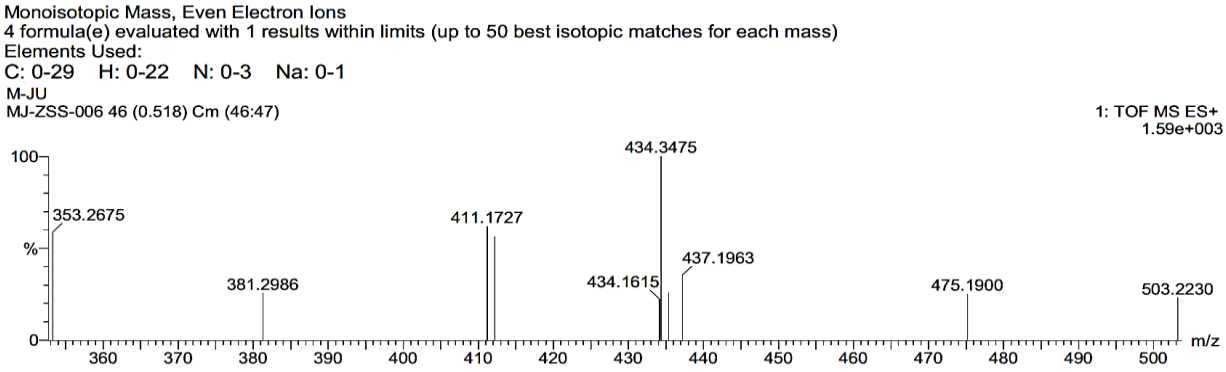

Minimum:				-1.5			
Maximum:		5.0	5.0	50.0			
Mass	Calc. Mass	mDa	PPM	DBE	i-FIT	i-FIT (Norm)	Formula
412.1805	412.1814	-0.9	-2.2	20.5	24.7	0.0	C29 H22 N3

Fig. S13 The HRMS of compound **8**.

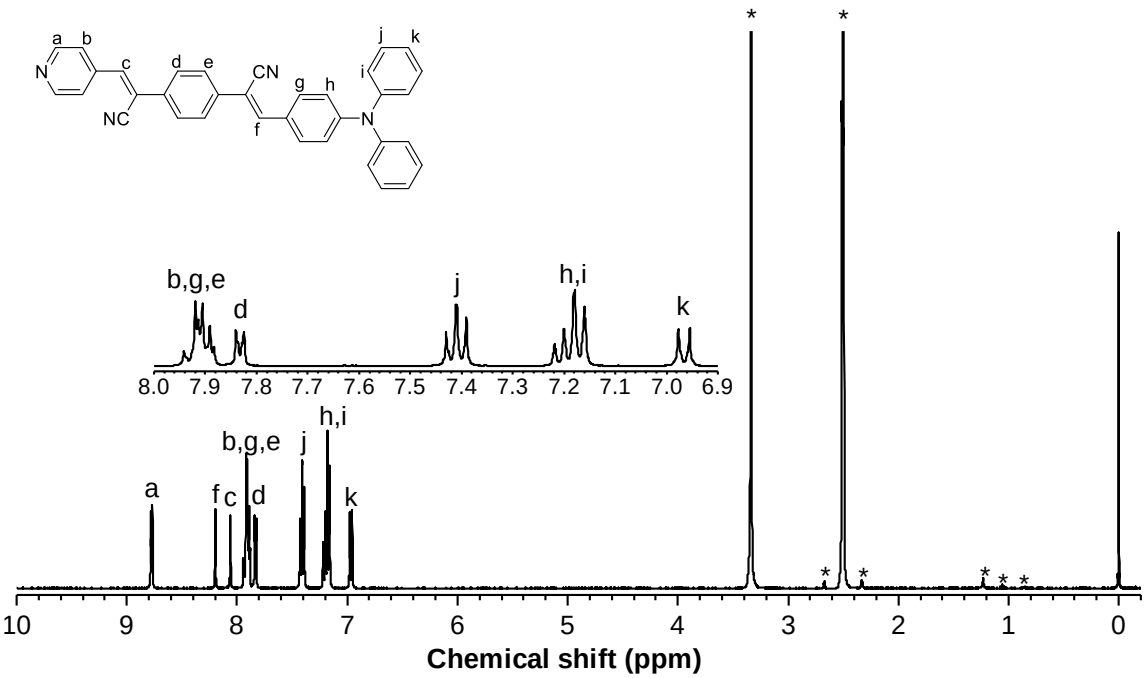

Fig. S14 The ^{1}H NMR spectrum of compound **9** in DMSO-d_6, where the solvent peaks are marked with asterisks.

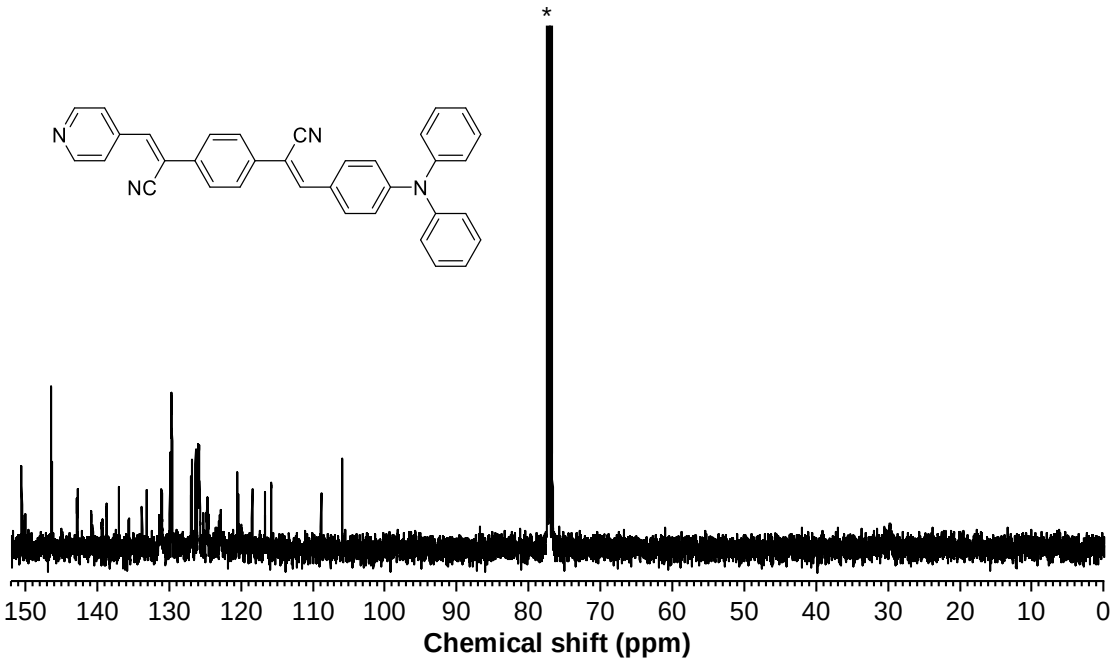

Fig. S15 The ^{13}C NMR spectrum of compound **9** in $CDCl_3$, where the solvent peaks are marked with asterisks.

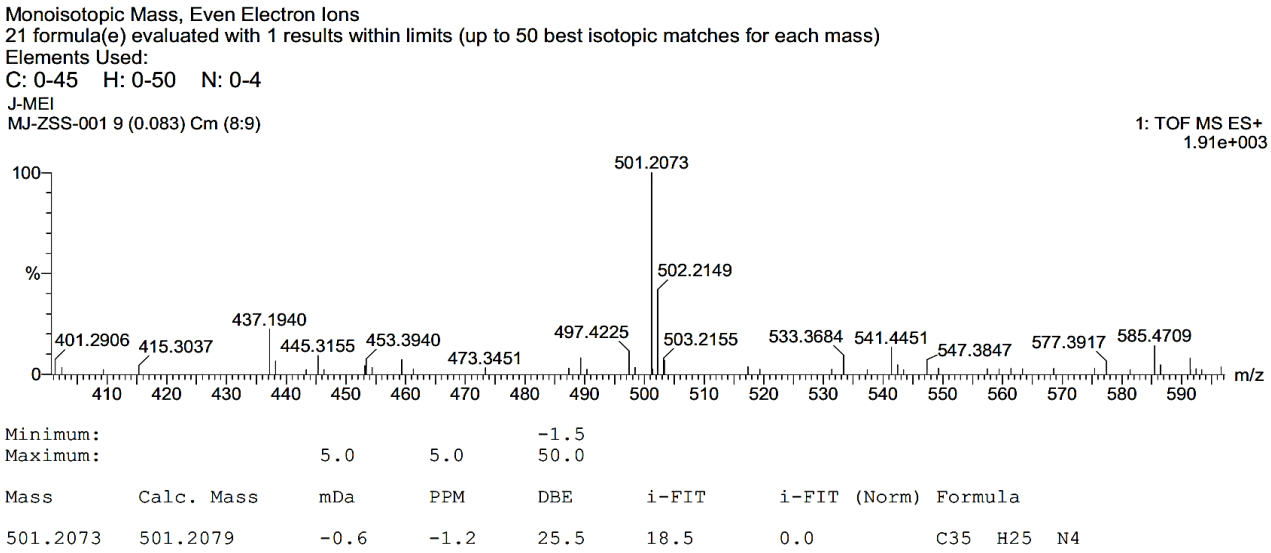

Minimum:				-1.5			
Maximum:		5.0	5.0	50.0			
Mass	Calc. Mass	mDa	PPM	DBE	i-FIT	i-FIT (Norm)	Formula
501.2073	501.2079	-0.6	-1.2	25.5	18.5	0.0	C35 H25 N4

Fig. S16 The HRMS of compound **9**.

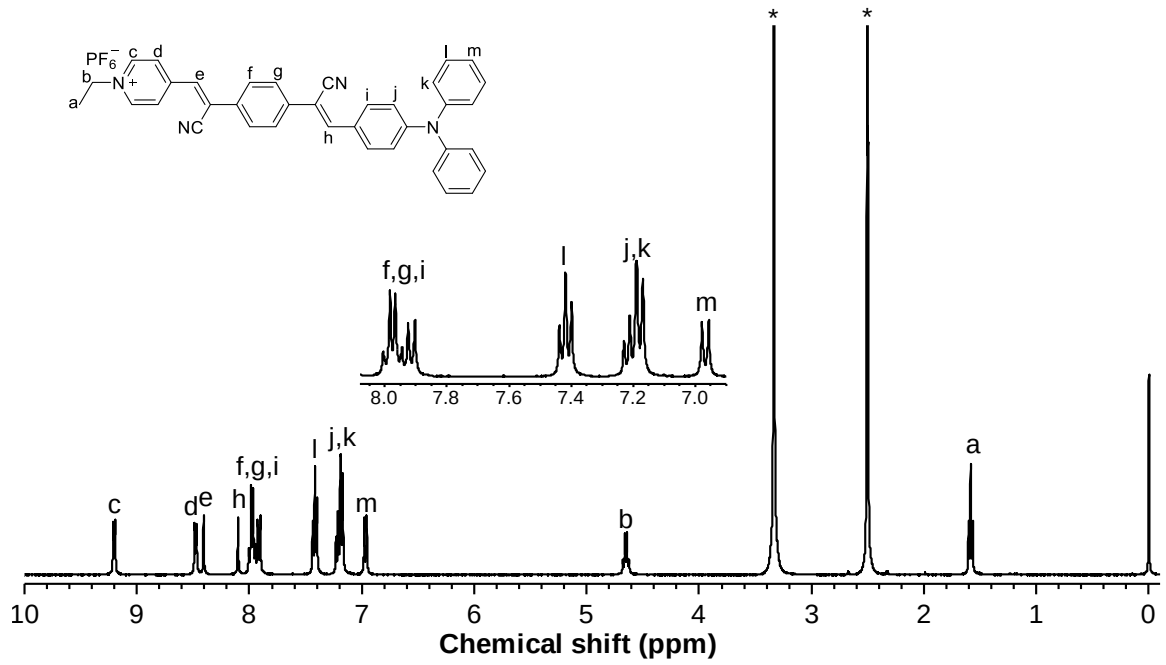

Fig. S17 The ^{1}H NMR spectrum of TPAPF$_6$ in DMSO-d_6, where the solvent peaks are marked with asterisks.

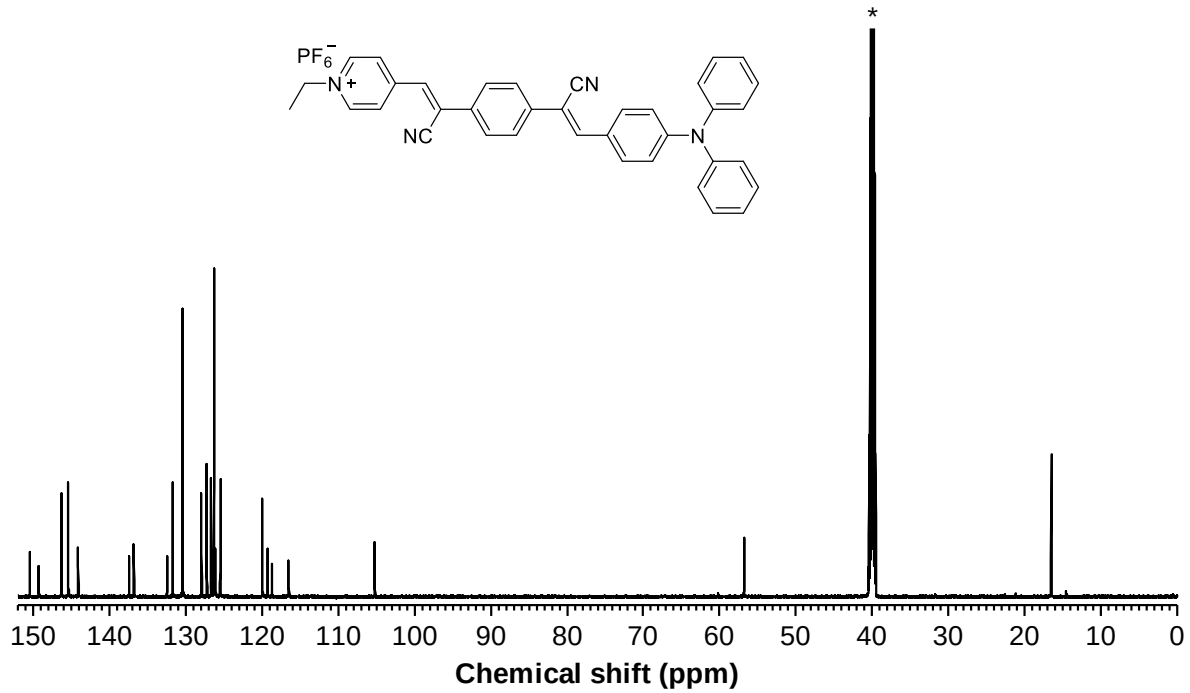

Fig. S18 The ^{13}C NMR spectrum of $TPAPF_6$ in DMSO-d_6, where the solvent peaks are marked with asterisks.

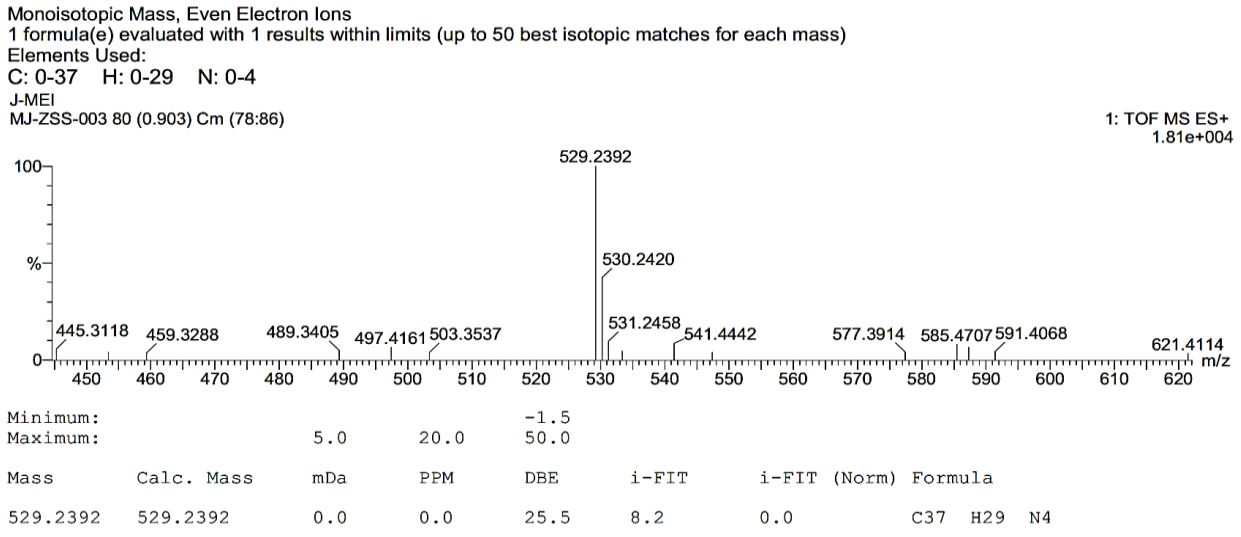

Minimum:				-1.5			
Maximum:		5.0	20.0	50.0			
Mass	Calc. Mass	mDa	PPM	DBE	i-FIT	i-FIT (Norm)	Formula
529.2392	529.2392	0.0	0.0	25.5	8.2	0.0	C37 H29 N4

Fig. S19 The HRMS of $TPAPF_6$.

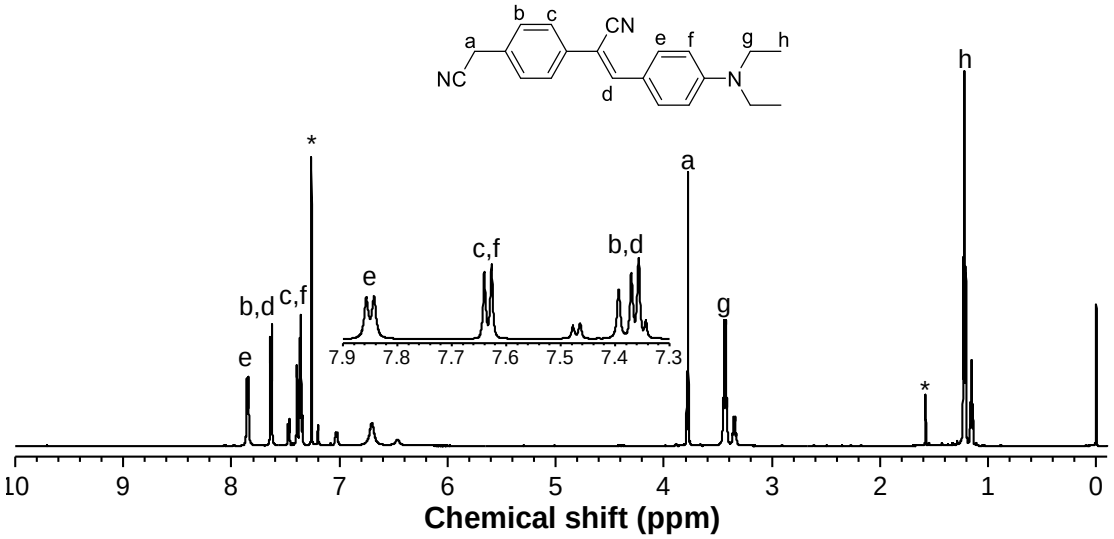

Fig. S20 The ^{1}H NMR spectrum of compound **10** in $CDCl_3$, where the solvent peaks are marked with asterisks.

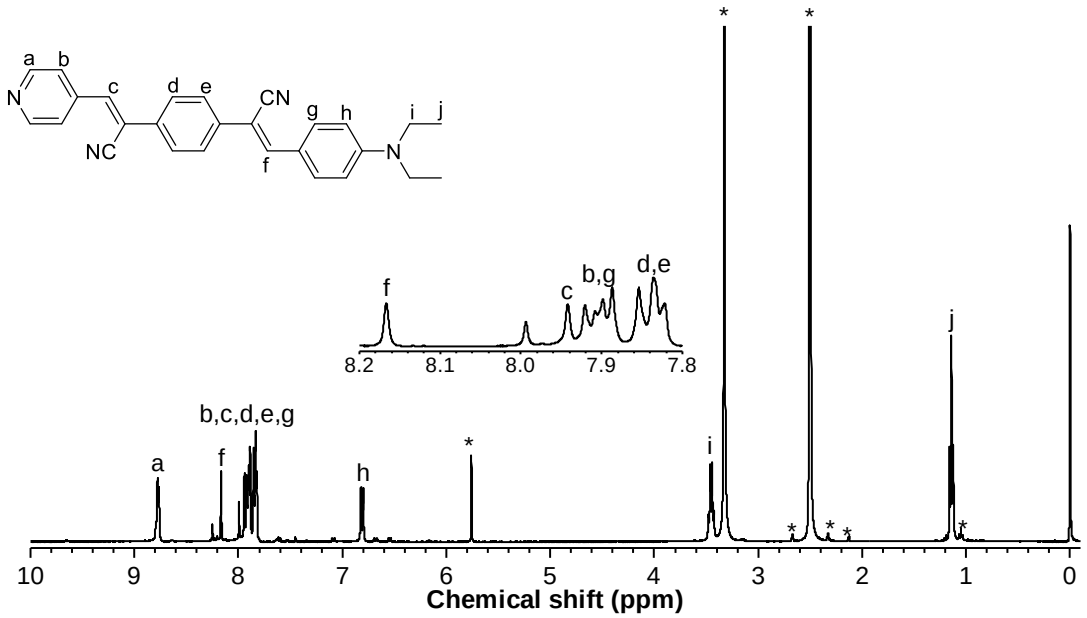

Fig. S21 The ^{1}H NMR spectrum of compound **11** in DMSO-d_6, where the solvent peaks are marked with asterisks.

Monoisotopic Mass, Even Electron Ions
11 formula(e) evaluated with 1 results within limits (up to 50 closest results for each mass)
Elements Used:
C: 0-27 H: 0-99 N: 0-4
J-MEI
MJ-ZSS-020 33 (0.359) Cm (28:33)

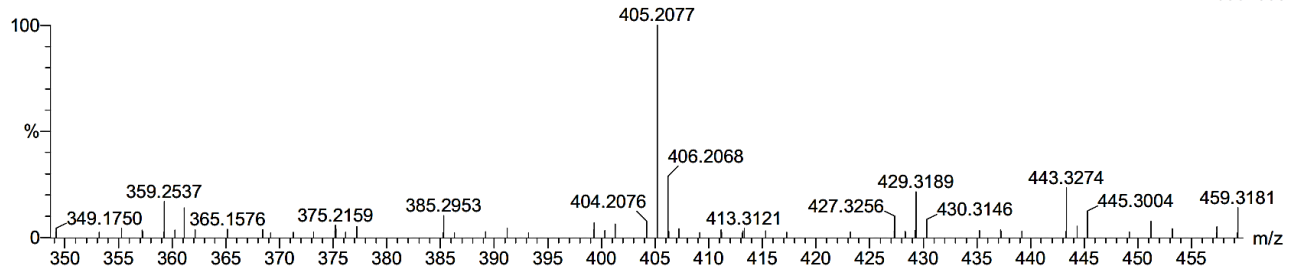

Minimum:				-1.5			
Maximum:		5.0	10.0	50.0			
Mass	Calc. Mass	mDa	PPM	DBE	i-FIT	i-FIT (Norm)	Formula
405.2077	405.2079	-0.2	-0.5	17.5	25.6	0.0	C27 H25 N4

Fig. S22 The HRMS of compound **11**.

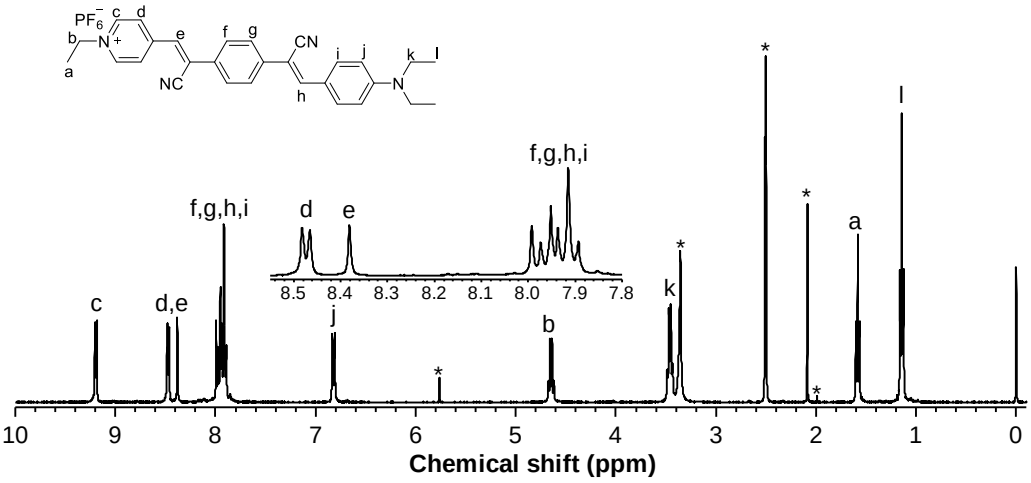

Fig. S23 The ^{1}H NMR spectrum of DEAPF$_6$ in DMSO-d_6, where the solvent peaks are marked with asterisks.

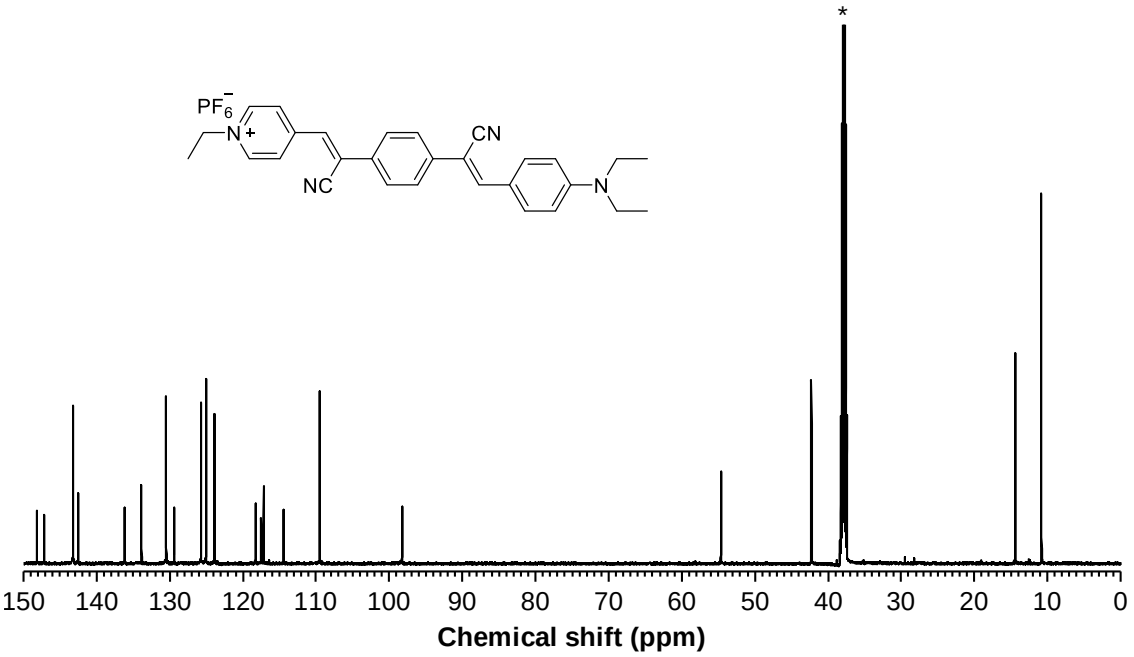

Fig. S24 The ^{13}C NMR spectrum of $DEAPF_6$ in DMSO-d_6, where the solvent peaks are marked with asterisks.

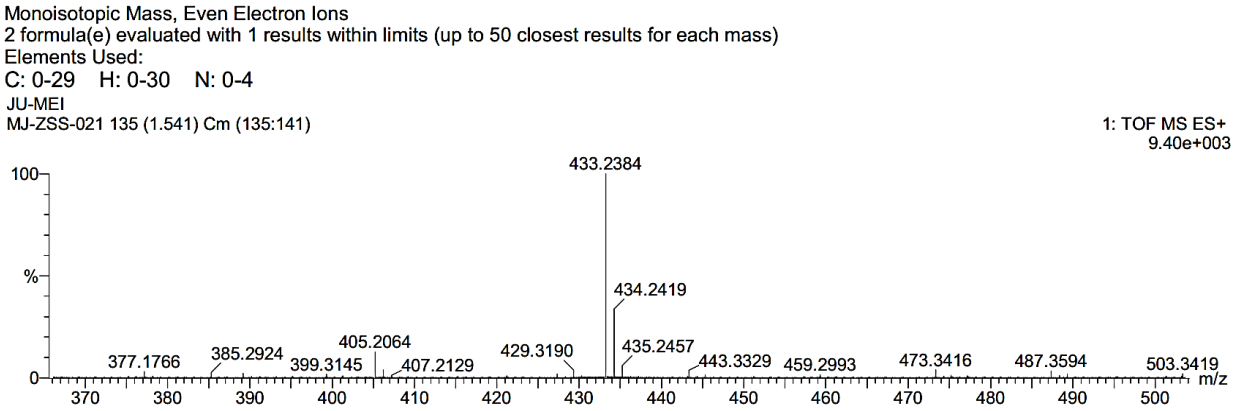

Minimum:				-1.5			
Maximum:		5.0	5.0	50.0			
Mass	Calc. Mass	mDa	PPM	DBE	i-FIT	i-FIT (Norm)	Formula
433.2384	433.2392	-0.8	-1.8	17.5	272.0	0.0	C29 H29 N4

Fig. S25 The HRMS of $DEAPF_6$.

Table S2 Hole-electron analysis parameters of these three photosensitizers at five excited states[a]

		E_{ex} (eV)	D (Å)	S_r	S_m	H (Å)	t (Å)	E_{coul} (eV)	HDI	EDI
$TPEPF_6$	$S_0 \rightarrow S_1$	2.050	11.986	0.30534	0.09953	4.317	8.136	1.512054	5.12	6.60
	$S_0 \rightarrow S_2$	2.812	7.738	0.60481	0.30697	5.237	2.873	2.451043	4.38	6.27
	$S_0 \rightarrow S_3$	2.950	5.782	0.63392	0.33685	4.986	1.255	2.812485	4.86	5.44
	$S_0 \rightarrow S_4$	3.291	14.226	0.22060	0.05766	4.236	10.665	1.157827	5.70	6.54
	$S_0 \rightarrow S_5$	3.359	13.553	0.19937	0.04376	4.237	10.133	1.202698	5.68	6.51
$TPAPF_6$	$S_0 \rightarrow S_1$	1.940	10.812	0.34536	0.10858	4.237	6.948	1.767370	7.49	6.78
	$S_0 \rightarrow S_2$	2.912	5.901	0.72278	0.42849	5.570	0.639	2.868374	5.30	5.26
	$S_0 \rightarrow S_3$	3.095	6.061	0.69455	0.40789	5.397	1.002	2.842617	5.63	5.21
	$S_0 \rightarrow S_4$	3.696	12.207	0.38368	0.15170	4.682	8.023	1.537000	6.31	6.54
	$S_0 \rightarrow S_5$	3.715	10.926	0.38548	0.13406	4.437	6.901	1.767509	5.80	6.35
$DEAPF_6$	$S_0 \rightarrow S_1$	2.060	9.346	0.37655	0.12659	3.968	5.692	2.090274	7.84	7.02
	$S_0 \rightarrow S_2$	3.167	4.534	0.75618	0.46208	5.183	–0.388	3.292498	6.08	5.51
	$S_0 \rightarrow S_3$	3.439	4.378	0.74304	0.45161	5.056	–0.422	3.361627	6.94	5.47
	$S_0 \rightarrow S_4$	3.723	3.652	0.42305	0.14626	2.862	1.368	4.084757	9.62	6.78
	$S_0 \rightarrow S_5$	3.821	9.601	0.24872	0.05906	3.156	7.017	1.872519	9.81	6.38

[a]Abbreviation: E_{ex}: Excitation energy; D: The distance between the centroids of hole and the electron; S_r: The average overlap level of holes and electrons. S_m: The minimum overlap level of holes and electrons. H: The overall average distribution of holes and electrons. t: The degree of separation of holes and electrons; E_{coul}: Coulomb attraction energy between holes and electrons; HDI: Hole delocalization index; EDI: Electron delocalization index.

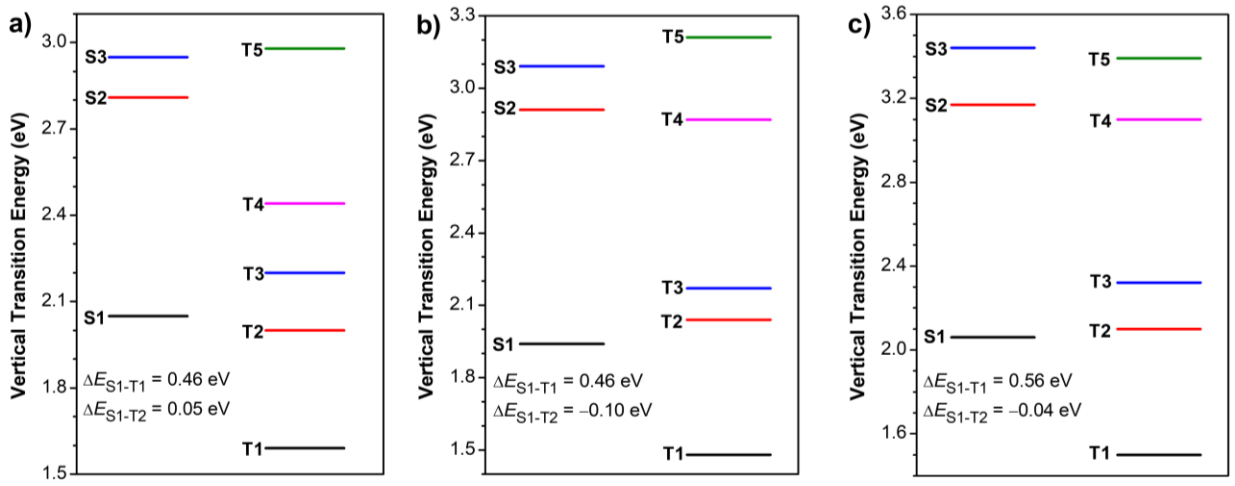

Fig. S26 Singlet (S)- and triplet (T)-state energy levels of a) $TPEPF_6$, b) $TPAPF_6$, and c) $DEAPF_6$.

Table S3 Calculated energy levels of the singlet (*S*) and triplet (*T*) excited states by density functional theory (DFT)[a]

	$TPEPF_6$			$TPAPF_6$			$DEAPF_6$		
n	*S* (eV)	*T* (eV)	$\Delta E_{S1\text{-}Tn}$ (eV)	*S* (eV)	*T* (eV)	$\Delta E_{S1\text{-}Tn}$ (eV)	*S* (eV)	*T* (eV)	$\Delta E_{S1\text{-}Tn}$ (eV)
1	2.05	1.59	0.46	1.94	1.48	0.46	2.06	1.50	0.56
2	2.81	2.00	0.05	2.91	2.04	–0.10	3.17	2.10	–0.04
3	2.95	2.20	–0.15	3.09	2.17	–0.23	3.44	2.32	–0.26
4	3.29	2.44	–0.39	3.70	2.87	–0.93	3.72	3.10	–1.04
5	3.36	2.98	–0.93	3.71	3.21	–1.27	3.82	3.39	–1.33
6	3.38	3.19	–1.14	3.74	3.32	–1.38	3.98	3.59	–1.53

[a] Abbreviation: $\Delta E_{S1\text{-}Tn}$: The energy gaps (ΔE) between the lowest singlet excited state (S_1) and triplet excited state (T_n).

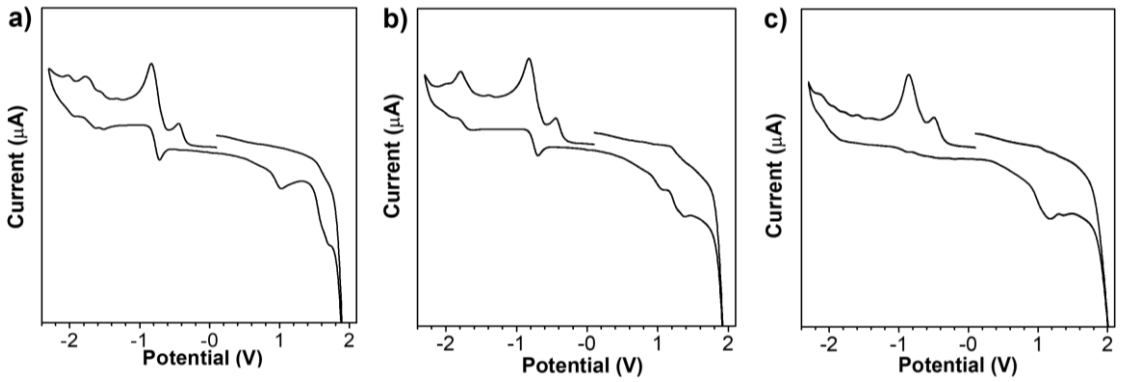

Fig. S27 Cyclic voltammograms (CVs) of a) $TPEPF_6$, b) $TPAPF_6$, and c) $DEAPF_6$ in the *N*,*N*′-dimethylformamide (DMF) solution (c = 10 μM). The CVs were determined by using 0.1 M *n*-Bu_4NPF_6 as the supporting electrolyte, saturated calomel electrode (SCE) as the reference electrode, Pt disk and Pt wire as counter electrodes, and ferrocene was used as internal standard.

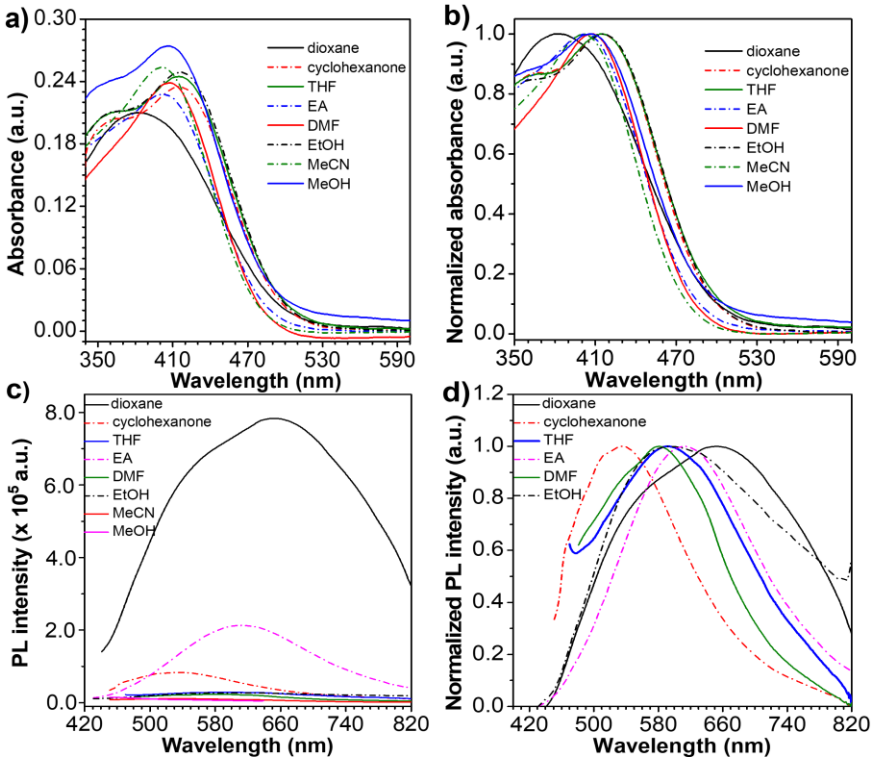

Fig. S28 a) The UV-Vis and b) normalized UV-Vis spectra of $TPEPF_6$ in different solvents with various polarities; c) Fluorescence (FL) spectra and d) normalized FL spectra of $TPEPF_6$ in different solvents with various polarities. c = 10 μM.

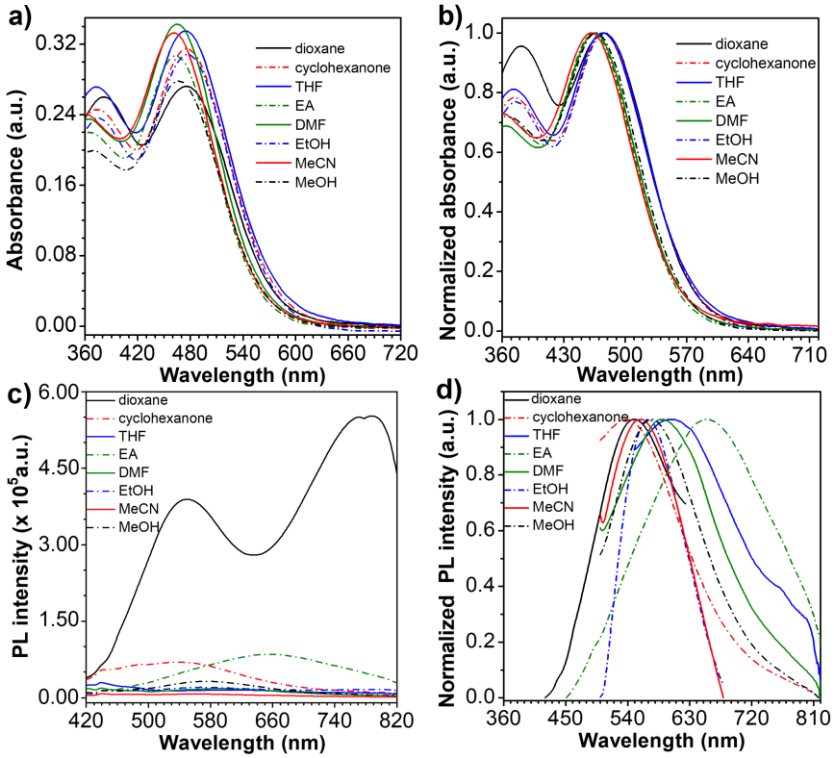

Fig. S29 a) The UV-Vis and b) normalized UV-Vis spectra of $TPAPF_6$ in different solvents with various polarities; c) FL spectra and d) normalized FL spectra of $TPAPF_6$ in different solvents with various polarities. c = 10 μM.

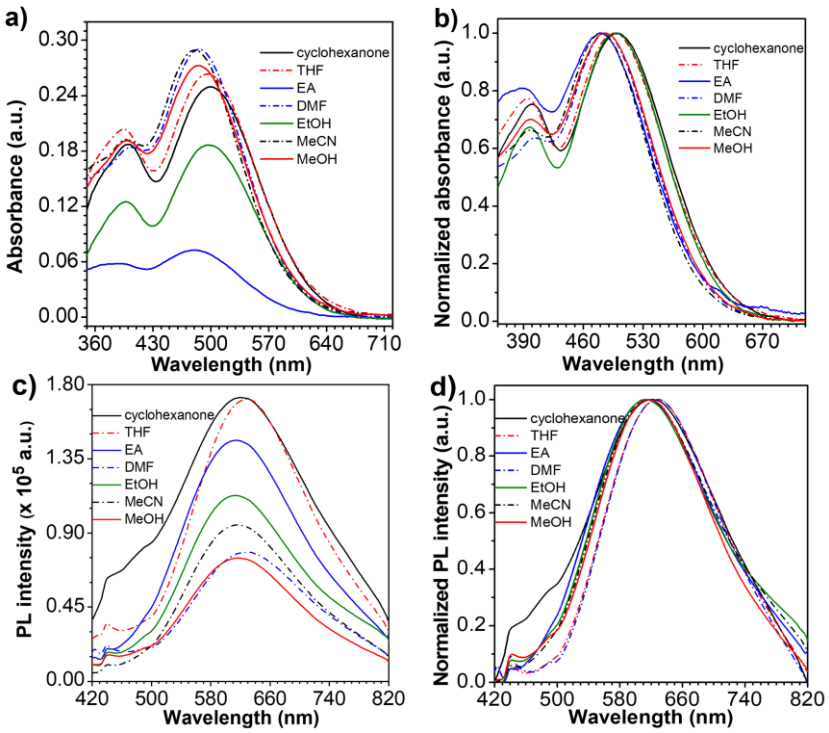

Fig. S30 a) The UV-Vis and b) normalized UV-Vis spectra of $DEAPF_6$ in different solvents with various polarities; c) FL spectra and d) normalized FL spectra of $DEAPF_6$ in different solvents with various polarities; c = 10 μM.

To address the AIE effect in aqueous solution, we have carried out a series of experiments.

Firstly, we used the biocompatible DMSO and water to construct the binary solvent system. In this solvent system, DMSO is supposed to be a good solvent to the AIE-PSs developed in our work and water is supposed to be a relatively poorer solvent. However, as depicted in Fig. S31, the fluorescence of all these three compounds is not monotonously increased with the increase of water fraction (f_w). To figure out the reason for this phenomenon, we carried out the DLS measurements of $TPEPF_6$, $TPAPF_6$ and $DEAPF_6$ in the DMSO/water mixtures with different water fractions (Fig.s S32–S34). It is clearly that the DLS results are well consistent with the fluorescence spectra. In the DMSO/water mixtures with water fractions of 0% and 10%, the particle sizes of all these three compounds cannot be detected by DLS, suggesting their good solubility in DMSO. Moreover, in the DMSO/water mixtures with water fractions of 80%, 90% and 99%, the particle sizes of all these three compounds also cannot be detected by DLS, suggesting their good water miscibility and high solubility in the mixtures of DMSO/water with high water fractions. This is because that the three molecules developed by us all have a π-conjugated skeleton with cationic group, which makes the compounds amphiphilic. Combining the results of fluorescence and DLS measurements, it can be seen that for each compound, the larger aggregate size corresponds to stronger fluorescence, suggesting the AIE properties.

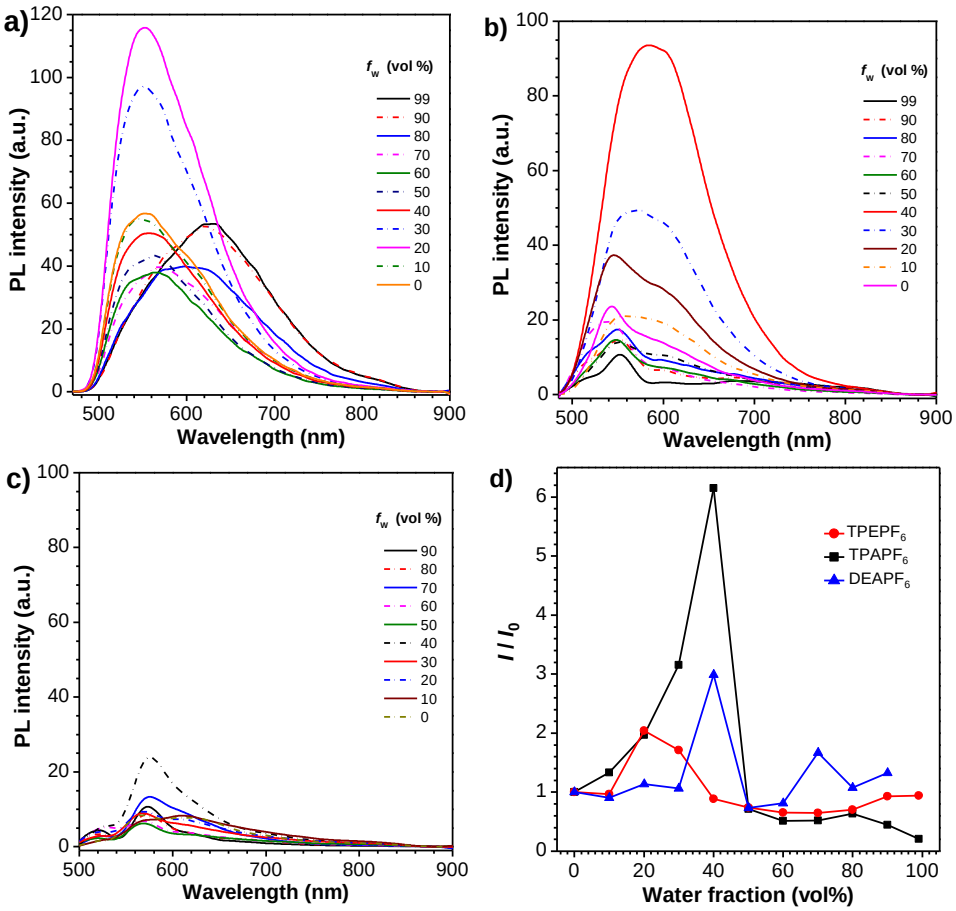

Fig. S31 a), b) and c) The fluorescence spectra of a) $TPEPF_6$, b) $TPAPF_6$ and c) $DEAPF_6$ in the DMSO/water mixtures with different water fractions (f_ws). λ_{ex} = 400 nm for $TPEPF_6$; λ_{ex} = 465 nm for $TPAPF_6$; λ_{ex} = 475 nm for $DEAPF_6$; *c* = 10 μM. d) The plots of I/I_0 of $TPEPF_6$, $TPAPF_6$, and $DEAPF_6$ in the DMSO/water mixtures *versus* the fractions of water.

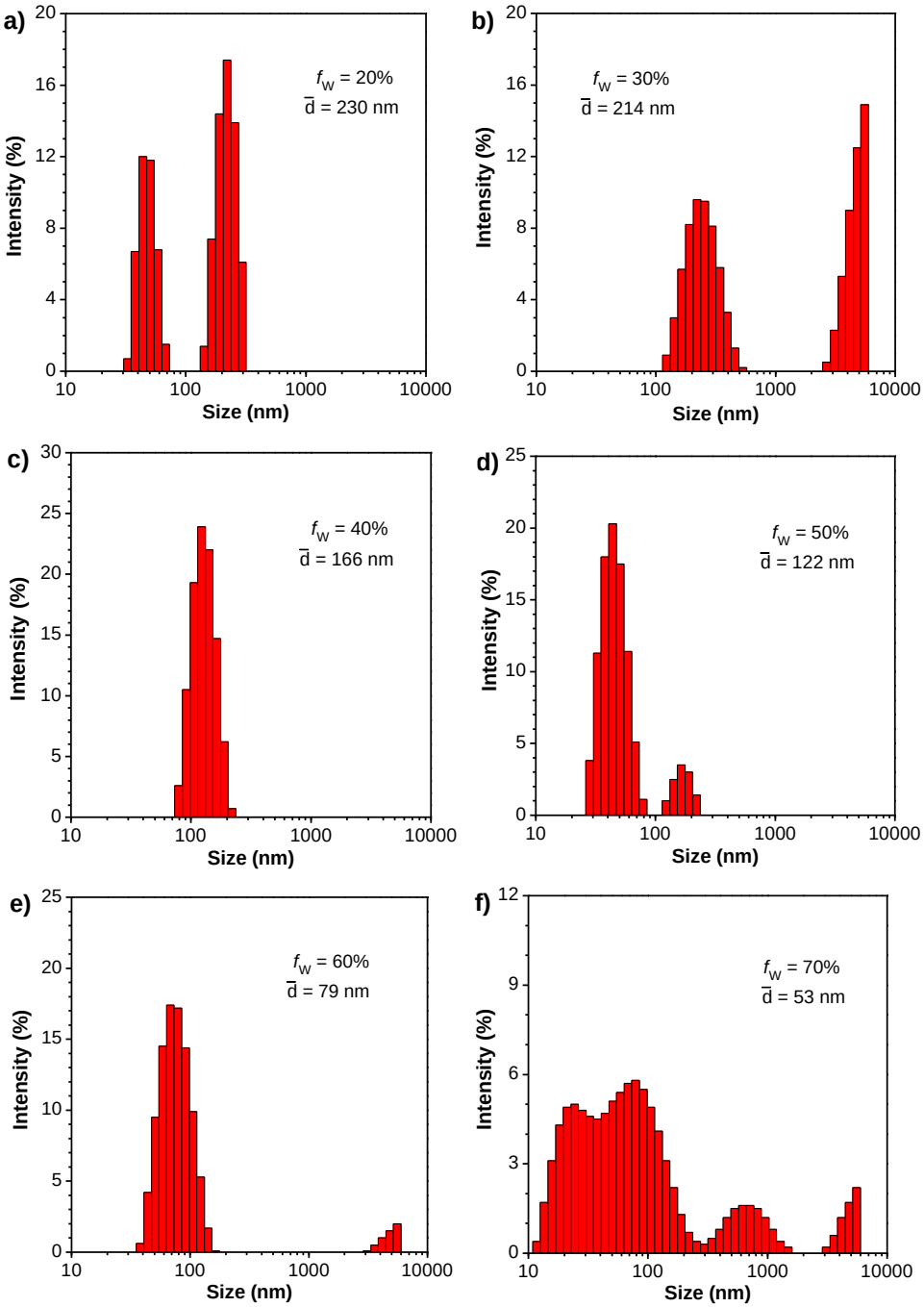

Fig. S32 Size distribution of $TPEPF_6$ in DMSO/water mixtures with different water fractions (f_ws), measured by dynamic light scattering (DLS).

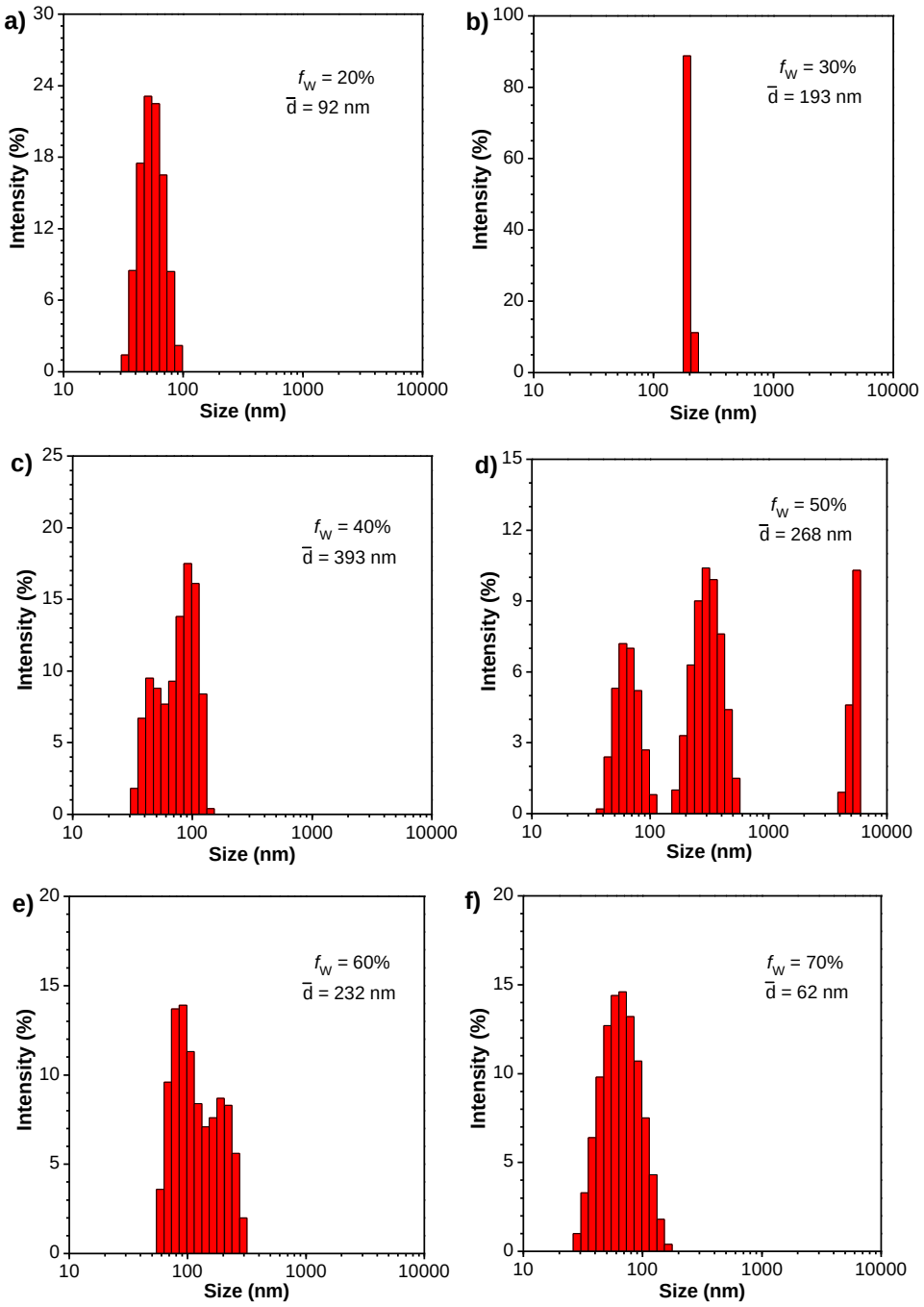

Fig. S33 Size distribution of $TPAPF_6$ in DMSO/water mixtures with different water fractions (f_ws), measured by dynamic light scattering (DLS).

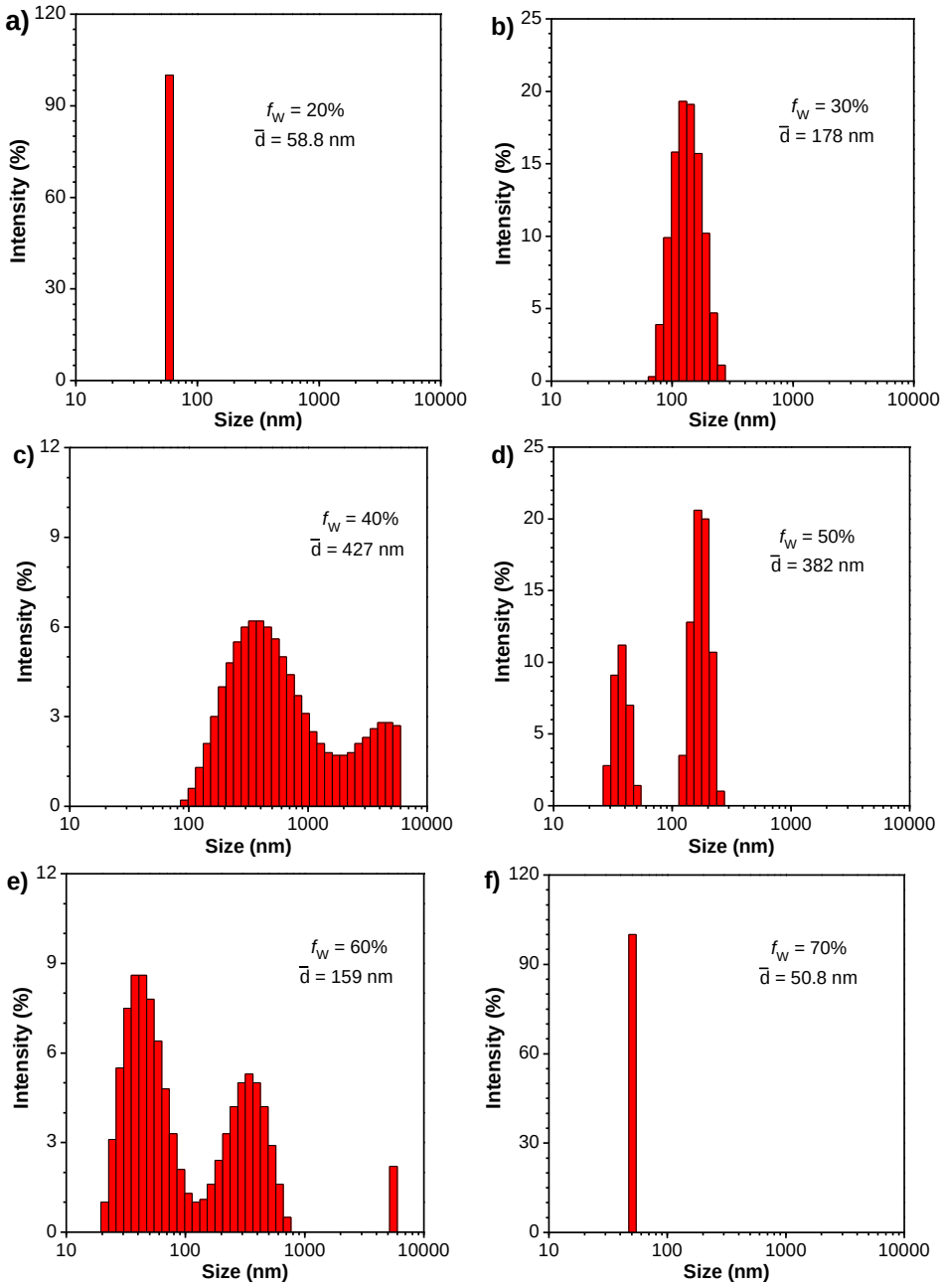

Fig. S34 Size distribution of $DEAPF_6$ in DMSO/water mixtures with different water fractions (f_ws), measured by dynamic light scattering (DLS).

To achieve a more direct demonstration of the AIE properties of our compounds in aqueous solution, we implemented the investigation on the fluorescence behaviors and the size distributions of these three compounds in the mixtures of DMSO/water (v/v = 1/99) with different compound concentrations (10, 20, 40, 60, 80, and 100 μM; Fig.s S35–S40). As we know, high concentration is prone to result in aggregation. As shown in Fig.s S35, S37 and S39, the fluorescence of all these three compounds gets intensified by the increase of compound concentration. Such a phenomenon is proved to be associated with the AIE effect with the aid of the DLS results displayed in Fig.s S36, S38 and S40. It should be noted that at a concentration of 10 or 20 μM ($TPEPF_6$ and $DEAPF_6$) or 10, 20, 40 μM ($TPAPF_6$), the average diameters of all the three compounds in the DMSO/water mixtures (1/99, v/v) cannot be detected by the DLS. While the concentration reaches 40 μM ($TPEPF_6$ and $DEAPF_6$) and 60 μM ($TPAPF_6$), nanoaggregates or even microaggregates are detected. As the compound concentration increases, the average

diameter grows larger, and the fluorescence gets stronger, clearly demonstrating the AIE feature of these compounds.

It thus can be concluded that the AIE properties are the inherent attribute of our PSs.

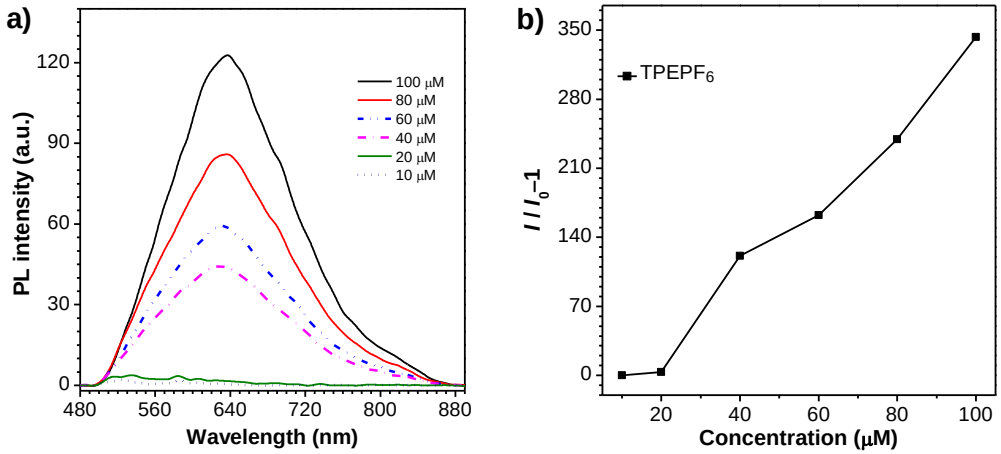

Fig. S35 a) The fluorescence spectra of $TPEPF_6$ in the DMSO/water mixtures (1/99, v/v) with different concentrations of $TPEPF_6$. b) The plot of I/I_0–1 of $TPEPF_6$ in the DMSO/water mixtures (1/99, v/v) *versus* the concentration of $TPEPF_6$.

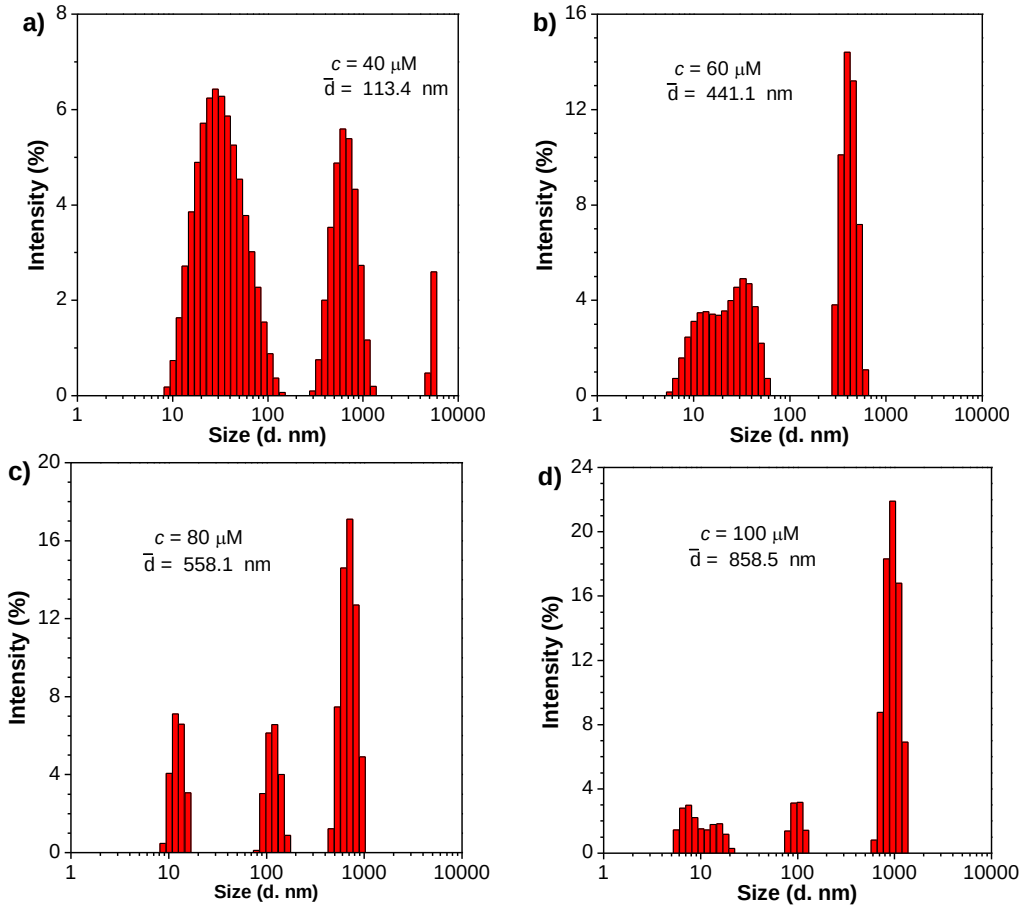

Fig. S36 Size distribution of $TPEPF_6$ in the DMSO/water mixtures (1/99, v/v) with different concentrations of $TPEPF_6$, measured by dynamic light scattering (DLS).

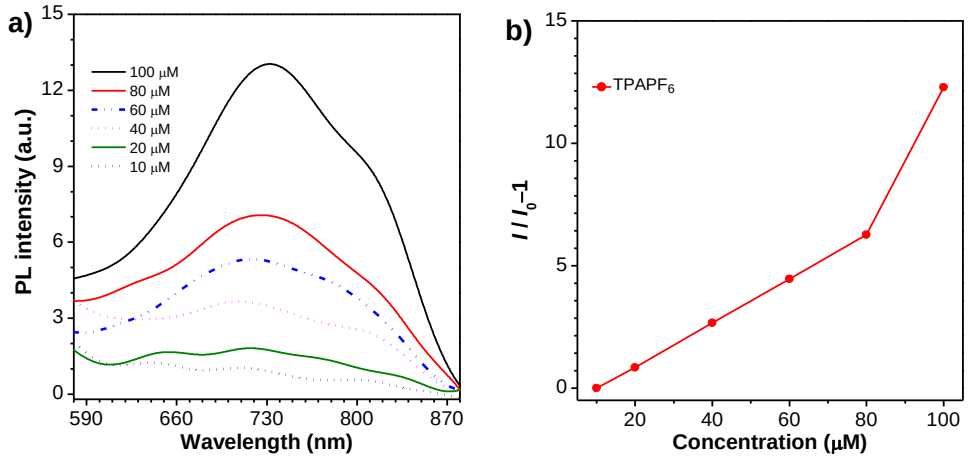

Fig. S37 a) The fluorescence spectra of $TPAPF_6$ in the DMSO/water mixtures (1/99, v/v) with different concentrations of $TPAPF_6$. b) The plot of I/I_0–1 of $TPAPF_6$ in the DMSO/water mixtures (1/99, v/v) *versus* the concentration of $TPAPF_6$.

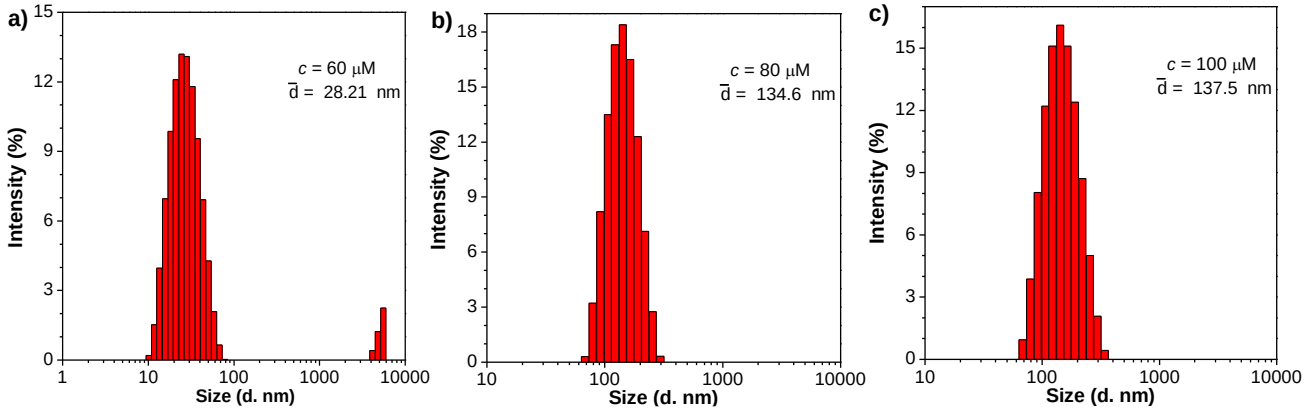

Fig. S38 Size distribution of $TPAPF_6$ in the DMSO/water mixtures (1/99, v/v) with different concentrations of $TPAPF_6$, measured by dynamic light scattering (DLS).

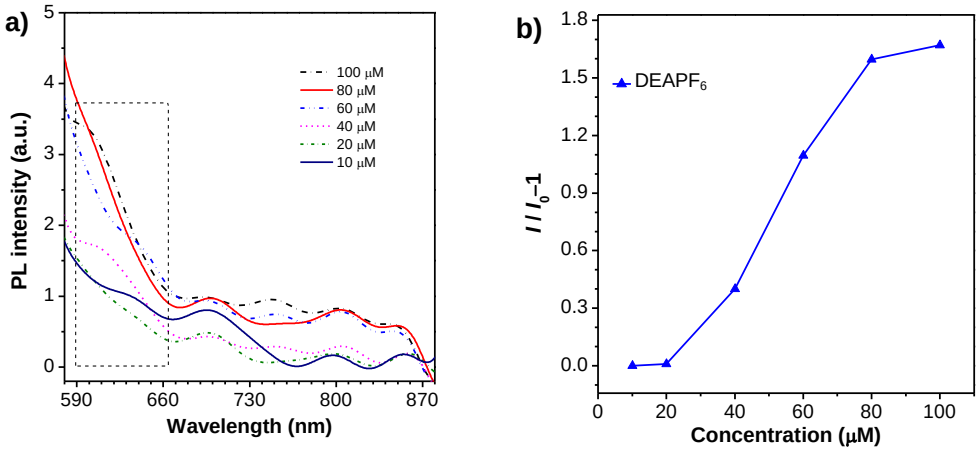

Fig. S39 a) The fluorescence spectra of $DEAPF_6$ in the DMSO/water mixtures (1/99, v/v) with different concentrations of $DEAPF_6$. b) The plots of I/I_0–1 of $DEAPF_6$ in the DMSO/water mixtures (1/99, v/v) *versus* the concentration of $DEAPF_6$.

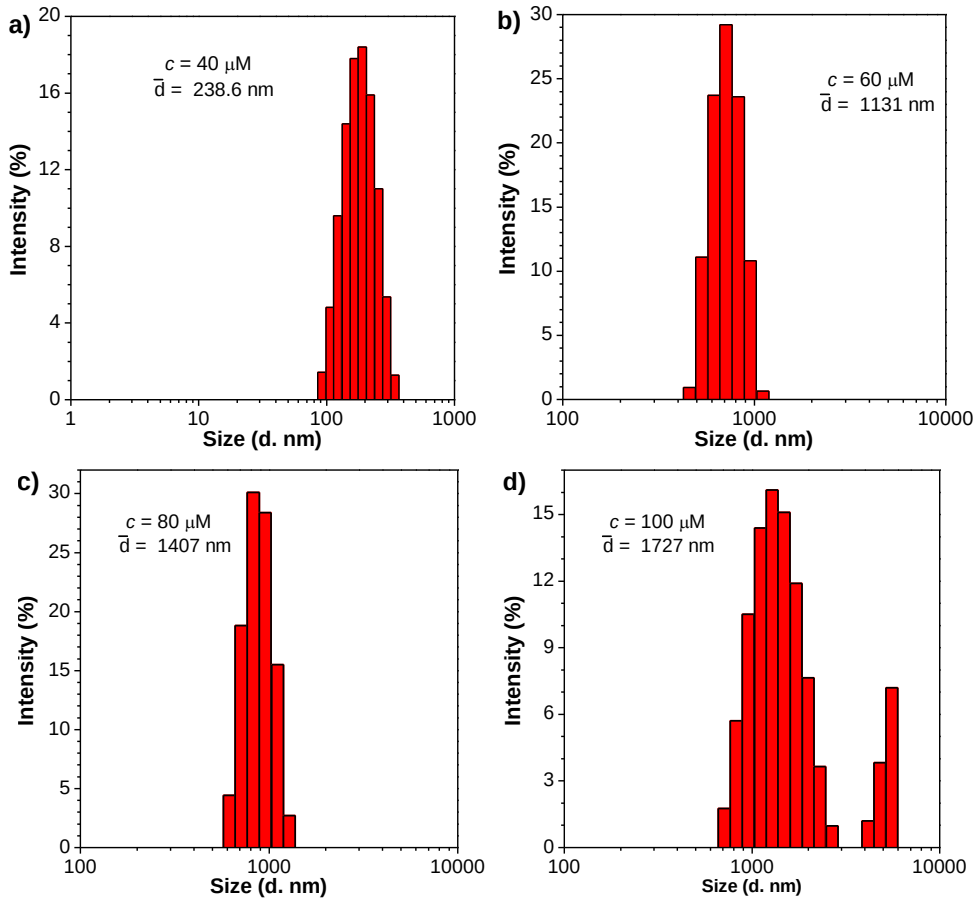

Fig. S40 Size distribution of $DEAPF_6$ in the DMSO/water mixtures (1/99, v/v) with different concentrations of $DEAPF_6$, measured by dynamic light scattering (DLS).

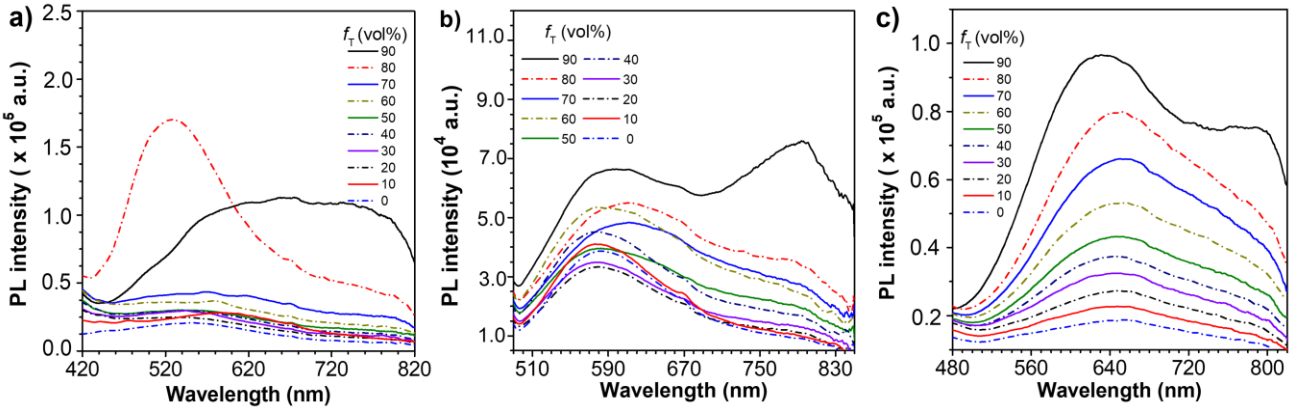

Fig. S41 FL spectra of a) $TPEPF_6$, b) $TPAPF_6$ and c) $DEAPF_6$ in the DMSO/toluene mixtures with different toluene fractions (f_Ts). λ_{ex} = 400 nm for $TPEPF_6$; λ_{ex} = 465 nm for $TPAPF_6$; λ_{ex} = 475 nm for $DEAPF_6$; c = 10 μM.

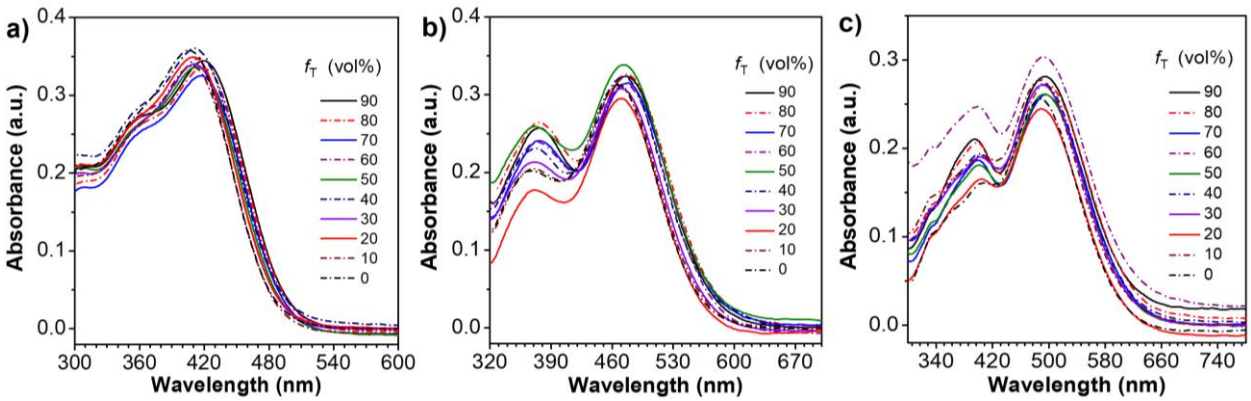

Fig. S42 The UV-Vis spectra of a) $TPEPF_6$, b) $TPAPF_6$, and c) $DEAPF_6$ in the DMSO/toluene mixtures with different toluene fractions (f_Ts), c = 10 μM.

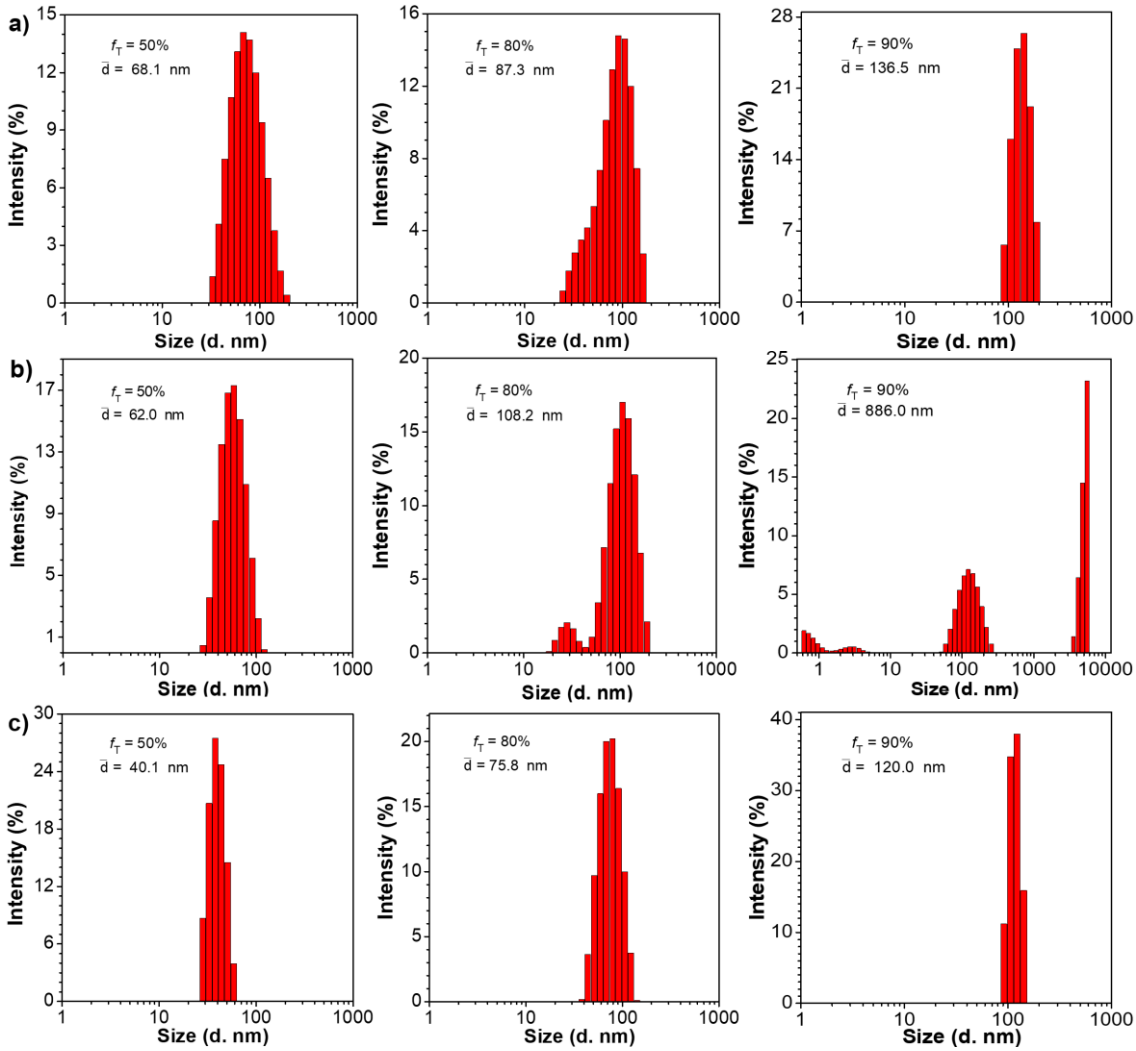

Fig. S43 Size distribution of a) $TPEPF_6$, b) $TPAPF_6$, and c) $DEAPF_6$ in DMSO/toluene with different toluene fractions (f_Ts), measured by dynamic light scattering (DLS).

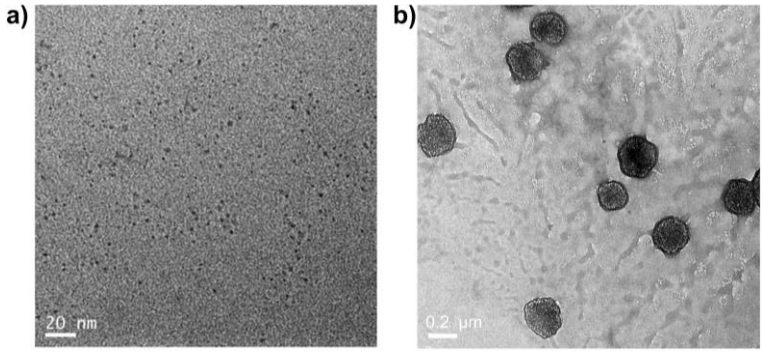

Fig. S44 TEM images of $TPEPF_6$ in DMSO/toluene with different toluene fractions (f_Ts). a) f_T = 80 vol%, b) f_T = 90 vol%.

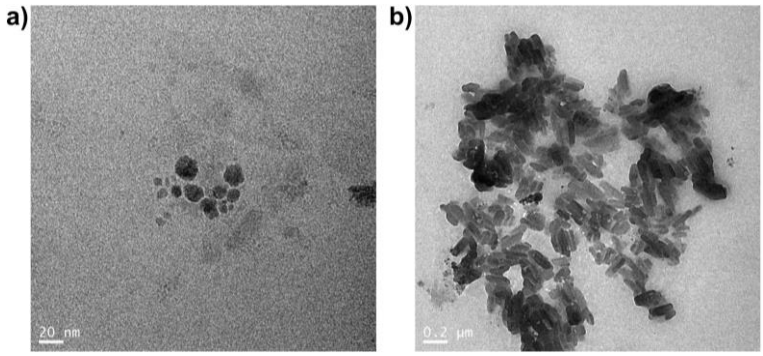

Fig. S45 TEM images of $TPAPF_6$ in DMSO/toluene with different toluene fractions (f_Ts). a) f_T = 80 vol%, b) f_T = 90 vol%.

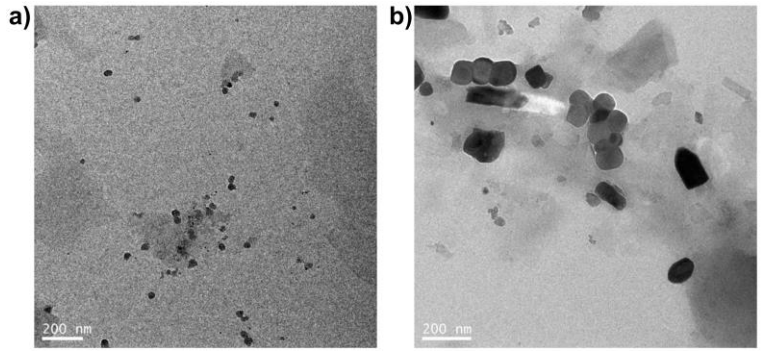

Fig. S46 TEM images of $DEAPF_6$ in DMSO/toluene with different toluene fractions (f_Ts). a) f_T = 80 vol%, b) f_T = 90 vol%.

The average hydrodynamic diameters of the aggregates formed by $TPEPF_6$, $TPAPF_6$, and $DEAPF_6$ in the mixtures of DMSO/toluene (v/v, 1/9) are about 137, 886, and 120 nm, respectively, as indicated by DLS (Fig. S33). Obvious aggregate formation can be clearly seen in TEM images (Fig. S34–S36), which is in good agreement with the DLS data.

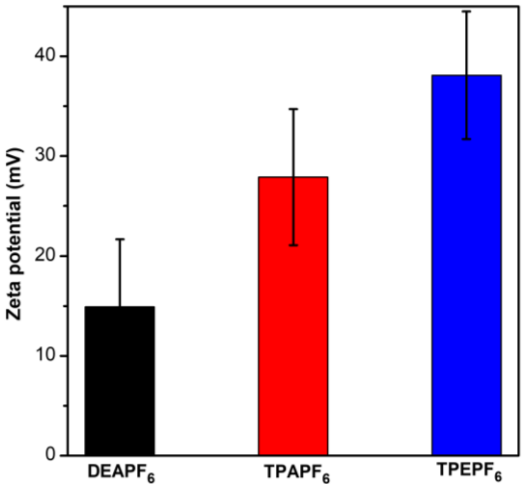

Fig. S47 Zeta potential of $TPEPF_6$, $TPAPF_6$ and $DEAPF_6$ characterized by DLS in aqueous solution (containing 1 vol% DMSO).

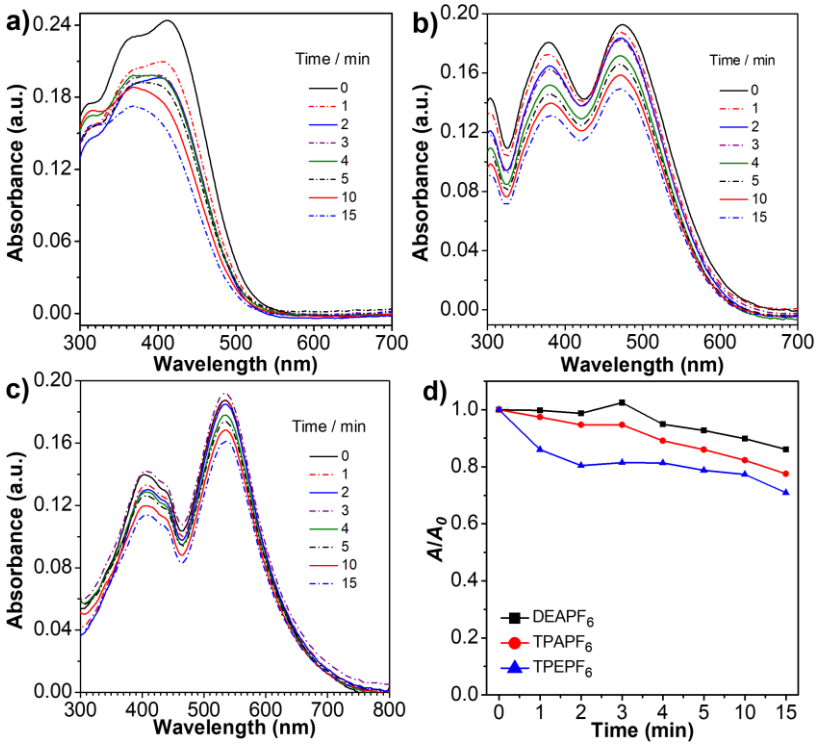

Fig. S48 UV-Vis absorption spectra of a) $TPEPF_6$, b) $TPAPF_6$ and c) $DEAPF_6$ after being irradiated for different time by white light (25 mW/cm^2). d) Plots of the relative absorbance of these three AIE-PSs under white-light irradiation, where A_0 and A is the absorbance before and after light irradiation, respectively.

Table S4 Crystal data and structure refinement for $TPAPF_6$.

Compound name	$TPAPF_6$	
CCDC number	No. 2165738	
Empirical formula	$C_{38.50}H_{37}F_6N_{6.50}OP$	
Formula weight	751.71	
Temperature	296 K	
Wavelength	1.54178 Å	
Crystal system	Triclinic	
Space group	P-1	
Cell parameters	a = 13.844(3) Å	α = 83.878(14)°
	b = 14.078(3) Å	β = 87.451(14)°
	c = 20.216(5) Å	γ = 75.021(14)°
Volume	3783.8(16) $Å^3$	
Z	4	
Density (calculated)	1.320 mg/m^3	
Absorption coefficient	1.246 mm^{-1}	
F(000)	1562.0	
Crystal size	0.4× 0.2 × 0.1 mm^3	
Theta range for data collection	3.3 to 67.4°	
Index ranges	–16<=h<=16, –16<=k<=16, –23<=l<=23	
Reflections collected	12711	
Independent reflections	12711 [R(int) = 0.058]	
Completeness of data	98.6 %	
Absorption correction	Multi-scan (θ_{max} = 65.1°, θ_{min} = 2.2°)	
Max. and min. transmission	0.633 and 0.753	
Refinement method	Full-matrix least-squares on F^2	
Final R indices [I>2sigma(I)]	R = 0.0999, wR2 = 0.0.3054	
Largest diff. peak and hole	0.55 and −0.43 e. $Å^{-3}$	

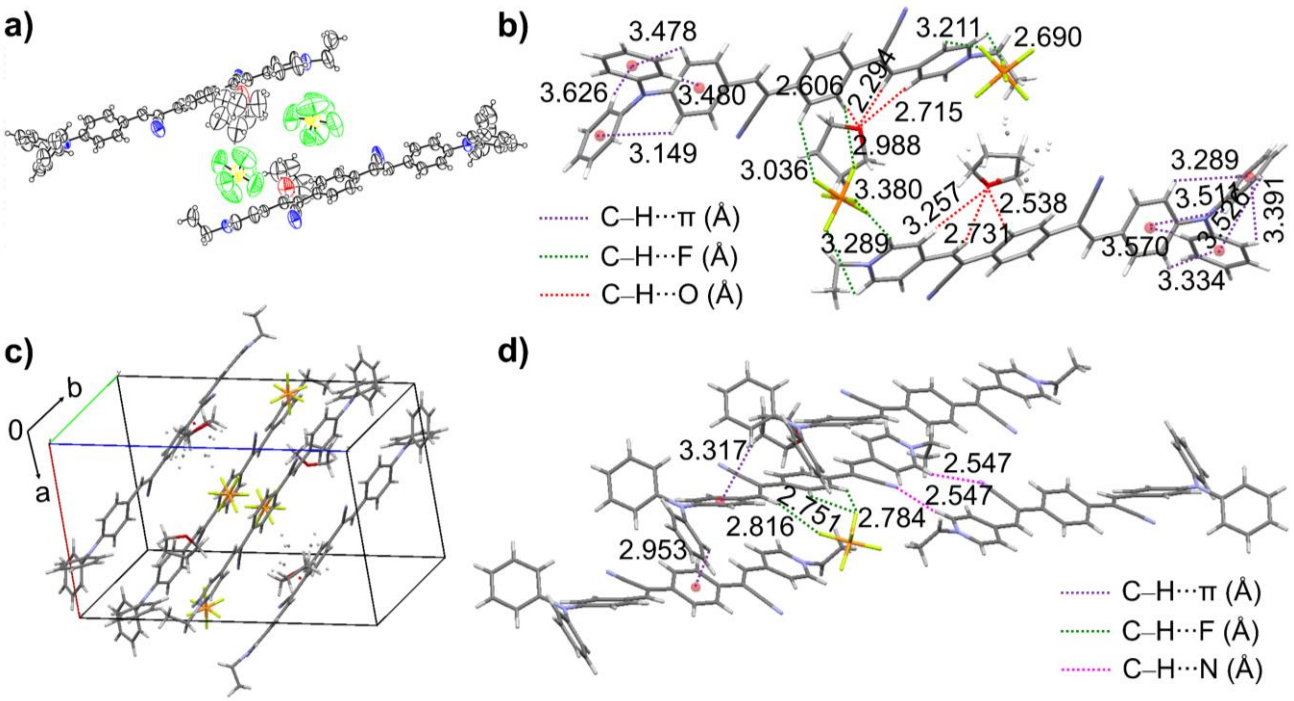

Fig. S49 a) The ORTEP of $TPAPF_6$ determined by the X-ray crystallography; b) The intramolecular interactions in the molecules of $TPAPF_6$ and the short contacts between the molecules of $TPAPF_6$ and the tetrahydrofuran (THF); c) Molecular packing of $TPAPF_6$ in a single crystal cell; d) The intermolecular short contacts of between the neighboring $TPAPF_6$ molecules. The data have been deposited at the Cambridge Crystallography Data Centre with the CCDC number of 2165738.

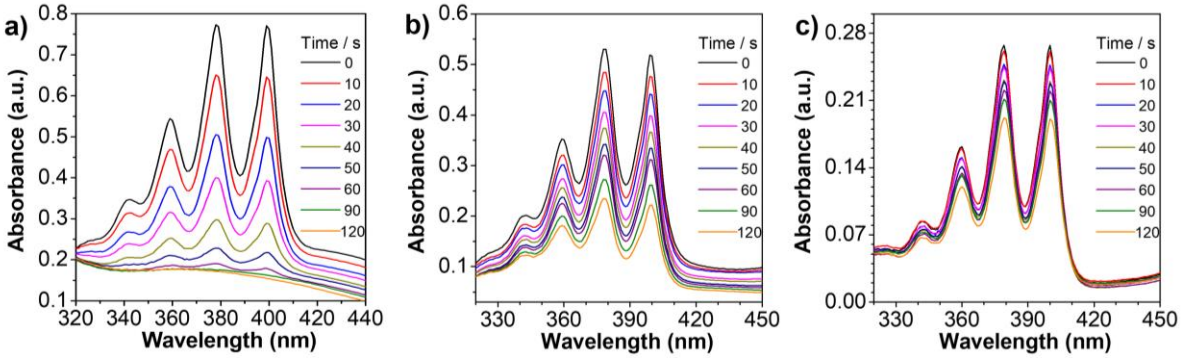

Fig. S50 UV-Vis spectra of ABDA in the presence of a) $TPEPF_6$, b) $DEAPF_6$, or c) Rose Bengal, after being irradiated for different time by white light (25 mW/cm^2) in the mixture of DMSO/water (v/v = 1/100). [ABDA] = 5×[PS]. To avoid the inner-filter effect, the absorption maxima of the PSs were adjusted to about 0.2 OD, and the corresponding concentrations were applied for the measurements.

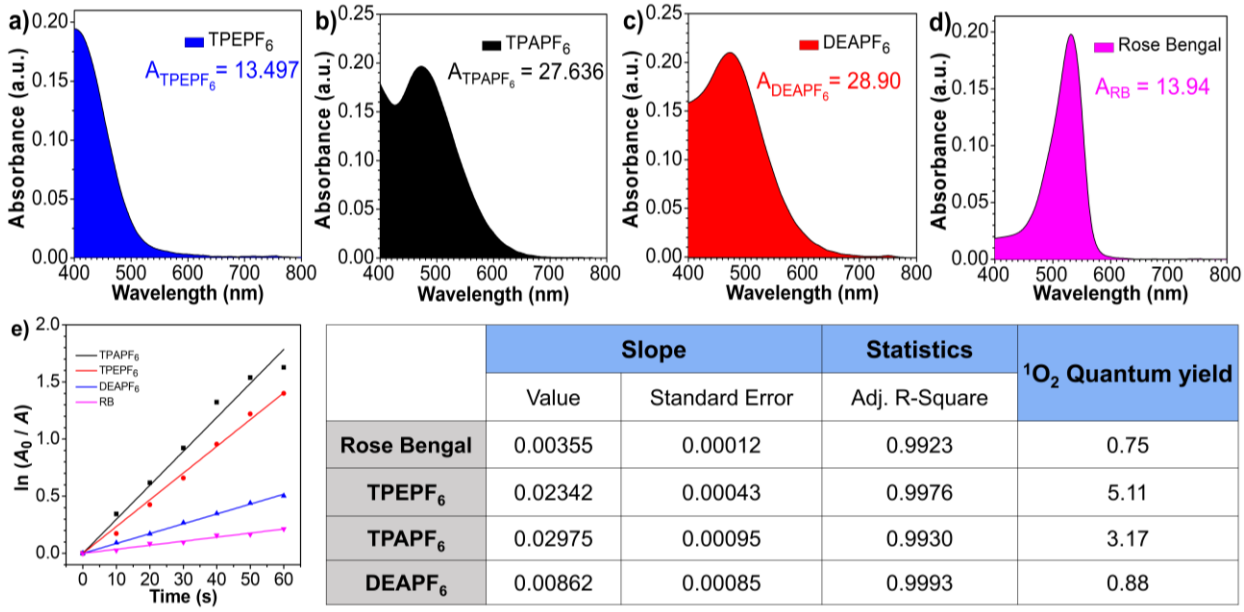

	Slope		Statistics	$^1O_2$ Quantum yield
	Value	Standard Error	Adj. R-Square	
Rose Bengal	0.00355	0.00012	0.9923	0.75
$TPEPF_6$	0.02342	0.00043	0.9976	5.11
$TPAPF_6$	0.02975	0.00095	0.9930	3.17
$DEAPF_6$	0.00862	0.00085	0.9993	0.88

Fig. S51 The absorption spectra of a) $TPEPF_6$, b) $TPAPF_6$, c) $DEAPF_6$, and d) Rose Bengal in the range of 400–800 nm. e) Time-dependent $^1O_2$ generation kinetics deduced from the decomposition rates of ABDA in the presence of different PSs under white-light irradiation in the mixture of DMSO/water (v/v = 1/100). A_0 = absorption of ABDA at 378 nm without light irradiation. A = real-time absorbance of ABDA at 378 nm at different irradiation time. [ABDA] = 5×[PS]. Light power density = 25 mW/cm^2. The table shows the optical parameters of these photosensitizers calculated according to ln (A_0/A).

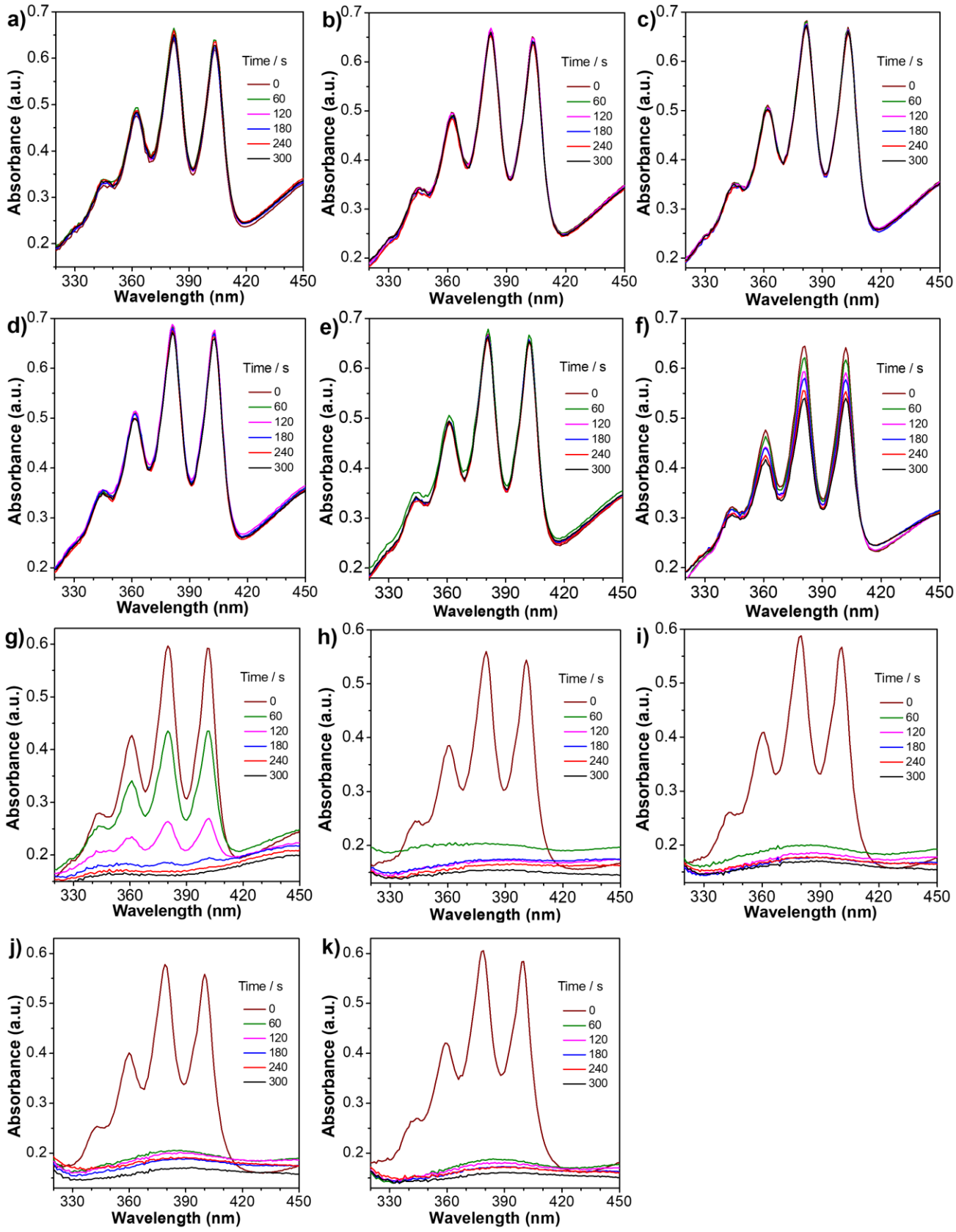

Fig. S52 UV-Vis spectra of ABDA in the presence of $TPAPF_6$ (1×10^{-5} M) in the DMSO/water mixture with a water fraction of a) 0, b) 10 vol%, c) 20 vol%, d) 30 vol %, e) 40 vol %, f) 50 vol %, g) 60 vol %, h) 70 vol %, i) 80 vol %, j) 90 vol %, and k) 98 vol % under white-light irradiation.

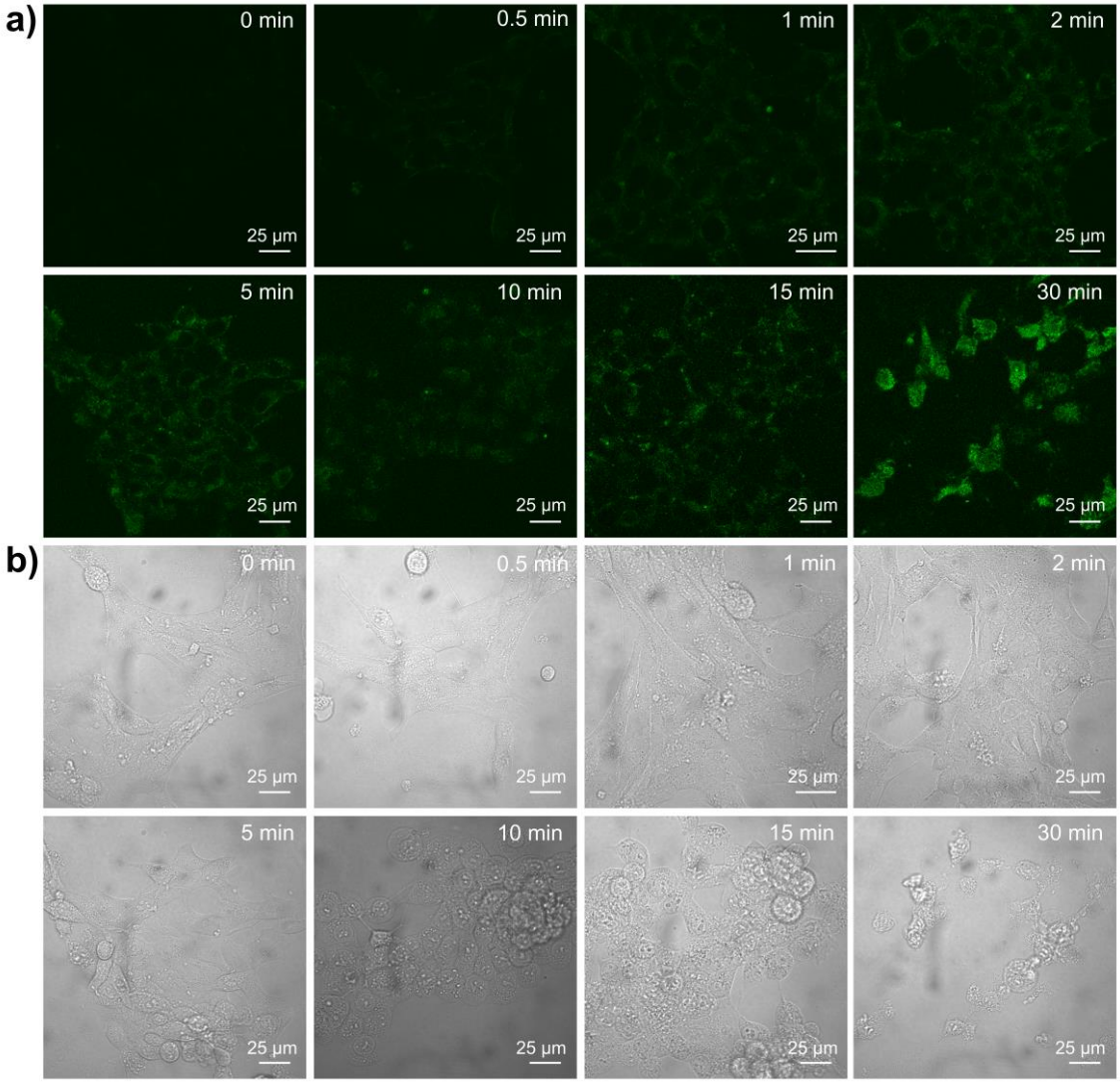

Fig. S53 Detection of intracellular $^1O_2$ by SOSG staining in 4T1 cells incubated with $TPEPF_6$. a) Fluorescence and b) bright-field images of different irradiation time; SOSG, λ_{ex} = 488 nm, λ_{em} = 500–530 nm; [SOSG] = 5 μM.

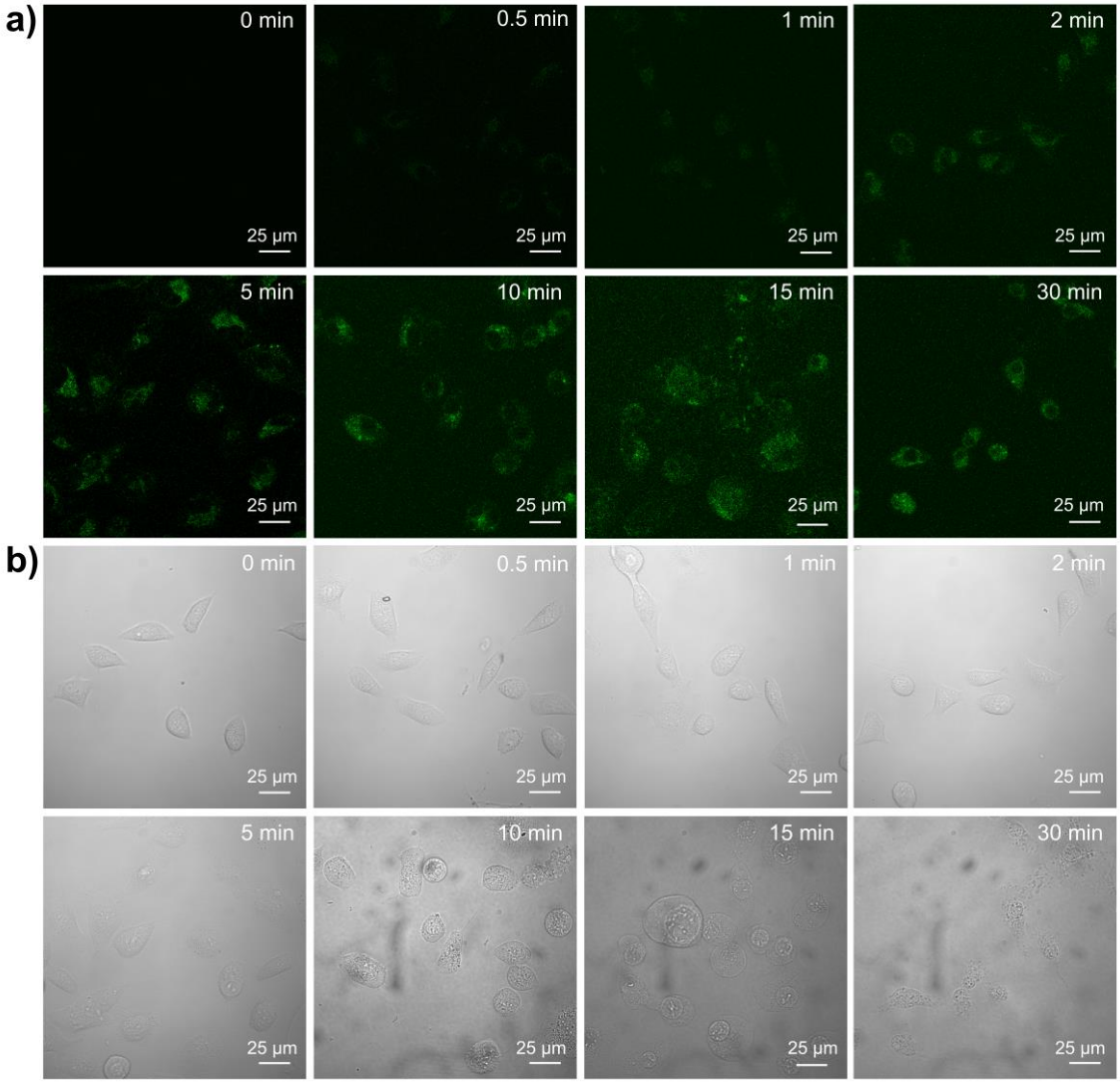

Fig. S54 Detection of intracellular $^1O_2$ by SOSG staining in SK-OV-3 cells incubated with $TPEPF_6$. a) Fluorescence and b) bright-field images of different irradiation time; SOSG, λ_{ex} = 488 nm, λ_{em} = 500–530 nm; [SOSG] = 5 μM.

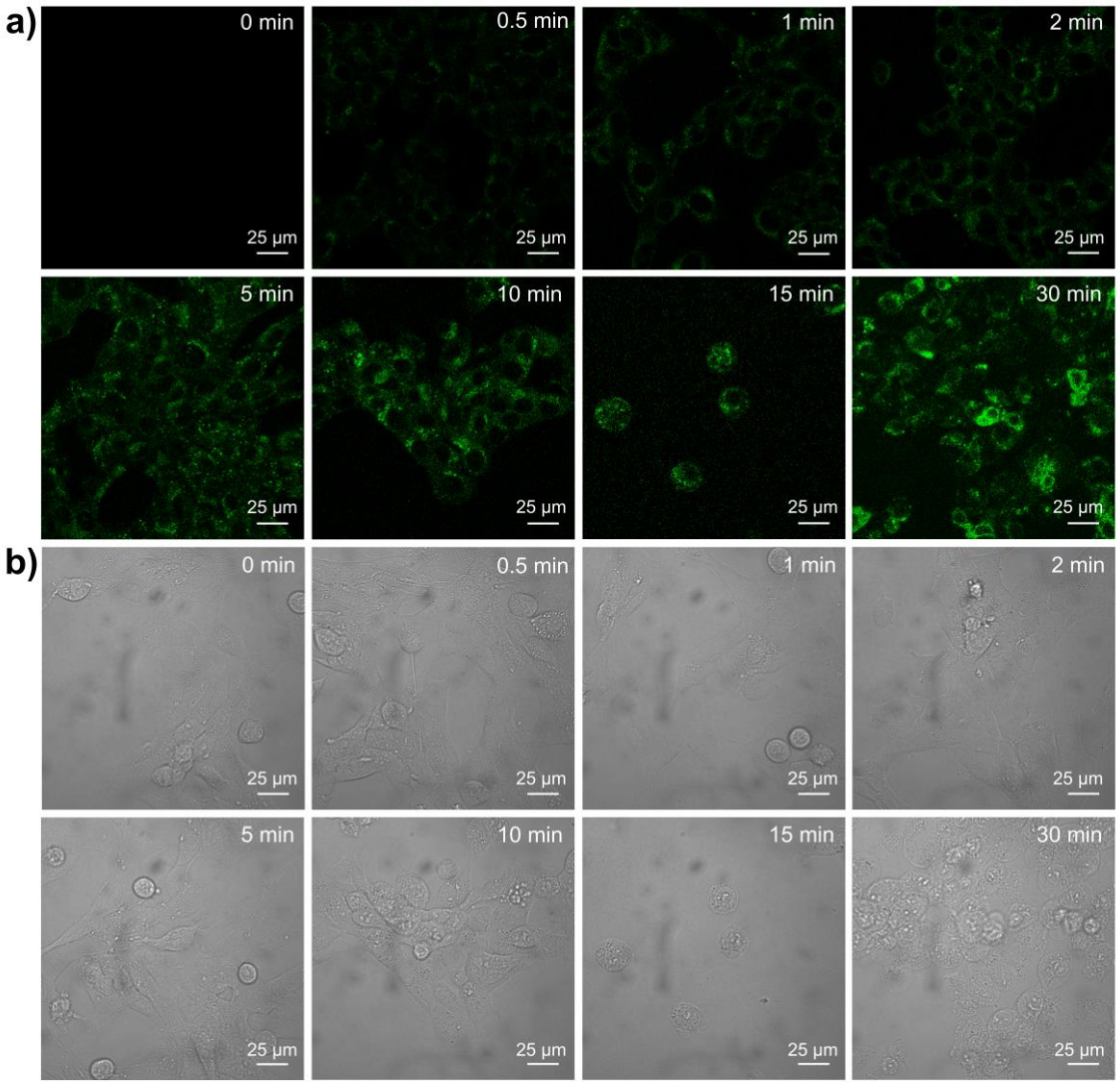

Fig. S55 Detection of intracellular $^1O_2$ by SOSG staining in 4T1 cells incubated with $TPAPF_6$. a) Fluorescence and b) bright-field images of different irradiation time; SOSG, λ_{ex} = 488 nm, λ_{em} = 500–530 nm; [SOSG] = 5 μM.

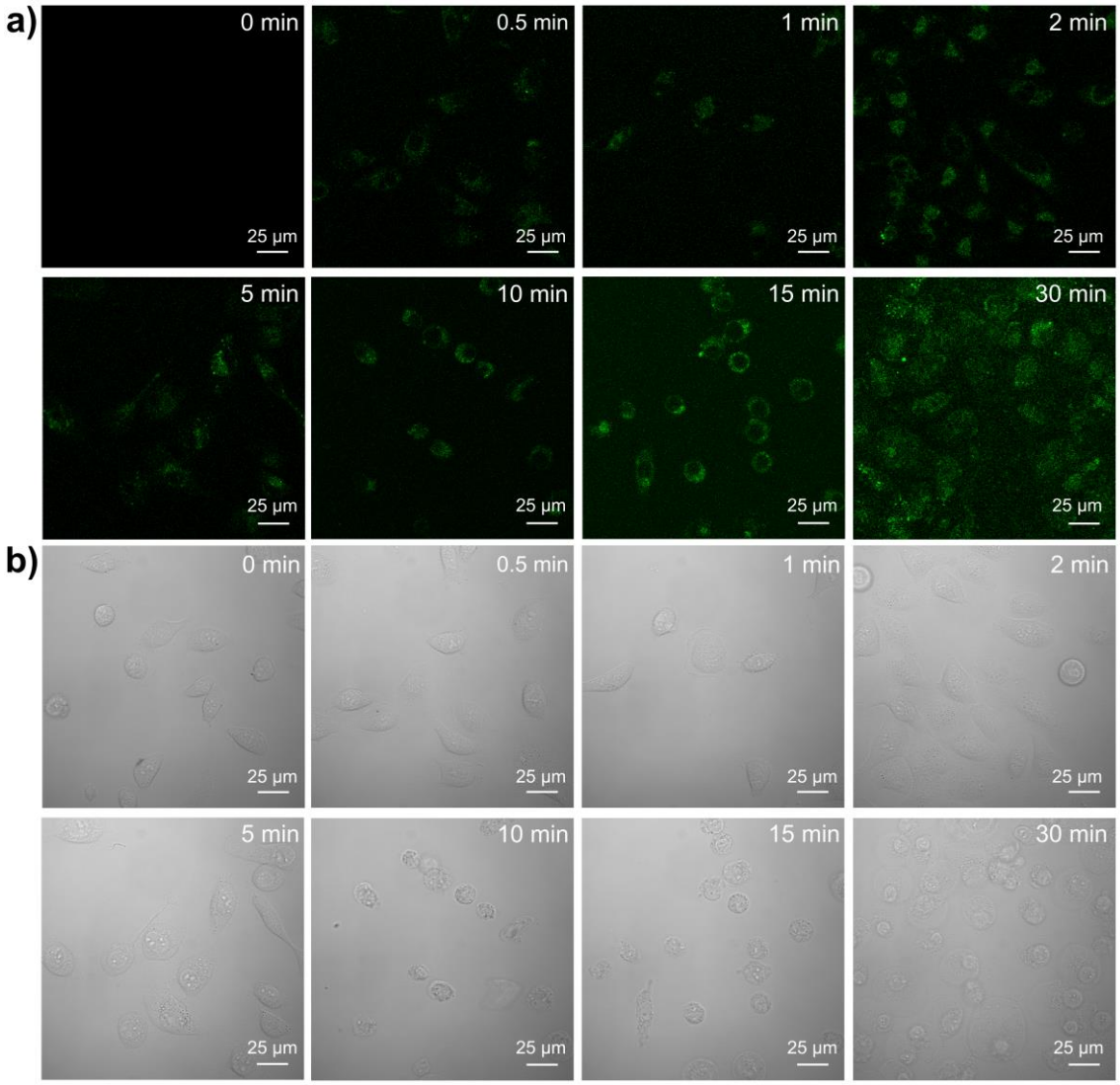

Fig. S56 a) Detection of intracellular $^1O_2$ by SOSG staining in SK-OV-3 cells incubated with $TPAPF_6$. a) Fluorescence and b) bright-field images of different irradiation time; SOSG, λ_{ex} = 488 nm, λ_{em} = 500–530 nm; [SOSG] = 5 μM.

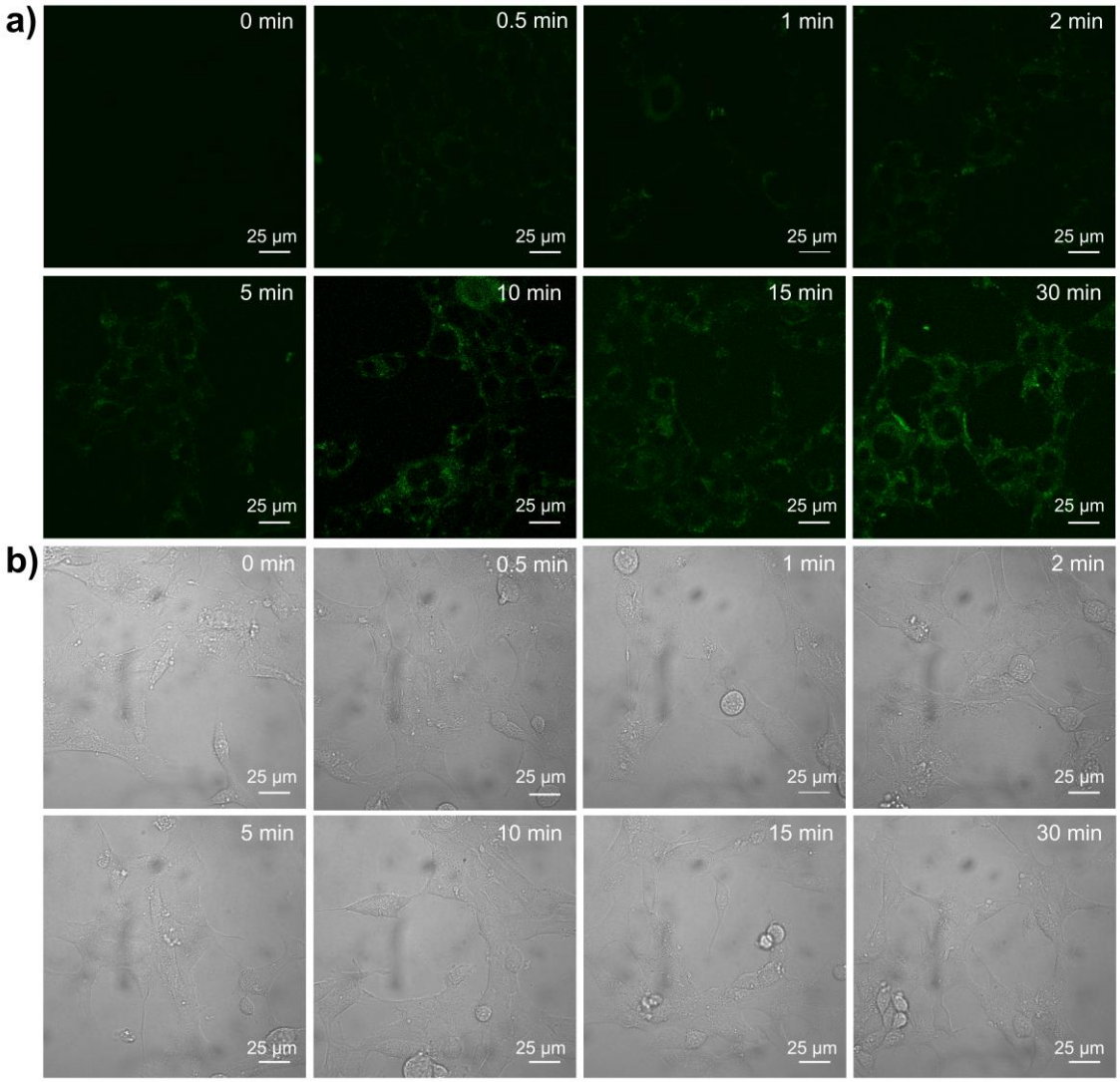

Fig. S57 Detection of intracellular $^1O_2$ by SOSG staining in 4T1 cells incubated with $DEAPF_6$. a) Fluorescence and b) bright-field images of different irradiation time; SOSG, λ_{ex} = 488 nm, λ_{em} = 500–530 nm; [SOSG] = 5 μM.

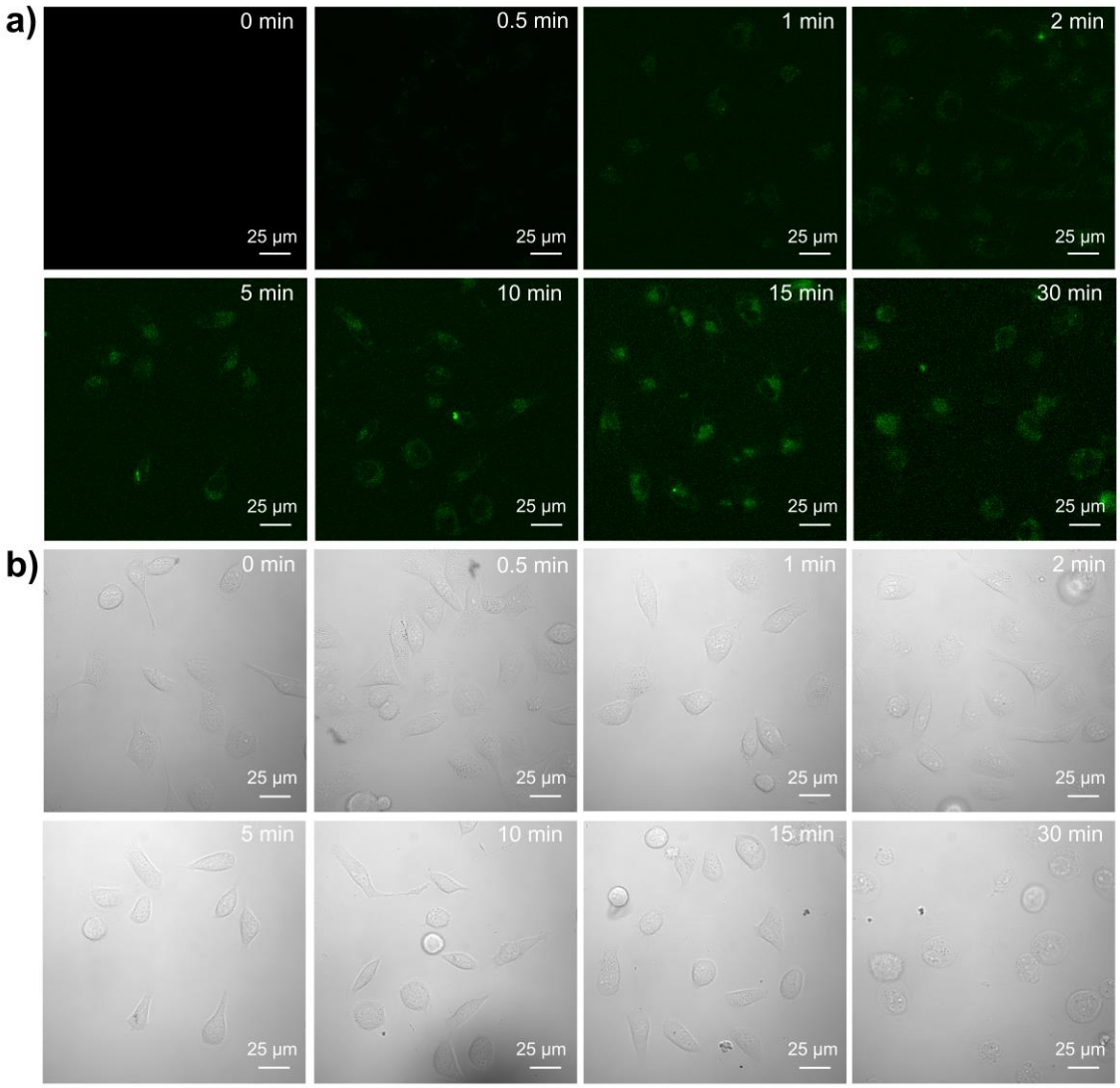

Fig. S58 Detection of intracellular $^1O_2$ by SOSG staining in SK-OV-3 cells incubated with $DEAPF_6$. a) Fluorescence and b) bright-field images of different irradiation time; SOSG, λ_{ex} = 488 nm, λ_{em} = 500–530 nm; [SOSG] = 5 μM.

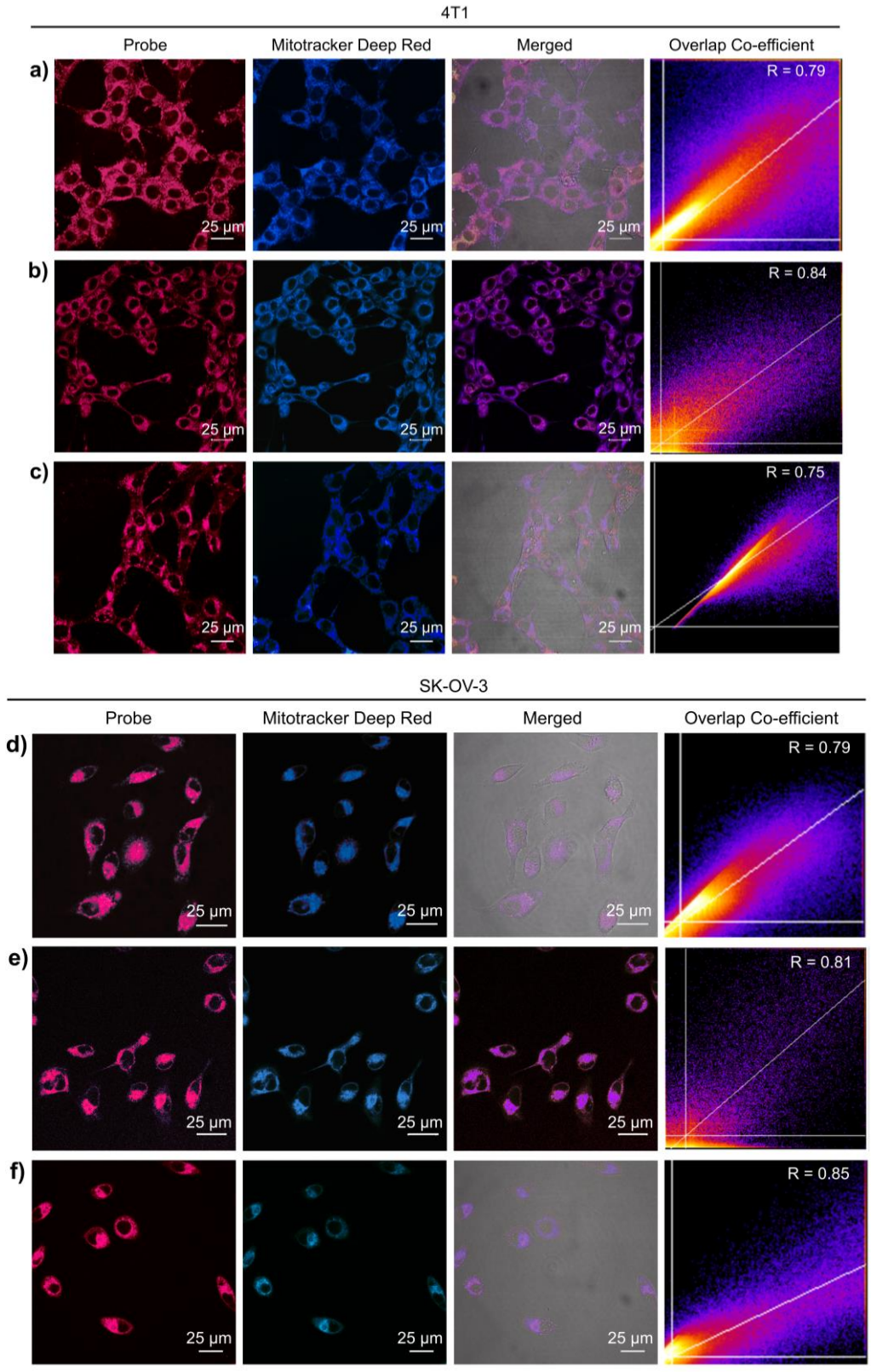

Fig. S59 Co-localization and overlapping coefficients assessed by the Pearson's correlation coefficient (R) of 4T1 and SK-OV-3 cells pre-incubated with MitoTracker® Deep Red FM and then further incubated with 10 μM of a), d) $TPEPF_6$, or b), e) $TPAPF_6$, or c), f) $DEAPF_6$ for 1 h, respectively. MitoTracker® Deep Red FM, λ_{ex} = 647 nm, λ_{em} = 655–675 nm; $TPEPF_6$, λ_{ex} = 405 nm, λ_{em} = 570–630 nm; $TPAPF_6$ and $DEAPF_6$, λ_{ex} = 488 nm, λ_{em} = 670–730 nm; [MitoTracker® Deep Red FM] = 250 nM; [AIE-PSs] = 10 μM.

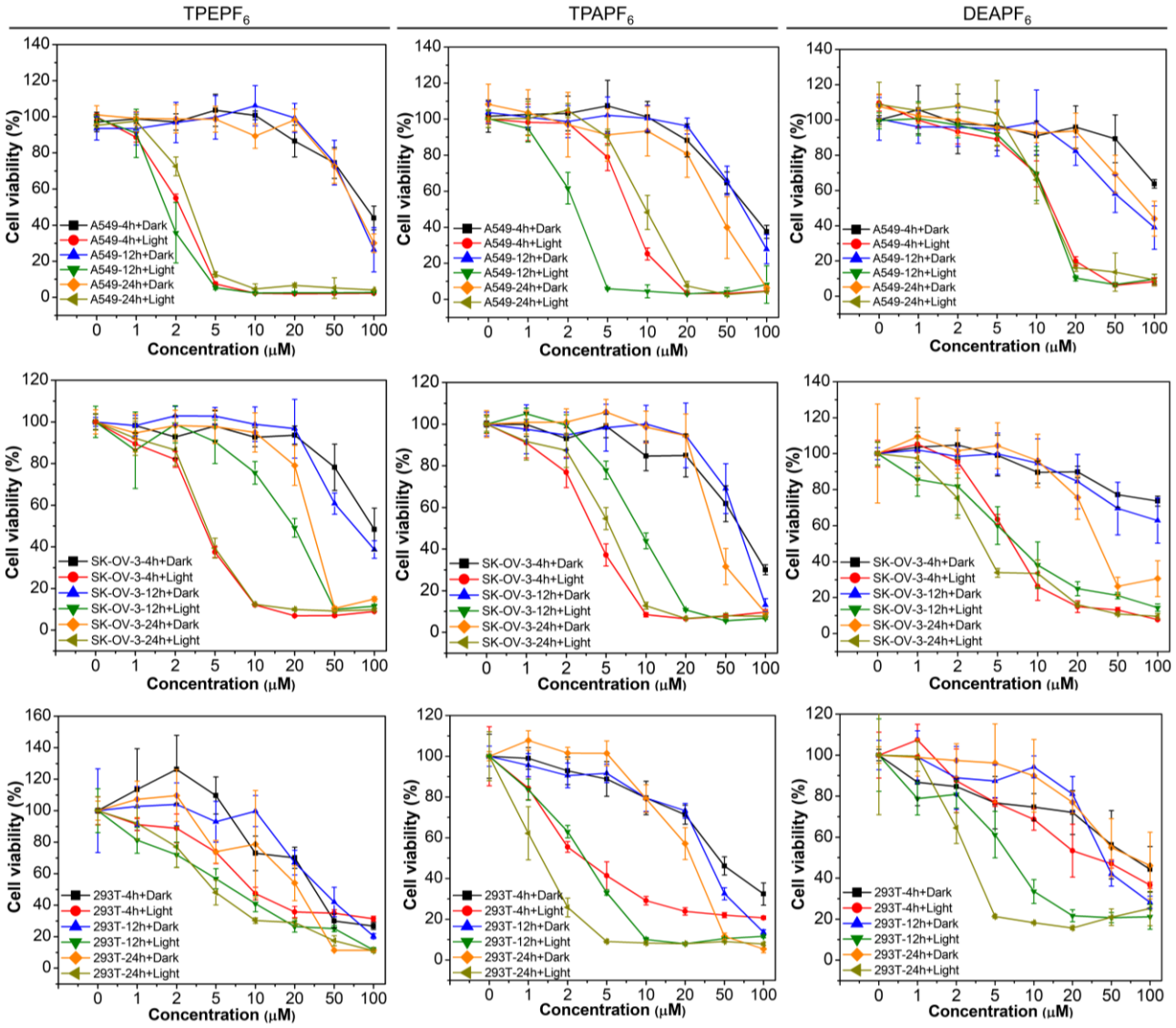

Fig. S60 Relative viabilities of cancer cells (A549 and SK-OV-3 cells) and normal cells (293T cells) treated with $TPEPF_6$, $TPAPF_6$, and $DEAPF_6$, respectively, at various concentrations under darkness or white-light irradiation (100 mW/cm^2, 30 min) and further being incubated for 4 h, 12 h and or 24 h. Data represent mean value ± standard deviation, $n = 6$.

Table S5 Dark- and Photo-cytotoxicity (IC_{50} [μM]) of $TPEPF_6$, $TPAPF_6$ and $DEAPF_6$ towards different cell lines[a]

Compound	A549		293T		SK-OV-3		4T1	
	Dark	Photo	Dark	Photo	Dark	Photo	Dark	Photo
$TPEPF_6$	71.68	3.12	40.37	6.62	74.61	4.73	104.68	4.81
$TPAPF_6$	67.08	10.03	29.64	0.78	59.86	5.20	50.67	3.98
$DEAPF_6$	67.05	11.65	47.92	4.18	131.07	5.31	98.68	3.79

[a] The IC_{50} value is calculated by Statistical Product and Service Solutions (SPSS) software. Data shown are values from three replicates.

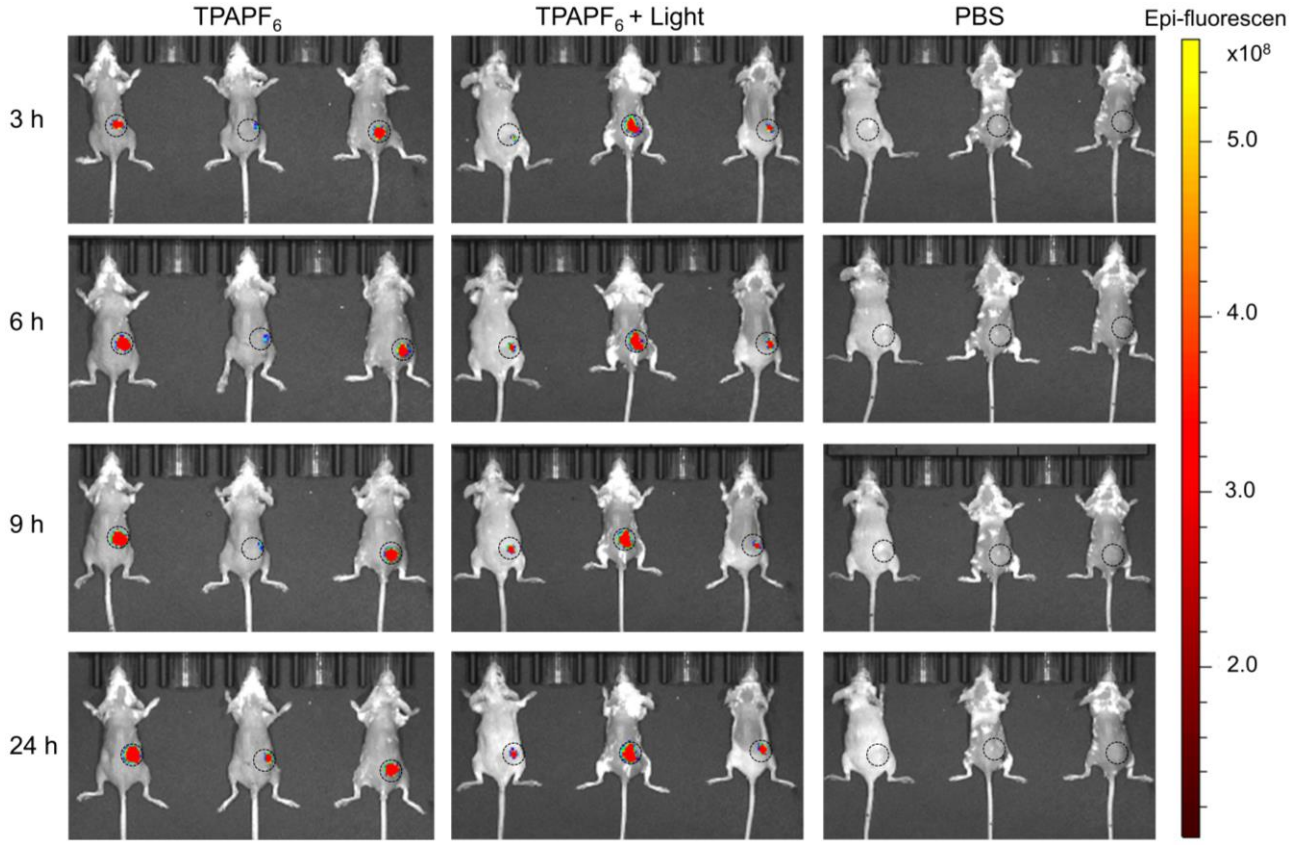

Fig. S61 *In vivo* fluorescence imaging of BALB/*c* mice bearing 4T1 tumor (black circles) over time after intratumoral administration of $TPAPF_6$ (n = 3 per group). λ_{ex} = 465 nm, λ_{em} = 760 nm.

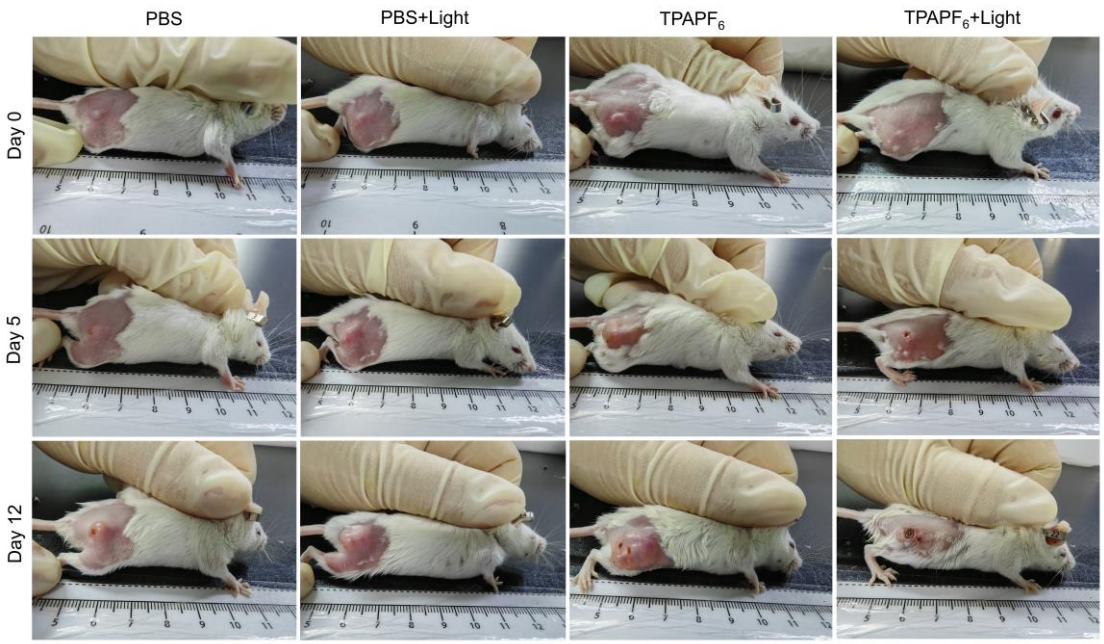

Fig. S62 Photographs of 4T1 tumour-bearing mice in different groups on day 0, 5 and 12 during the treatment process.

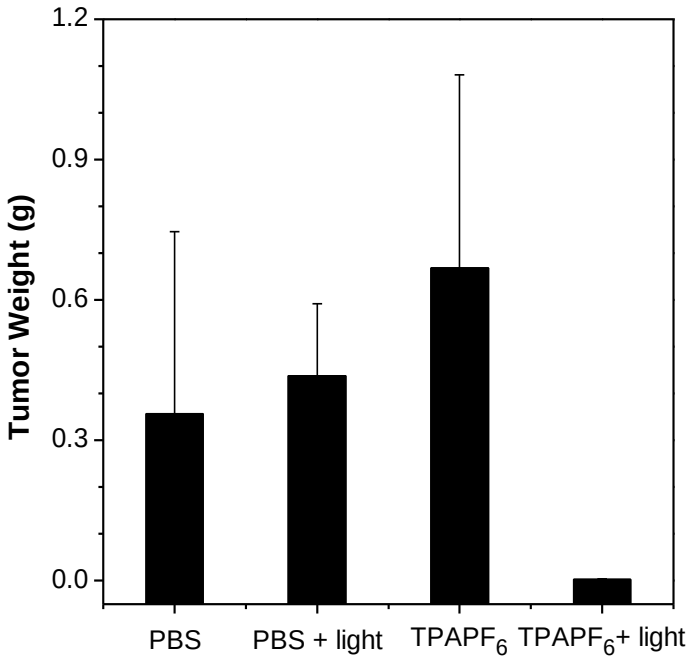

Fig. S63 Weights of the tumors resected from the four groups of mice at day 12 after treatment.

Table S6 The ratio of tumor weight to body weight at day 12 post treatment.

Group	Number	tumor weight (g)	body weight (g)	tumor weight/body weight
PBS	1	0.980	19.1	5.13%
	2	0.078	16.9	0.46%
	3	0.140	17.9	0.78%
	4	0.085	18.8	0.45%
	5	0.501	18.9	2.65%
	Mean	0.357	18.3	1.90%
	SD	0.390	0.9	2.03%
PBS+Light	1	0.444	16.4	2.71%
	2	0.607	18.0	3.37%
	3	0.305	17.9	1.70%
	4	0.572	18.6	3.08%
	5	0.263	16.7	1.57%
	Mean	0.438	17.5	2.49%
	SD	0.154	0.9	0.81%
$TPAPF_6$	1	0.896	17.8	5.03%
	2	0.661	17.2	3.84%
	3	1.113	17.9	6.22%
	4	0.662	18.0	3.68%
	5	0.011	17.4	0.06%
	Mean	0.669	17.7	3.77%
	SD	0.413	0.3	2.31%
$TPAPF_6$+Light	1	0.004	16.4	0.02%
	2	0	17.4	0.00%
	3	0.004	17.4	0.02%
	4	0.003	17.1	0.02%
	5	0.003	17.5	0.02%
	Mean	0.003	17.2	0.02%
	SD	0.002	0.5	0.01%

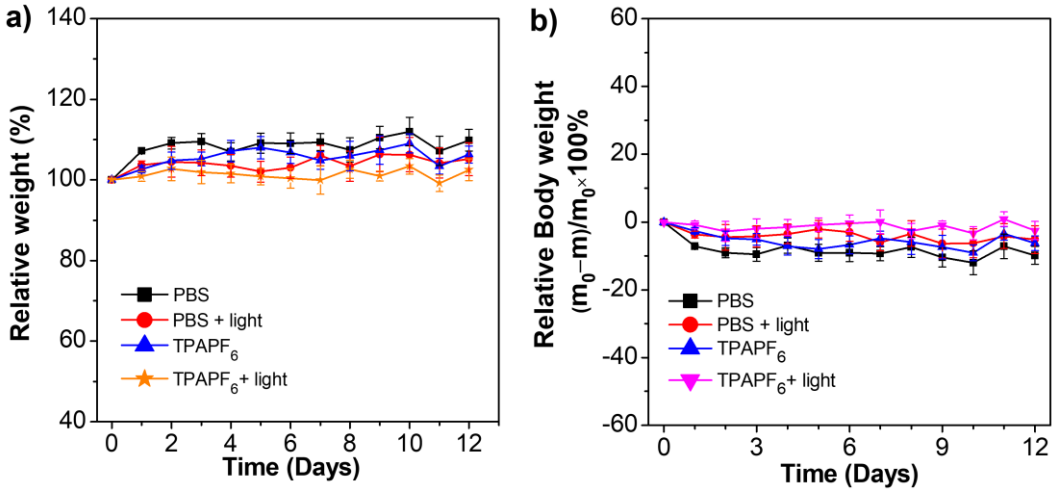

Fig. S64 a) Tumour growth curves of mice after different treatments (n = 5). b) The percentage of "body weight loss", where m_0 is the initial body weight while m is the body weight at different time after treatment.

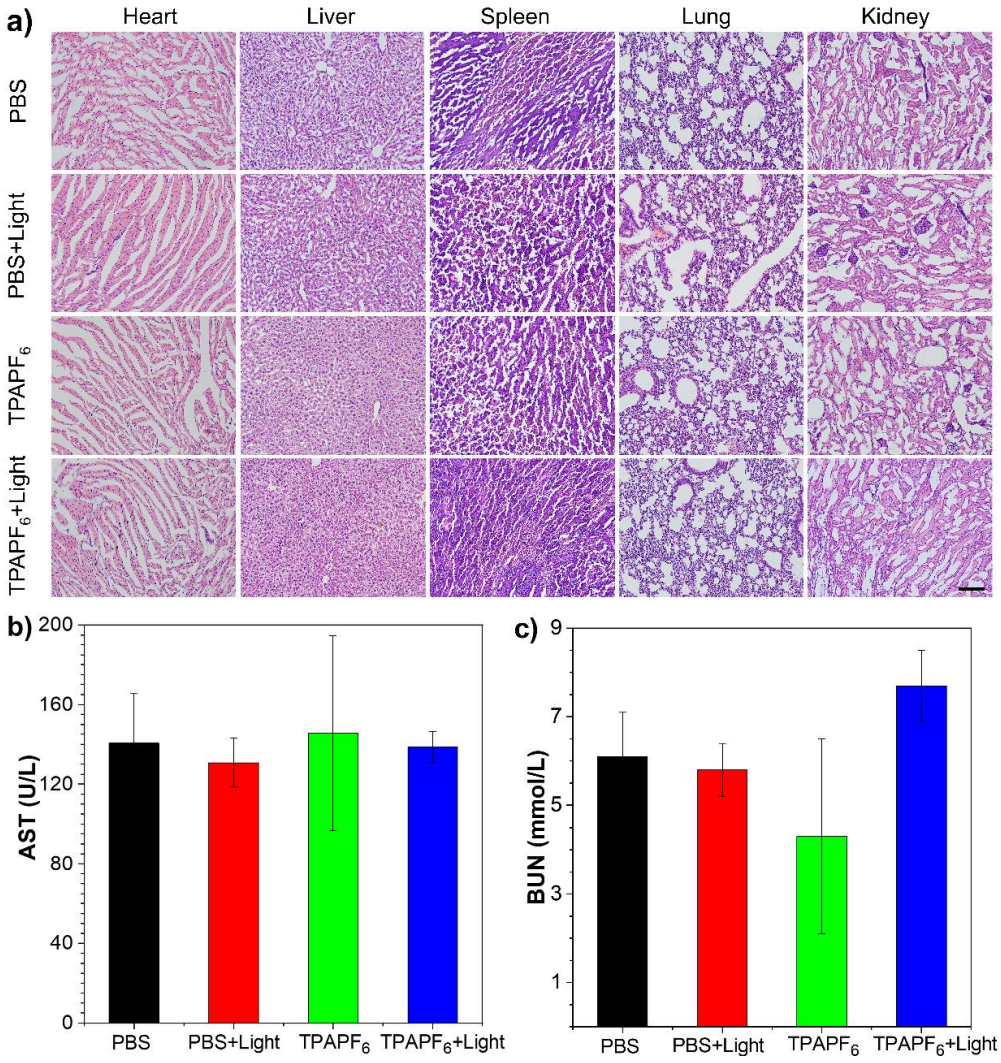

Fig. S65 a) H&E staining images of the major organs (heart, liver, spleen, lung, kidney) sections from the four groups of mice at day 12 after treatment. Scale bar = 100 μm. b, c) Blood biochemistry indices (aspartate aminotransferase (AST) and blood urea nitrogen (BUN)) of the mice obtained at day 11 after treatment. Data are presented as the mean ± SD (n = 5).

References

S1 Z. Liu, T. Lu and Q. Chen, *Carbon*, 2020, **165**, 461–467.

S2 W. Xu, M. M. S. Lee, J. Nie, Z. Zhang, R. T. K. Kwok, J. W. Y. Lam, F. Xu, D. Wang and B. Z. Tang, *Angew. Chem. Int. Ed*., 2020, **59**, 9610–9616.

S3 M. Baglan and S. Atilgan, *Chem. Commun.*, 2013, **49**, 5325–5327.